Synthesis and characterization of molecules for gold (III) catalysis

Karl Stefan Norén

Master Thesis, Department of Chemistry
Organic chemistry
60 credits

UNIVERSITY OF OSLO

03/2023

2023

Synthesis and characterization of molecules for gold (III) catalysis

Karl Stefan Norén

http://www.duo.uio.no/

Printing: Reprosentralen, Universitetet i Oslo

Acknowledgment

The experimental work done for this master's thesis was conducted in the Tilset group at the Department of Chemistry, University of Oslo. It summarizes all the results I have achieved under the supervision of Professor Mats Tilset and Doctor Ainara Nova Flores.

First, I would like to give a sincere and humble thanks Professor Mats Tilset. For holding a presentation about the wonders of organometallic chemistry so compelling that it convinced me to change my master program from analytical to organic chemistry. For giving me the opportunity to work on this project. For always taking time for questions and giving solid professional advice to any problems I was facing. But perhaps above all, always inspiring confidence, strength, and passion after each discussion we had. This has been especially important throughout the corona pandemic. Also, a thanks to Doctor Ainara Nova for an interesting and well-structured introduction to DFT although it was never implemented into the master project.

I would also like to thank all great people in the Tilset group that I spent many hours in the lab with. Especially Stian Årvik for indulging in my many questions and half-baked ideas and Inga Schmidtke for guiding me through her previous work.

I would also direct a big thanks to my good friend Trond Sivert Moe for always having my back and supporting me through put the project.

Lastly, I want to thank my family and friends for always believing in me and all encouragement you have provided throughout the years.

Stefan Norén

Oslo March 2023

Abstract

This thesis consists of two parts where the first part is an investigation of the catalytic reactivity of an (N,C,C) gold(III) pincer complex with substituted hexenynes, including the synthesis of the substituted hexenynes. The second part focuses on the synthesis of precursor gold(III) complexes that will hopefully lead to completely new gold(III) complexes or simplify the synthesis of the existing gold(III) complexes.

The synthesis of 4-phenyl-1-hexen-5-yne and 3-phenyl-1-hexen-5-yne was successful and a by-product was isolated and elucidated to be hexa-1,2,5-trien-1-ylbenzene. The synthesis procedure of 4-phenyl-1-hexen-5-yne was improved to yield a pure product without the by-product present.

Three previously demonstrated catalytic reactions were recreated to validate the catalytic activity of the (N,C,C) gold(III) pincer complex towards the cycloisomerization of hexenynes. 3-phenyl-1-hexene-5-yne was only successfully synthesized once due to unknown circumstances. It was therefore not possible to investigate the catalytic activity of this species.

In the second part two ligands were synthesized and characterized, 5-bromo-2-(4-bromophenyl)pyridine and 5-bromo-2-phenylpyridine. These ligands were successfully cyclometalated into the wanted precursors (N,C) gold(III) 5-bromo-2-(4-bromophenyl)pyridine complex and (N,C) gold(III) 5-bromo-2-phenylpyridine complex. Only (N,C) gold(III) 5-bromo-2-phenylpyridine complex was isolated.

Abbreviations

APPI–MS	Atmospheric pressure photoionization mass spectrometry
2D	two–dimensional (NMR)
br	broad (NMR)
COSY	correlation spectroscopy (NMR)
d	doublet (NMR)
equiv.	equivalents
ESI–MS	electrospray ionization mass spectrometry
HMBC	heteronuclear multiple–bond correlation spectroscopy (NMR)
HSQC	heteronuclear single–quantum correlation spectroscopy (NMR)
J	coupling constant (NMR)
m	multiplet (NMR)
m/z	mass-to-charge ratio (MS)
NaOBz	Sodium benzoate
NMR	nuclear magnetic resonance
NOESY	nuclear Overhauser effect spectroscopy (NMR)
PIFA	(Bis(trifluoroacetoxy)iodo)benzene
ppm	parts per million (NMR)
ppy	2-phenylpyridine
q	quartet (NMR)
rac-BINAP	(±)-2,2′-Bis(diphenylphosphino)-1,1′-binaphthalene
rt	room temperature
s	singlet (NMR)
t	triplet (NMR)
tpy	2-(p-tolyl)pyridine
TLC	Thin layer chromatography
Å	Angstrom

Overview of key compounds

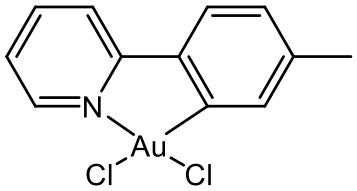

Au(III) Cl_2(tpy)

Au(tpy)Cl_2

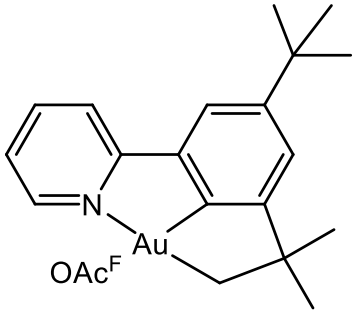

(N,C,C) Au(III) pincer complex

AuPincOAc^F

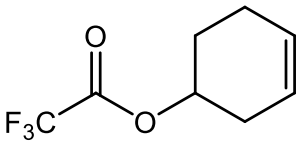

cyclohex-3-en-1-yl 2,2,2-trifluoroacetate

C1

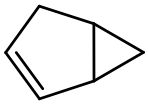

bicyclo[3.1.0]hex-2-ene

C2

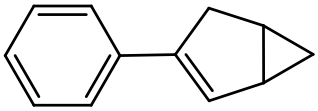

3-phenylbicyclo[3.1.0]hex-2-ene

C3

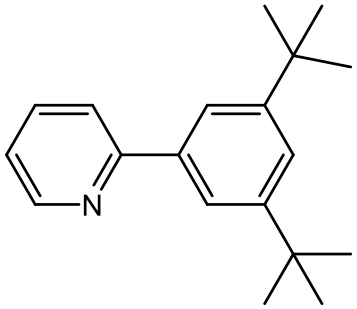

2-(3,5-di-*tert*-butylphenyl)pyridine

L1

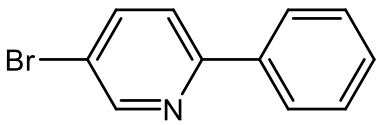

5-bromo-2-phenylpyridine

L2

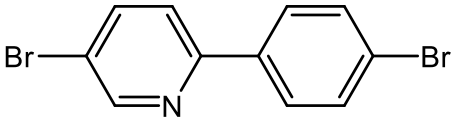

5-bromo-2-(4-bromophenyl)pyridine

L3

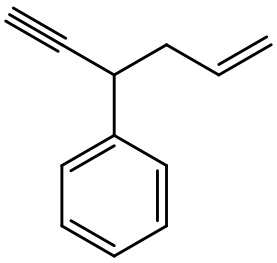

4-phenyl-1-hexen-5-yne

R1

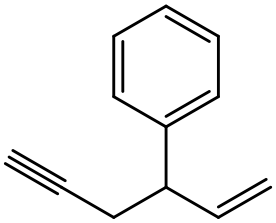

3-phenyl-1-hexen-5-yne

R2

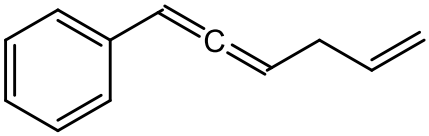

hexa-1,2,5-trien-1-ylbenzene

R3

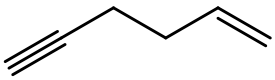

hex-1-en-5-yne

R4

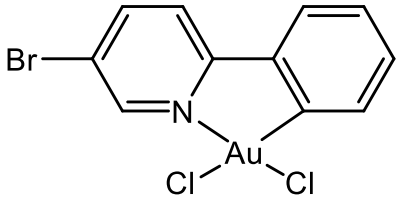

(N,C) Au(III) 5-bromo-2-phenylpyridine

P1

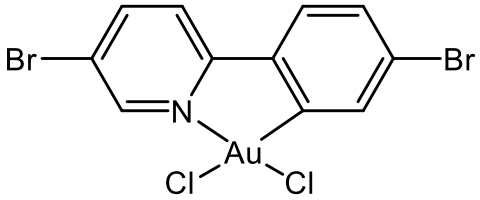

(N,C) Au(III) 5-bromo-2-(4-bromophenyl)pyridine

P2

The compounds are numbered by type:

C = Catalytic product

L = Ligand

R = Reagent in catalytic studies

P = Precursor

Table of contents

*Appendix sorted alphabetically.

1 Introduction

1.1 Gold

If it is one metal that has captured humankinds' fascination and reverence, it is gold. Spanning back several thousand years, gold has been used as jewellery, status symbols, religious artefacts, money, and colouring agent. Gold has even been used in the monetary system to define the value of currency called the gold standard[1].

Gold belongs to group 11 with the atomic number 79 in the periodic table. Interesting physical properties of gold include a melting point at 1337 K and a boiling point at 3129 K[2], a smaller than expected atomic radius and a unique shiny yellow metal colour. These attribute deviations are all due to the relativistic effect[1]. Without the relativistic effect the melting and boiling point would be higher, the colour would be more like silver, and the atomic radius would be larger. Gold has the highest electron affinity and electronegativity of all transition metals, rivalled only by platinum. Gold also has a remarkably high redox potential at $E° = +1.68$ V, making it very resistant to attacks from oxygen and sulphur which is why it does not tarnish or corrode[3]. This resistance is the reason it can be found naturally in its elemental form and why it is called a noble metal. However pure gold is too soft and malleable to be used for anything requiring durability like tools or weapons and was historically mostly used for jewellery and adornments.

It is not until modern times that gold found widespread uses in more practical areas, maybe most noticeably in electronics[4]. But to a lesser-known degree it has also found uses in medicine such as Auranofin to treat rheumatoid arthritis[5], food additives (with metallic gold having its own E-number (E175)[6]) and dental care[7]. Gold has also been used as a colouring agent in glassmaking in the form of purple of Cassius and gold ruby. These colours are achieved by mixing gold nanoparticles into the glass, a technique that is still used today[1]. But more relevant to this thesis, gold has in the last 50 years been studied for its chemical and catalytic properties.

1.2 Gold catalysis

Gold, being a noble metal, is very resistant to oxidation and it is generally unreactive. So unreactive in fact, that it was believed not to have any catalytic properties of worth. In 1967[8] a patent for industrial application of oxidative acetoxylation of ethylene catalysed by Pd-Au showed improved selectivity and activity[9] over pure Pd catalyst. This reaction showed that gold was not totally inert, and it gained a bit of interest as a bimetallic catalyst. A few years later in the 1970s Bond and Sermon showed that the gold could be used as a catalyst and that its catalytic properties changed with the size of the nanoparticles[10]. However, it would not be until the late 1980s when Harut et al. published oxidation of carbon monoxide[11] and Hutchings et al. published hydrochlorination of acetylene[12] using gold nano particles as catalyst, that gold catalysis started getting real traction in the scientific community. Around the same time, it was proposed that gold could form catalytically active complexes in different oxidation states, primarily gold(I)[13], but also gold(III)[14]. Two important milestones for gold catalysis in the industry occurred in 1998 when Prati and Rossi showed that gold could promote selective oxidation of alcohols[15] and in 2005 when Hutchings et al. showed direct synthesis of hydrogen peroxide in non-explosive conditions[16]. Modern research into gold catalysis has discovered many more applications including epoxidation of propylene[17], water-gas shift[18] and C-C bond coupling[19]. Gold catalysis has since been implemented in many industrial processes, especially in chemical and pharmaceutical industry. Today interest in gold catalysis has exploded with almost eleven times as many articles published in the last four years[i] as previously published[20].

A great property of gold is that it often can be used in mild and ambient reaction conditions and gold complexes are less sensitive towards oxygen or water compared to other transition metal complexes. Gold's ability to activate alkene and alkynes for nucleophilic attacks and nucleophilic addition is a well-known fact and is key in gold catalysis. The general proposed reaction is shown in **Scheme 1**.

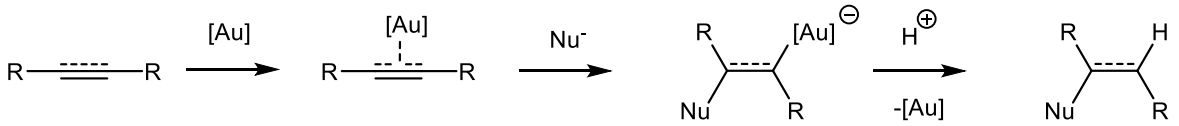

Scheme 1. General scheme for the activation of alkenes and alkynes toward nucleophilic attack at Au.

[i] Searching for "gold +catalysis" on SciFinder (30.01.2023) gave 400000 hits.

This ability to interact with alkenes and alkynes has earlier been explored by the Tilset group[20-22] and further exploration of gold's catalytic abilities will be the focus of this thesis. The catalytic background will be presented in more detail in subchapter 1.5. This is not to say that this is gold's only catalytic properties, it has also demonstrated other organometallic reactions such as reductive elimination, oxidative addition, transmetalation and migratory insertion but these will not be discussed further in this thesis.

1.3 Gold complexes

The simplest and most common form of organometallic gold complexes are gold salts that are activated in situ. Gold complexes are usually in an oxidation state of +1 or +3, however +2, +4, and +5 have also been reported[23, 24]. Gold(I) complexes are d^{10} 14 electron complexes with a preferred linear two-coordinate geometry as illustrated in **Figure 1**. Gold(I) complexes have been and continue to be more widely studied but they are not the focus of this thesis and will not be discussed further. It was demonstrated by Hashmi et al.[25] that the gold(III) complexes when compared with gold(I) complexes could catalyse certain reactions with higher selectivity, activity, and long-term stability. Gold(III) complexes are d^8 16 electron species that prefer a square planar four-coordinated geometry[26] as illustrated in **Figure 1**. Gold(III) complexes have become a main focus in the Tilset group and will be the focus of this thesis.

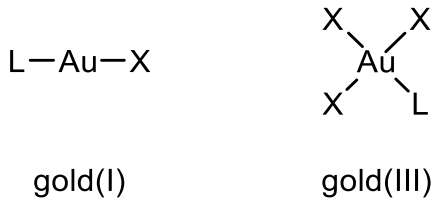

Figure 1. Preferred coordination geometries of gold(I), left, and gold(III), right, where X is anionic 1 electron donor and L is a neutral 2 electron donor.

Most gold(III) catalyses are done with simple salts such as $AuCl_3$, $HAuCl_4$, $KAuCl_4$, $NaAuCl_4$, and so forth[27]. One of the gold(III) reactions Hashmi et al.[25] studied is shown in **Scheme 2**.

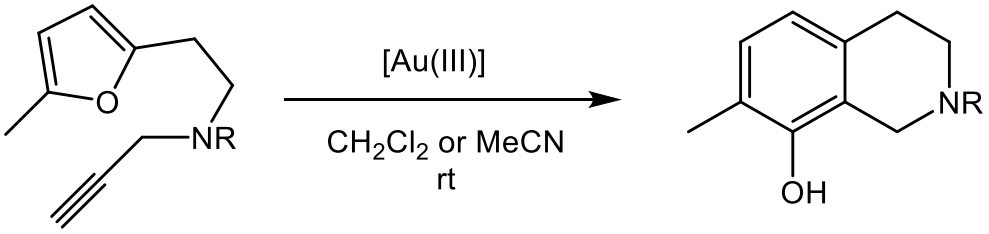

Scheme 2. Gold(III) catalysed phenol synthesis. (R= $SO_2C_6H_4Me$, 4-$NO_2C_6H_4SO_2$, $PhCH_2O_2C$)

In this study they showed the importance of the ligands attached to the gold centre[25]. For example, the simple salt $AuCl_3$ were only able to fully convert the simplest substrate (R = $SO_2C_6H_4Me$). To get full conversion of the more complex substrates a chelating (N,O)

pyridine ligand to gold(III) was needed. The (N,O) chelated gold(III) complex is shown in **Figure 2**.

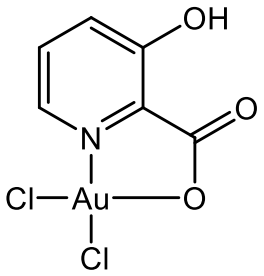

Figure 2. Gold(III) complex with a chelating 3-hydroxypicolinic acid ligand.

The chelated gold(III) complexes gained more attention after this and have since been used in several transformations. A subgroup of such chelated complexes are the gold(III) arylpyridines. One such complex $Au(ppy)Cl_2$ (ppy = 2-phenylpyridine) is air stable and not as hygroscopic or acidic as $AuCl_3$. Urriolabeitia et al. showed that $Au(ppy)Cl_2$ can catalyse the addition of 2-methylfuran to methyl vinyl ketone with good yields. This addition reaction is shown in Scheme 3[28].

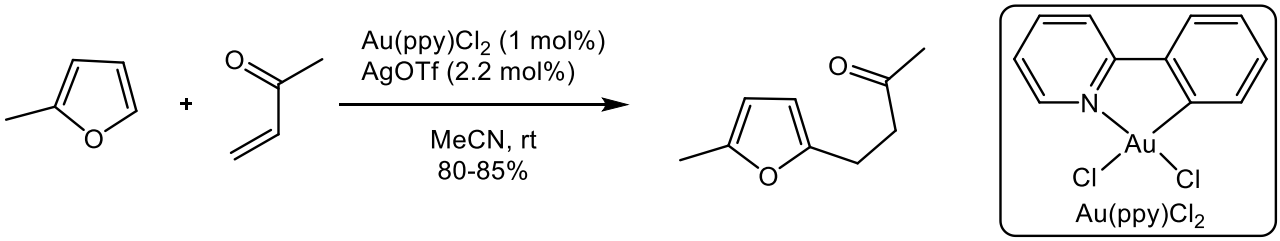

Scheme 3. Gold(III) catalysed addition of 2-methylfuran to methyl vinyl ketone.

The $Au(ppy)Cl_2$ mentioned above is a (N,C) cyclometalated gold(III) complex that resembles the complexes that have become the primary focus of the Tilset group.

Cyclometalated gold(III) complexes have come into the spotlight of research in recent years. This is because cyclometalated complexes stabilize the gold(III) centre and reduce the chance of reductive elimination reducing it to gold(I). Cyclometalation is the formation of a metallacycle with a metal carbon σ bond[29] most commonly in a two-step reaction. The first step in cyclometalation is metal coordinating with a heteroatom donor group (typically N,O,P or S). The second step closes the ring by intramolecular activation of a C-R bond, where C-H activation is by far the most common. A general cyclometalation reaction is illustrated in **Scheme 4**.

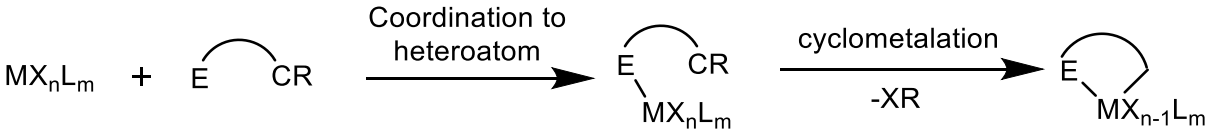

Scheme 4. General illustration of the two steps for cyclometalation, where E is heteroatom donor group and the most common case R=H

The ligands on the metal centre and the functional groups on the phenylpyridine, play a large role in the cyclometalation reaction and the resulting complexes' catalytic properties. The two most common gold ligands used by the Tilset group are chloride and trifluoroacetate. The trifluoroacetate is of interest as it is a larger and more reactive ligand then the corresponding chloride. Chloride was historically cheaper and easier to produce and has therefore been the subject of extensive investigations.

There are generally three different routes to perform gold cyclometalation. From an organic mercury precursor, halogen abstraction promoted with silver salts or direct coordination by heating[30, 31]. Of the three alternatives cyclometalation by heating is the most preferable, as it does not produce toxic mercury derivatives or need stoichiometric amounts of silver salts. This was pioneered by Leese and Constable in 1998[32], and has later been improved upon by the Tilset group in 2011, to a microwave assisted one-pot reaction. This one-pot procedure reduces the time needed for the reaction, increasing its ease of use while maintaining high yields.[33]

In 2022 Nevado et al.[34] showed a promising method using rhodium catalysed transmetalation of gold(III) complexes. This catalysed one-step synthesis does not produce any toxic waste, proceeds under milder conditions than previous mentioned methods, and shows promise of synthetic utility especially with electron deficient pyridines. Their mechanistical studies suggested that the transmetalation occurred by a Rh-to-gold(III) ligand transfer process, where C is first bonded to gold and then to N before releasing the catalytic rhodium complex. A generalized illustration of this reaction is shown in **Scheme 5**.

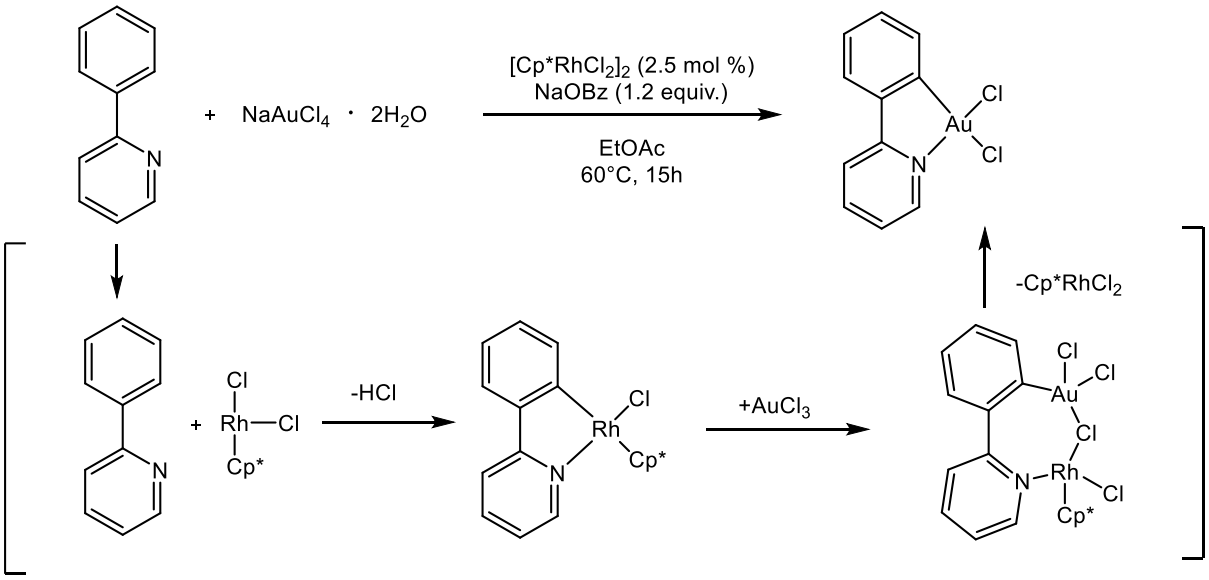

Scheme 5. Generalized illustration of Nevado et al.[34] rhodium catalysed gold(III) transmetalation reaction with summarized steps for the Rh-to-gold(III) ligand transfer. Where gold is first bonded to the activated Csp^2-H bond and then binds to the N atom.

The microwave assisted method developed by the Tilset group has enabled the synthesis of many variations of cyclometalated (N,C) gold(III) complexes[35] with relative ease, a few examples are shown in

Figure 3.

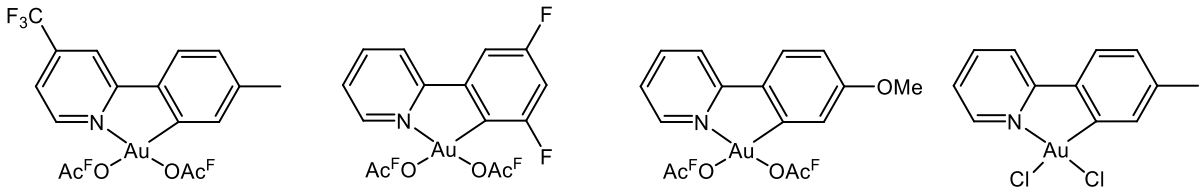

Figure 3. A few examples of cyclometalated gold(III) complexes synthesized by the Tilset group.

The standard procedure to synthesize such cyclometalated gold(III) complexes in the Tilset group, is to first synthesize the ppy-ligand with all wanted functional groups attached. The ligand is often synthesised by a Suzuki-coupling between a brominated pyridine and a phenylboronic acid. The ligand together with a gold salt is then heated in a microwave oven to yield the cyclometalated complexes as shown in **Scheme 6**.

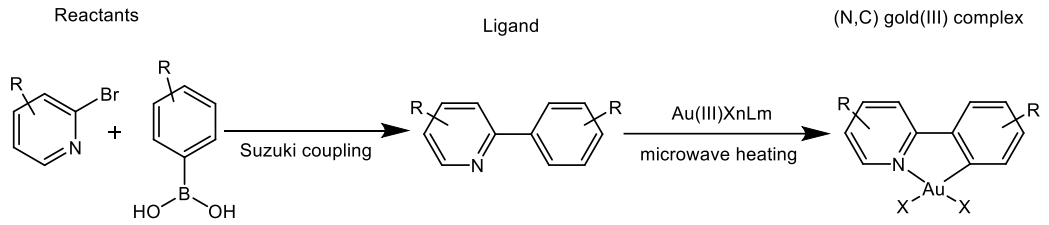

Scheme 6. A generalized illustration of a typical synthesis of a cyclometalated (N,C) gold(III) complex, note that the R and X in the schemes can be different substituents.

However, an interesting idea is to reverse the order and create a precursor cyclometalated gold complex that can then be diversified using different substitution reactions.

The advantage with this idea, is that the potential difficulties in the cyclometalation step can be circumvented. A problem might for example be the deactivation of the phenyl due to electron withdrawing substituents that make it impossible for the second step of cyclometalation to close the ring. Another known issue is that sensitive ligands may not survive the cyclometalation reaction conditions or the ligand might partake in unwanted side reactions. This will be further discussed in chapters in 3.1.4 and 3.1.5.

1.4 (N,C,C) Au(III) pincer complexes

Tridentate ligands that occupy adjacent sites in a metal complex are called pincer ligands and typically form a rigid geometry[36, 37]. The tridentate coordination of a pincer ligand provides strong bonds to the metal centre which gives the complex a high thermal stability. This thermal stability and rigidity allow the complexes to react with external ligands and reducing agents at high temperatures while still retaining the pincer coordination of the ligand. There are many types of pincer complexes reported such as (C,N,N), (N,C,N), (P,N,P), (O,N,O) etc.[38-40]. The most common gold(III) pincer complexes are probably (C,N,C) types derived from 2,6-diarylpyridines[39]. Traditionally gold(III) pincer complexes were synthesized by transmetalation from organomercury compounds just as with the cyclometalated (N,C) gold(III) complexes. However, Nevado et al. reported a mercury-free synthesis of a (N,C,C) gold(III) pincer complex with microwave assisted heating based on a 2-biphenylpyridine framework[41]. This synthesis was a two-step reaction where gold is first coordinated to the pyridine-N followed by cyclometalation by heating. The reported synthesis is illustrated in **Scheme 7**.

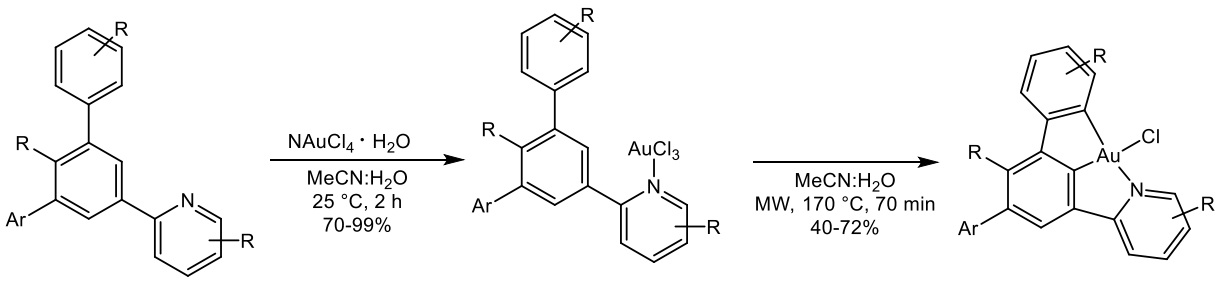

Scheme 7. Synthesis of gold(III) (N,C,C) pincer complexes reported by Nevado et al[41].

Most reported cyclometallations with gold(III) are via C(sp^2)-H activation and there are only a few examples involving C(sp^3)-H activation. Cinellu et al. reported a synthesis for a (N,N,C) pincer complex using $AgBF_4$ to activate C(sp^3)-H for cyclometalation[42]. In 2018 the Tilset group reported that a double cyclometalation via one C(sp^2)-H and one C(sp^3)-H activation was a possible pathway to synthesise the neutral (N,C,C) gold(III) pincer complex[43](**AuPincOAc^F**), illustrated in **Figure 4**.

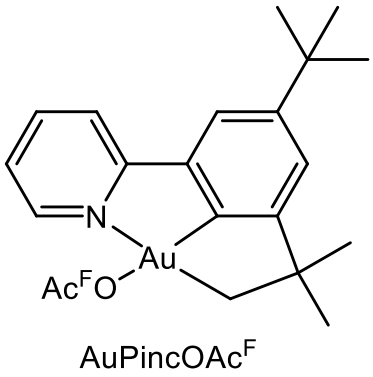

Figure 4. Illustration of **AuPincOAc^{F}** synthesised by a second cyclometalation through activation of a C(sp^3)-H bond.

This double cyclometalation utilized the one-pot microwave assisted procedure mentioned above. The second cyclometalation via C(sp^3)-H activation was achieved by having a large, sterically hindering, functional group on the phenyl. The functional group's interaction with the trifluoroacetate gold ligand distorts the Au(III) preferred square planar geometry making coordination to the C sterically favourable. This led to the additional cyclometalation step, where gold activates the C(sp^3)-H bond and releases one trifluoroacetate group to form the pincer complex that can relax back to square planar geometry.

AuPincOAc^{F} has been shown to be catalytically active towards small alkynes, be more robust and shown higher turnover numbers than comparable (N,C) gold(III) complexes. **AuPincOAc^{F}** has also shown catalytic activity promoting the cycloisomerization of substituted 1,5-hexenynes [21, 22].

1.5 Gold catalysis of reactions with alkenes/alkynes

Gold excels at increasing the electrophilicity of C-C multiple bonds making them susceptible to nucleophilic attack[25, 44]. One of simplest cases of such a catalytic cycle is shown in **Scheme 8**.

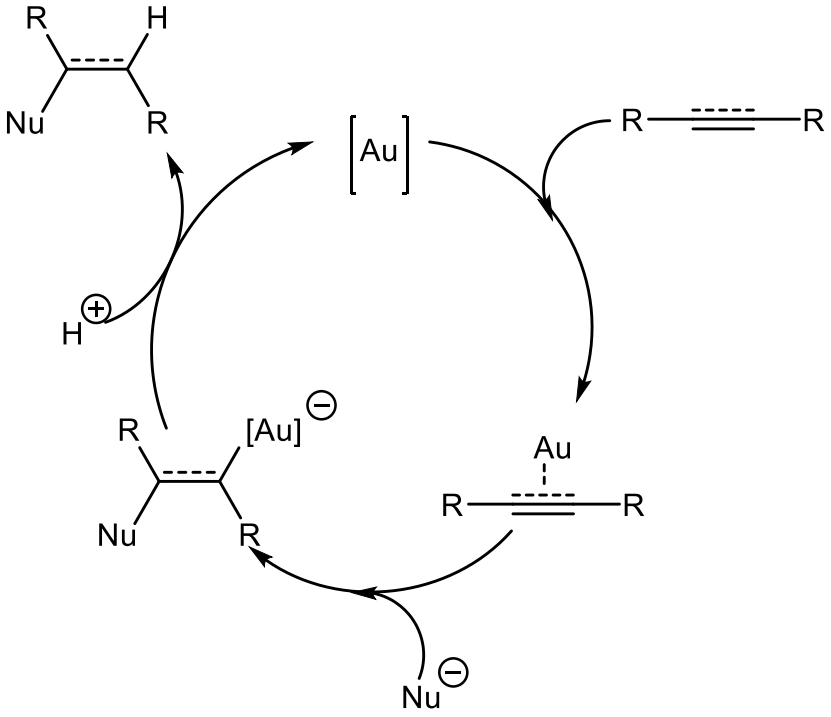

Scheme 8. Proposed general catalytic cycle for gold catalysed C-C multi band activation.

The gold catalyst may coordinate with the π-system of a multiple bond increasing its electrophilic character, readying it for a nucleophilic attack. This allows the formation of a gold alkyl/vinyl intermediate that undergoes protolytic cleavage to release the product and regenerate the gold catalyst.

Another catalytic ability of gold is the ability to catalyse rearrangements of enynes, where cycloisomerization reactions have been of particular interest[45-48]. Most such research focuses on the Alder-ene reactions of 1,6- and 1,7-enynes with a metal catalyst, which can lead to complex architectures by fully intramolecular processes. An example of a general metal

catalysed 1,6-enyne Alder-ene reaction is illustrated in **Scheme 9**.

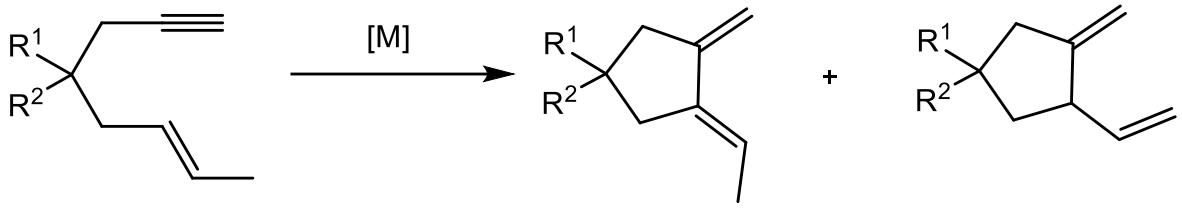

Scheme 9. General representation of a metal catalysed 1,6-enyne Alder-ene reaction.

Recently cycloisomerization of 1,5-enynes has come under investigation. For example, Toste et al. showed the formation of bicyclo[3.1.0]hexenes from 1,5-hexenyne catalysed with gold(I) complexes[49].

This bicycloisomerization has since been expanded upon and an example using gold(III) complexes as a catalyst was presented by Reeds et al.[50]. They used substituted 1,5-hexenynes in presence of silver salts where gold(III) complexes showed similar reactivity towards the enynes as gold(I) complexes did. The bicycloisomerization reported by Reeds et al.[50] is illustrated in **Scheme 10**.

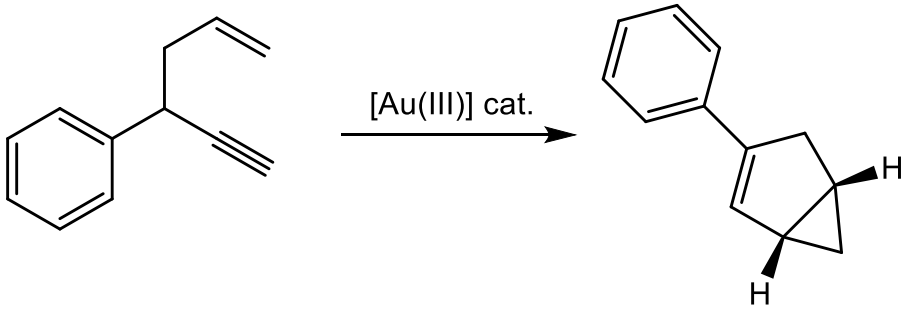

Scheme 10. General scheme for gold(III)–catalysed bicycloisomerization of 4-phenyl-1-hexen-5-yne to furnish 3-phenylbicyclo[3.1.0]hex-2-ene.

Cycloisomerization catalysed by gold(III) complexes has been further investigated by the Tilset group. It has been shown that gold(III) complexes exhibited reactivity towards smaller alkene/alkynes[20]. An example of this is the rearrangement of **R4** to **C1** catalysed with **AuPincOAc^{F}** as shown in **Scheme 11**.

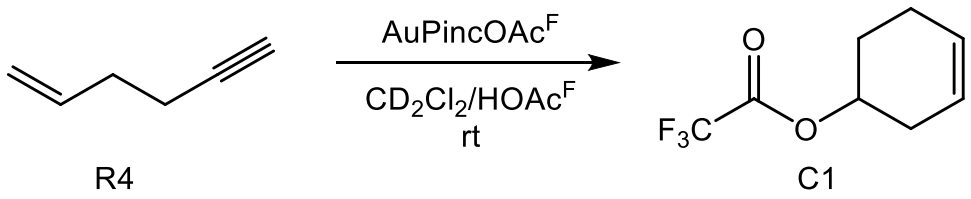

Scheme 11. Reaction of **R4** with AuPincOAc^{F} furnishing **C1**.

It was believed that the reaction involved the intermediate **C2**. To investigate this, TFE was used as solvent instead of DCM to slow down the reaction. With TFE as solvent the **C2** intermediate could be observed. However, when adding HOAc^{F} to react with **C2** to form **C1** an ether species was observed instead as shown in **Scheme 12**. It is unclear if the gold complex plays a role in the opening of the bicyclic ring or if this reaction is purely acid catalysed similar to what Freeman et al. described[51].

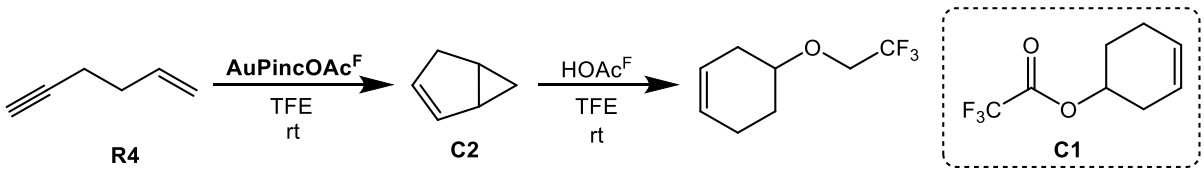

Scheme 12. Reaction of R4 with AuPincOAcF as catalyst in TFE leads to cycloisomerization into **C2**. When HOAc^{F} is added an ether is formed instead of the expected **C1**.

The same bicycloisomerization of substituted hexenynes as shown in **Scheme 10** has been reported using **AuPincOAc^{F}**[21, 22], but the product was never isolated. The substituted hexenynes have the advantage of being less volatile than their unsubstituted counterparts and should yield products that are easier to isolate. Further studies are needed on these reactions to determine their products and **AuPincOAc^{F}'s** role in the reaction. It is also of interest to determine if the reactions can take place under milder conditions. An exploration of reaction conditions/reaction products is presented in chapter 3.2.

2 Aim of project

This thesis consists of two parts. The first part is a further investigation in the catalytic properties of **AuPincOAc^{F}** reactivity towards substituted hexenynes that has previously been examined by the Tilset group. Earlier work conducted by the Tilset group will be replicated to provide a reference point before examining the reaction using different substituted hexenynes. The focus will be to determine if the cycloisomerization reaction takes place with phenyl substituted hexenynes and if it is catalysed by **AuPincOAc^{F}**. Milder reaction conditions will then be explored for the substituted hexenynes that show evidence of catalysed reactions. The reactions will be monitored by NMR to try and get as much information of the reactions as possible.

The second part will look at the possibility of synthesising cyclometalated gold(III) precursor complexes that can be further diversified. The general synthesis of such precursors is illustrated in **Scheme 13**.

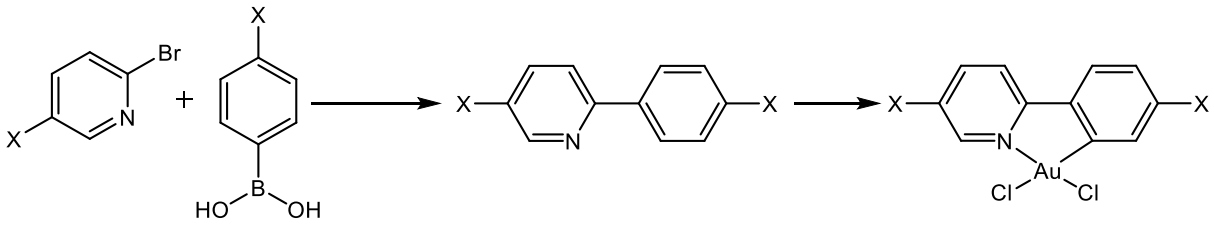

Scheme 13. An example of reaction scheme to cyclometalated precursor with, in this case, X being functional groups that can be easily substituted.

Currently, the ligand is synthesized with all wanted functional groups attached and then cyclometalated with the gold centre. But the idea behind the precursor, to diversify the ligand after cyclometalation, may open viable ways to synthesis new gold complexes. For example, adding functional groups that would normally not survive the cyclometalation conditions or very electron withdrawing groups that would deactivate the π-system of the ligand and in turn hinder the cyclometalation. Initially bromide will be used as functional groups for substitution with a Suzuki-Miyaura reaction to attach wanted substituents. A general example of a precursor reaction is shown in **Scheme 14**.

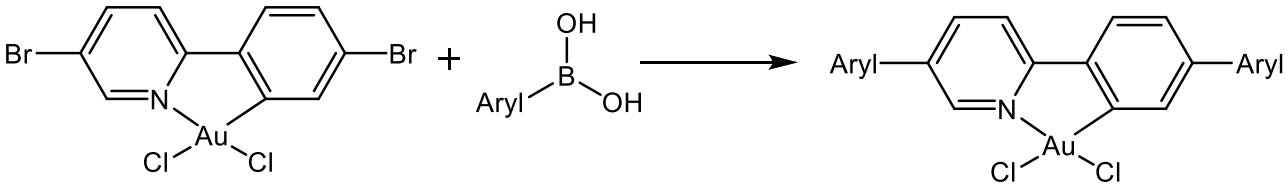

Scheme 14. A simplification of a Suzuki-Miyaura reaction with the cyclometalated gold precursor to attach a functional group.

Bromide was chosen because there are many readily available brominated pyridines and arylboronic acids and the Suzuki-Miyaura reaction is well-established in the Tilset group.

3 Results and discussion

All reactions presented in this chapter were conducted on a small scale (typical 100 - 600 mg) and monitored by TLC and/or NMR spectroscopy unless stated otherwise. Eluents, if different from original procedure, were chosen based on TLC testing.

3.1 Synthesis and characterization

3.1.1 (N,C,C) Au(III) pincer complex

To gain experience with the microwave assisted cyclometalation reaction mentioned in 1.3, the synthesis of **Au(tpy)Cl$_2$** is often used as a tutoring reaction in the Tilset group. The complex was synthesized following the procedure reported by Shaw et al.[33] shown in **Scheme 15** with a 68% yield.

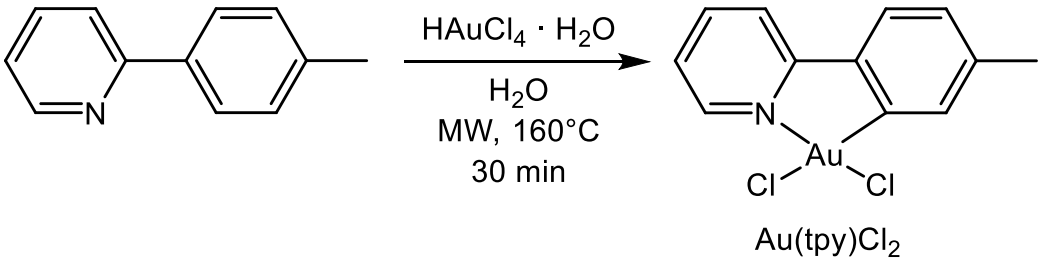

Scheme 15. Microwave-assisted synthesis of **Au(tpy)Cl$_2$**.

The isolated product was analysed with ^{1}H NMR (**A 1**), six signals were observed in the aromatic region along with one singlet in the aliphatic region. The assignment of signals to the molecule is shown in 6.2.1. This is in accordance with the reported NMR values[33].
ESI-MS analysis of the compound does not show the main ion peak but an adduct peak m/z 458 [M + Na] and a fragmented peak m/z 400 [M – Cl]. The corresponding expected isotope pattern[52] from naturally abundant ^{35}Cl and ^{37}Cl is also observed, m/z 460 [M + Na] (65% intensity of m/z 458) and m/z 402 [M – Cl] (32% intensity of m/z 400).
Analysis showed that the desired product **Au(tpy)Cl$_2$** was synthesised and isolated. Although the yield was lower than previously reported, product levels were sufficient to consider the method viable.

Synthesis of **L1**, used as ligand for synthesis of **AuPincOAc^{F}**, utilizes a Suzuki-Miyaura coupling shown in **Scheme 16**. This synthesis is based on the previously established procedure for ligand synthesis reported by the Tilset group[35, 43, 53]. Reacting 2-bromopyridine with (3,5-Di-tert-butylphenyl)boronic acid resulted in **L1** at a yield of 89%.

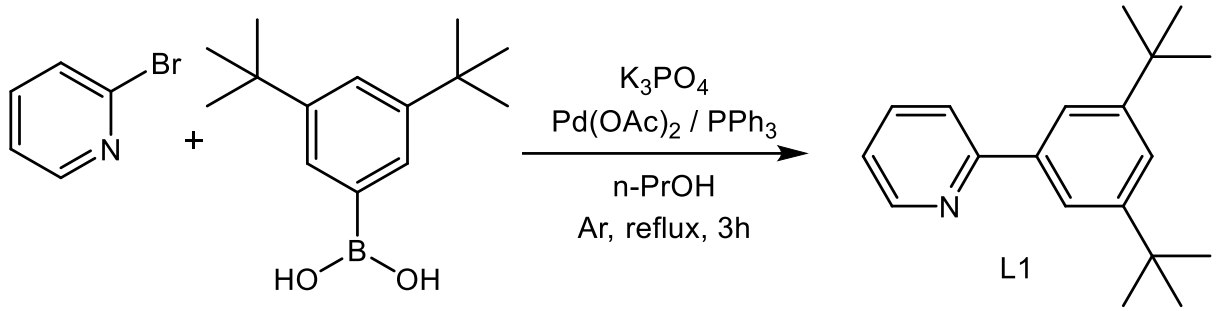

Scheme 16. Synthesis of **L1** via Suzuki-Miyaura coupling.

L1 was analysed with ^{1}H NMR (**A 6**) and the spectrum was in agreement with previously reported data[43] and no impurities was observed. **L1** was also analysed with ESI-MS that showed an expected main ion peak at m/z 268 [M+H] and corresponding isotope peak from ^{13}C at m/z 269 [M+H] (21% intensity of m/z 268). Assignment of ^{1}H NMR signals to the molecule are shown in 6.2.2.

AuPincOAc^{F} was synthesized from **L1** and $Au(OAc)_3$ at an 82% yield using the microwave assisted procedure developed by Holmsen et al.[43] shown in **Scheme 17**.

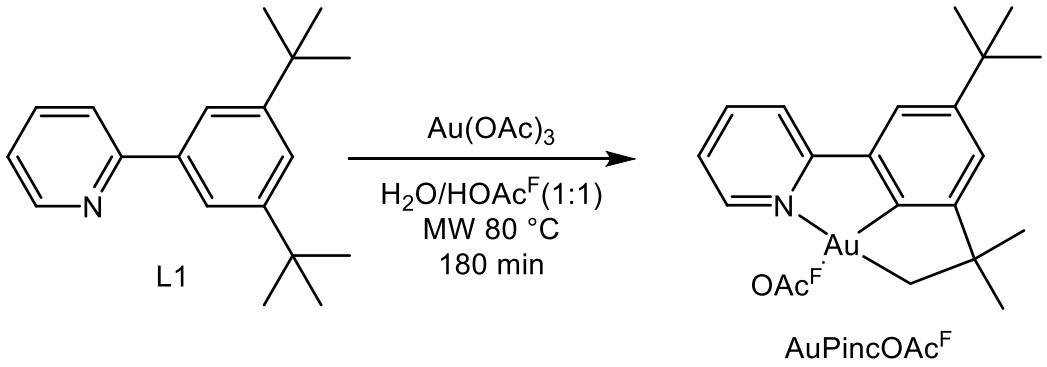

Scheme 17. Microwave assisted synthesis of **AuPincOAc^{F}**.

The product was analysed with ^{1}H NMR and the characteristic signal at 3.15 ppm for the CH_2 bridge to gold is observed as well as the two signals at 1.37 and 1.38 ppm integrating to a total of 15H (9+6) accounting for all methyl groups. The splitting of the signals in the

aromatic region also correspond well with previously reported NMR data[43].

AuPincOAc^{F} was also analysed with ESI-MS where the peak at m/z 520 could be [M - OAc^{F} + Cl + Na] with corresponding isotope peak with the right intensity at m/z 522 [M - OAc^{F} + Cl + Na] (33% intensity) and the peak at m/z 462 might be [M - OAc^{F}] (85% intensity). NMR signal assignments to the molecule are shown in 6.2.3.

The synthesis presented so far has been recreated successfully and all results are in accordance with what is previously reported[33, 43]. With **AuPincOAc^{F}** synthesized, the next step was to synthesis the substituted hexenynes, **R1** and **R2**, for the catalytic investigation.

3.1.2 4-phenyl-1-hexen-5-yne

R1 was synthesized using the reported procedure[50, 54] shown in **Scheme 18**.

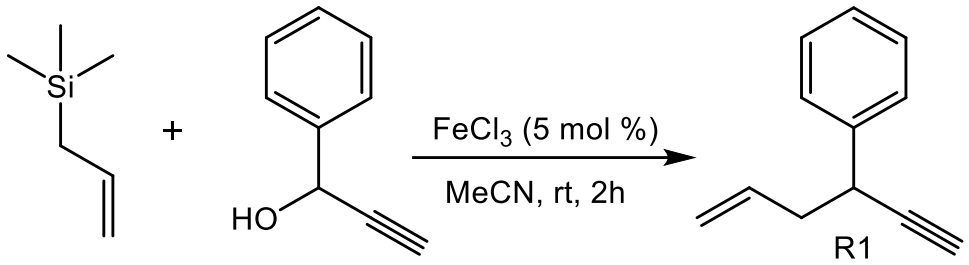

Scheme 18. Fe(III) catalysed substitution reaction of 1-phenylprop-2-yn-1-ol with allyltrimethylsilane.

1-phenylprop-2-yn-1-ol and allyltrimethylsilane were reacted in dry acetonitrile in the presence of iron(III) chloride at room temperature for 2 hours under inert conditions. The crude product was purified by flash chromatography using pure hexane as eluent. **R1** was obtained as a slightly yellow oil at a yield of 58%. The product was analysed with ^{1}H NMR and all the signals reported in the literature[21, 50] were observed in the spectrum (assignment of signals can be found in 6.2.4). However, there were also a considerable amount of impurities as shown in **Figure 5**.

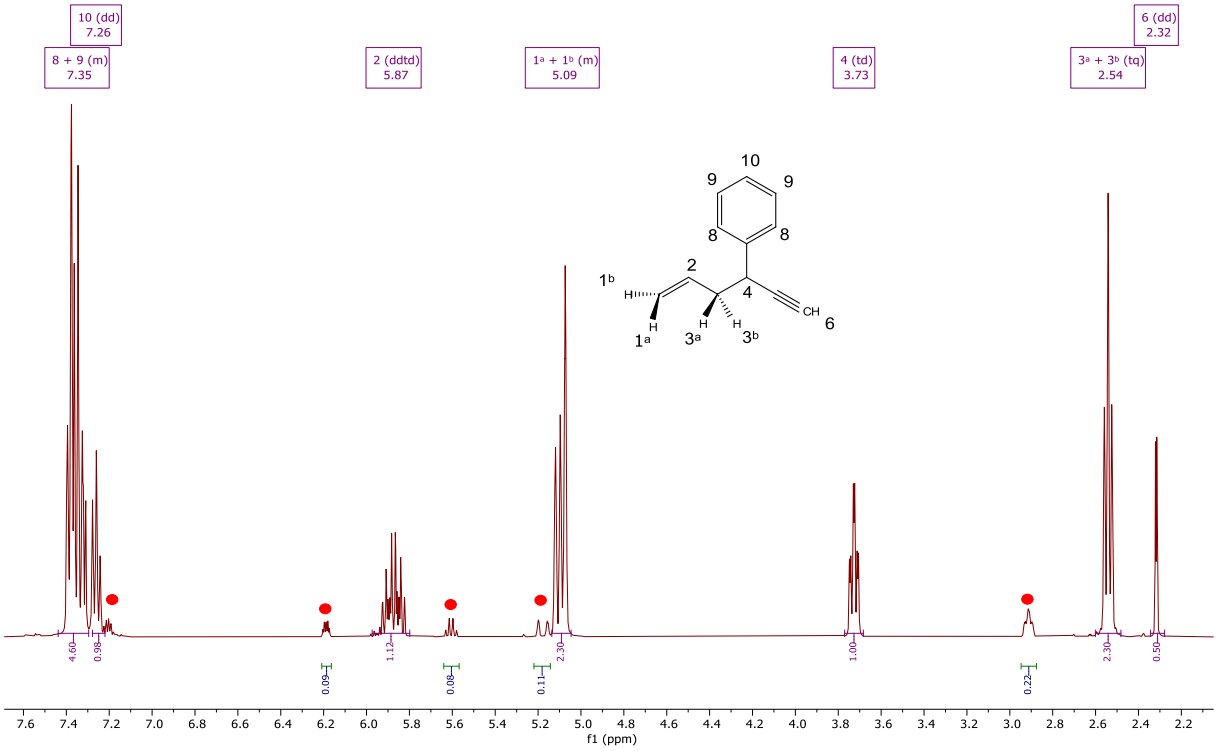

Figure 5. ^{1}H NMR (400 MHz, $CDCl_3$) spectrum of **R1** with assigned signals indicated with numbers and impurities indicated with a red dot.

As **R1** was going to be used in the catalytic studies, a high purity was desirable. As an impurity of roughly 8-11% could significantly affect the catalytic reaction as the impurities would be present in concentrations of the same order of magnitude as the catalyst. There is no spectrum attached in the supplementary information provided by Reeds et al.[50] or Zhan et al.[54] so it could not be established if the observed impurities were also present in their final product. However, the same impurities have been observed in the previous synthesis conducted by the Tilset group using the same procedure[21].

To separate the impurities from the product a new flash chromatography utilizing an eluent system consisting of 25:75 EtOAc / distilled hexane was used. This configuration achieved separation of two compounds, although trailing was observed in the TLC tests. Three different sets of fractions were collected determined by TLC, the first compound, a mix of the two and the second compound. With the solvent removed all three sets had a slight yellow colour as before. The different fractions were analysed with ^{1}H NMR, however as seen in Figure 6 no significant improvement in purity was achieved.

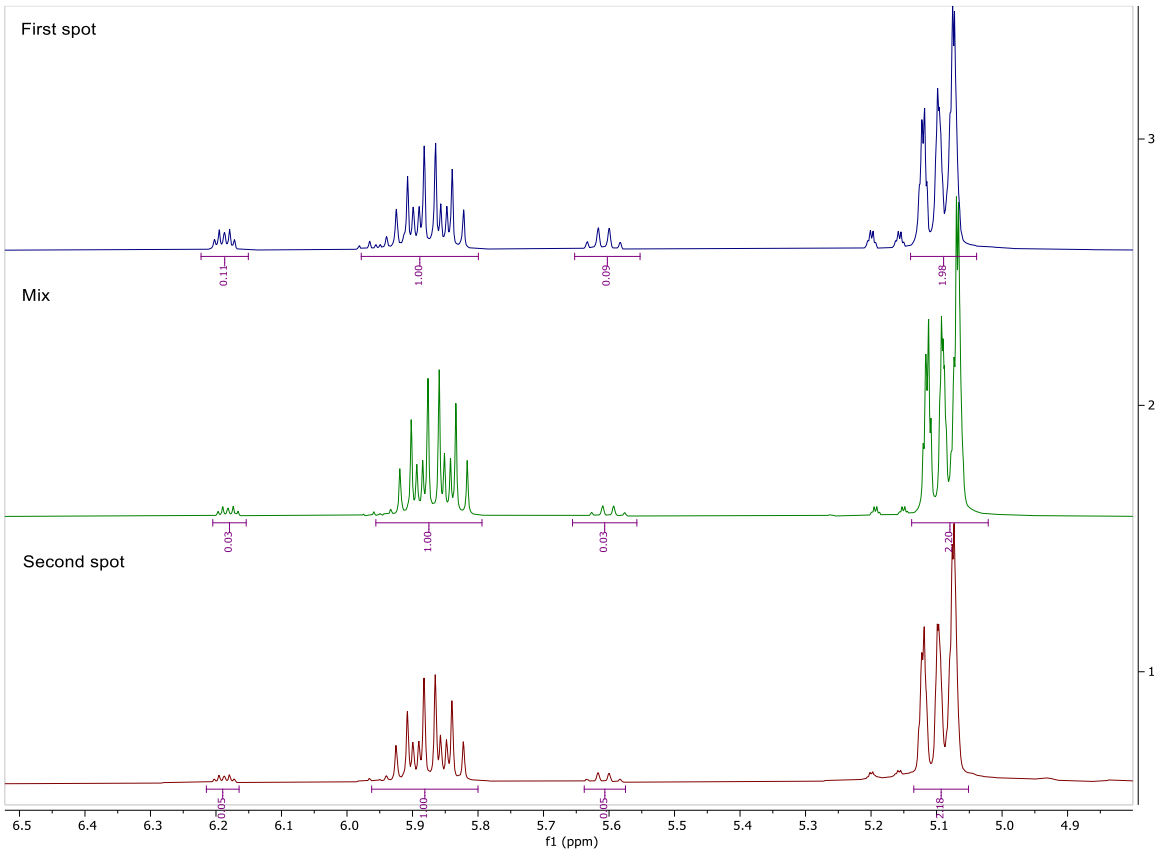

Figure 6. ^{1}H NMR (400 MHz, $CDCl_3$) spectra of the 3 sets of collected fractions after second column showing the alkene region.

As the fraction containing a mix of the two compounds had the lowest ratio of impurities (approximately 3%), it appears that the spots observed in TLC do not to correspond with the impurities. This might indicate an NMR silent impurity or a molecule similar in structure to the wanted product not easily separated on a column. One explanation for the impurities could be product coordinated with left over $FeCl_3$ as this would alter the shifts in NMR. Fe^{3+} could also explain the slight yellow colour observed[55].

To evaluate this hypothesis a liquid-liquid extractions was performed on a small sample of the impure product, using DCM as organic phase and saturated $NaHCO_3$ as the aqueous phase. After mixing and separation of the two phases 1M NaOH was added to each phase with the aim to form $Fe(OH)_3$ that would precipitate out as a solid. No change was observed when NaOH was added to the aqueous phase. However, when added to the organic phase it turned a bright orange, but no precipitate formed. The organic phase was dried with Na_2SO_4 and passed through a silica plug using DCM as eluent. The solvent was removed and analysed with ^{1}H NMR as shown in **Figure 7**.

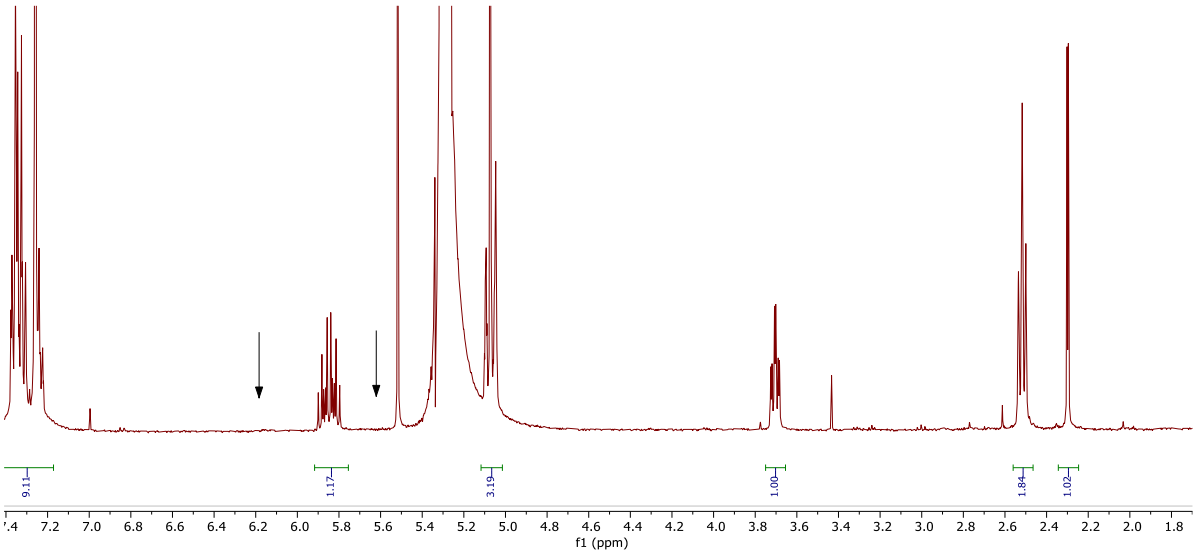

Figure 7. ^{1}H NMR (400 MHz, $CDCl_3$) spectrum of the extracted organic phase filtered through a silica plug showing the aromatic and alkene region, the arrows shows that the impurities are gone. The large signal at 5.3 ppm is DCM.

The ^{1}H NMR spectrum revealed that the impurities had been removed either by the liquid-liquid extraction, addition of NaOH or the silica plug. It is unlikely that the silica plug is the cause of this, as previous eluent testing for the column had not shown any separation using pure DCM.

To test if it was the liquid-liquid extraction that was the key to isolating **R1**, the step of adding NaOH was omitted in the second attempt. Another portion of the impure product was liquid-liquid extracted with DCM and $NaHCO_3$ and the organic phase dried with Na_2SO_4 and passed through a silica plug. A new ^{1}H NMR spectrum was recorded shown in **Figure 8**.

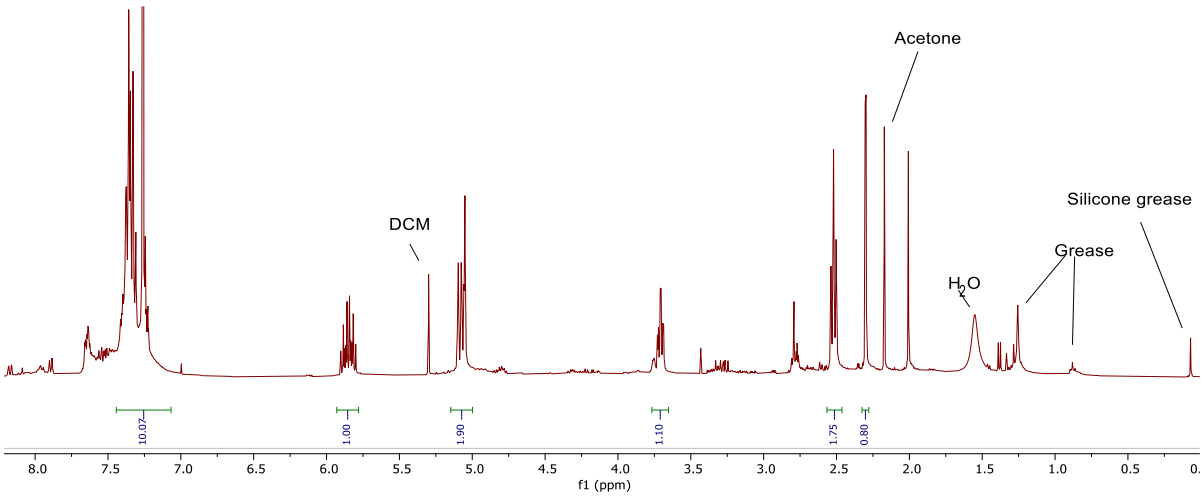

Figure 8. ^{1}H NMR (400 MHz, $CDCl_3$) spectrum of the extracted organic phase filtered through a silica plug. With some impurities identified. Signals with integrations indicates the desired product.

As can be observed in the spectra the impurities are gone indicating that the liquid-liquid extraction is indeed the key to obtaining pure **R1**. However, a lot of new impurities are evident in the spectra shown in **Figure 8**. Some of these can be identified such as acetone used to wash the NMR tube, DCM that was not properly evaporated, a water signal from the solvent and grease. The remaining unexplained new impurities seen in **Figure 8** are most likely explained by cross contamination from the rotavapor.

Another procedure to synthesis **R1**, reported by Weng et al.[56], uses the same starting reagents but a different catalyst, [bis(trifluoroacetoxy)iodo]benzene (PIFA), the reaction shown in **Scheme 19**.

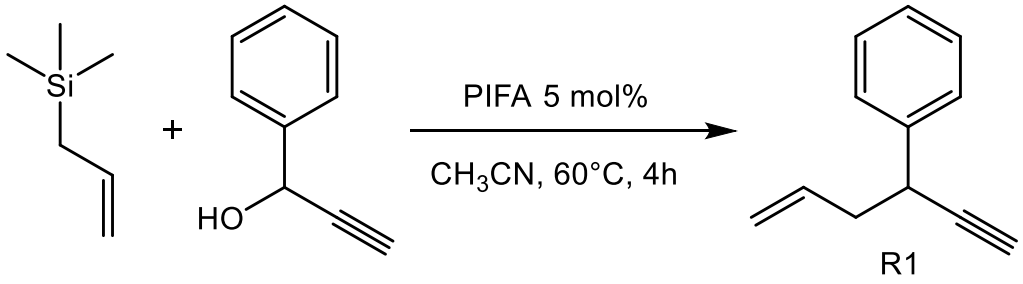

Scheme 19. PIFA catalysed substitution reaction of propargylic alcohol with allyltrimethylsilane.

In their supplementary information the NMR spectrum of the product shows no trace of the unwanted impurities. It is worth noting that they have almost the same work up steps as were tried in the last purification presented above but utilized EtOAc instead of DCM as eluent. The rest of the impure product was purified using the work up steps from Weng's procedure. This successfully removed the impurities, however new impurities are observed that most likely do not stem from the liquid-liquid extraction or silica plug but again from cross contamination, as shown in **Figure 9**.

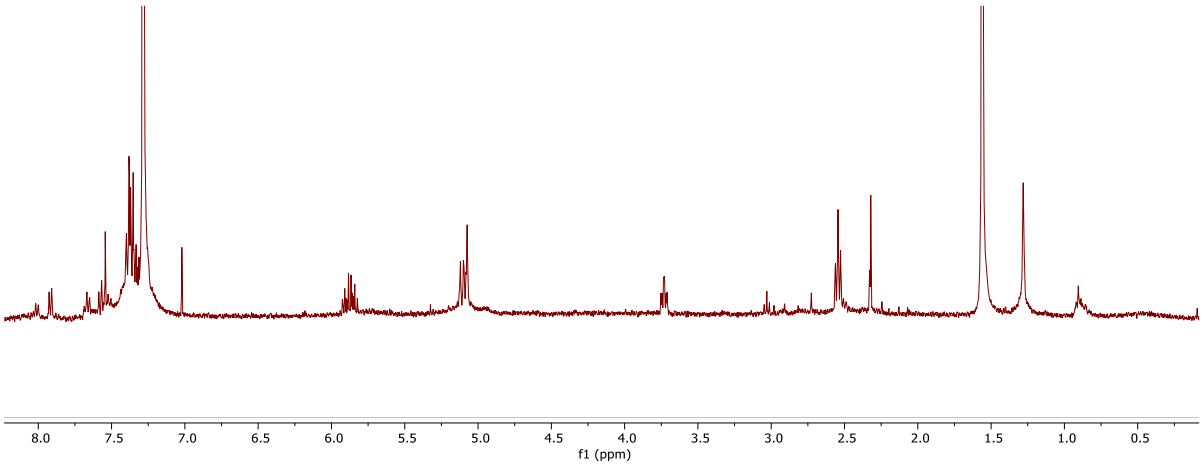

Figure 9. ^{1}H NMR (400 MHz, $CDCl_3$) spectrum of **R1** purified using Weng's work up. With some unknown impurities.

As Weng et al.'s alternative procedure had proven to furnish a pure product, it was used for the next two attempts of synthesising **R1.** The crude product from these two attempts were analysed with ^{1}H NMR shown in **Figure 10** however, only traces of product can be observed.

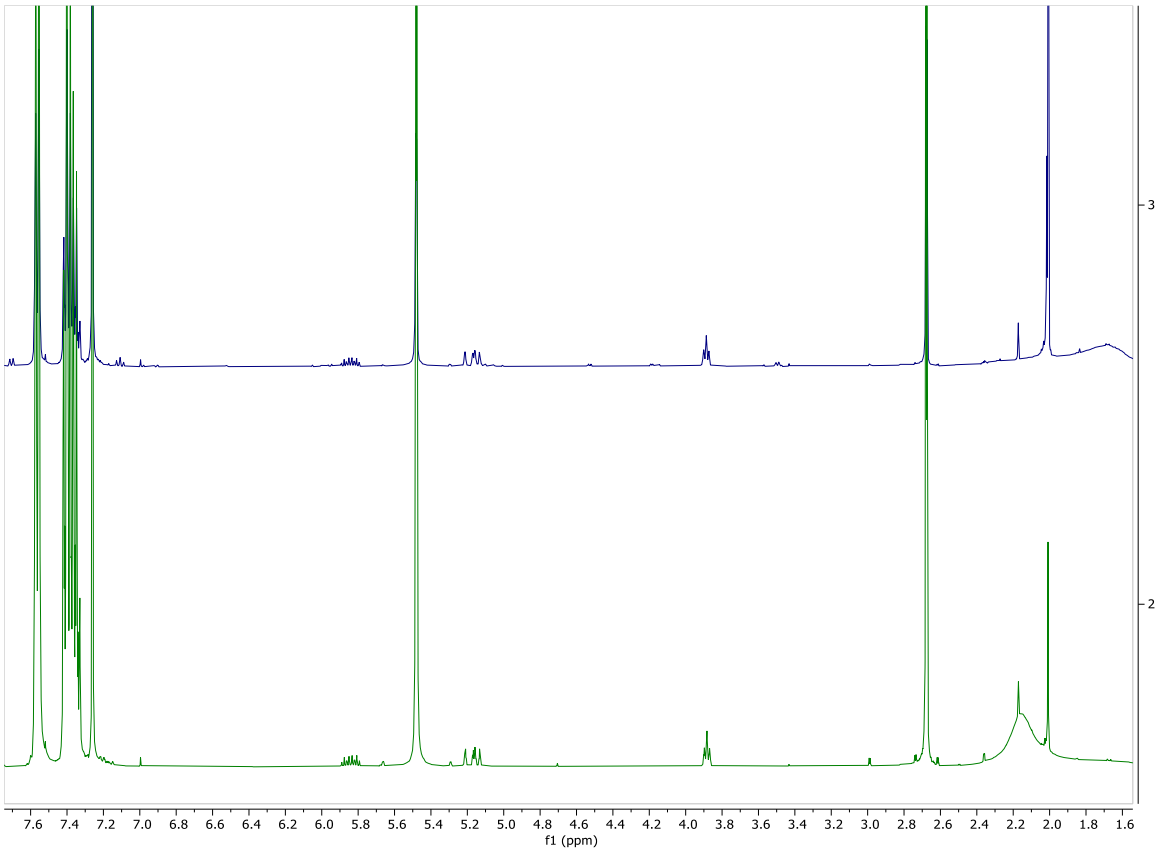

Figure 10. ^{1}H NMR (400 MHz, $CDCl_3$) spectrum of crude product from synthesis using PIFA as catalyst.

It is possible that the synthesis failed due to the age of the PIFA (opened in 2012). However, ^{1}H NMR analysis of the PIFA corresponded nicely with reference spectrum provided by

Sigma Aldrich and under visible inspection nothing seemed off about the compound. However since the synthesis conducted using the procedure published by Reeds et al.[50] was successful, no further attempts were made to determine the cause of the failed synthesis using PIFA as a catalyst.

Another attempt of synthesizing **R1** was conducted using the procedure from Reeds et al. combined with the work up from Weng et al. The ^{1}H NMR spectrum of the crude product from this combined procedure showed the same impurities as in the first attempt, as can be seen in **Figure 11**.

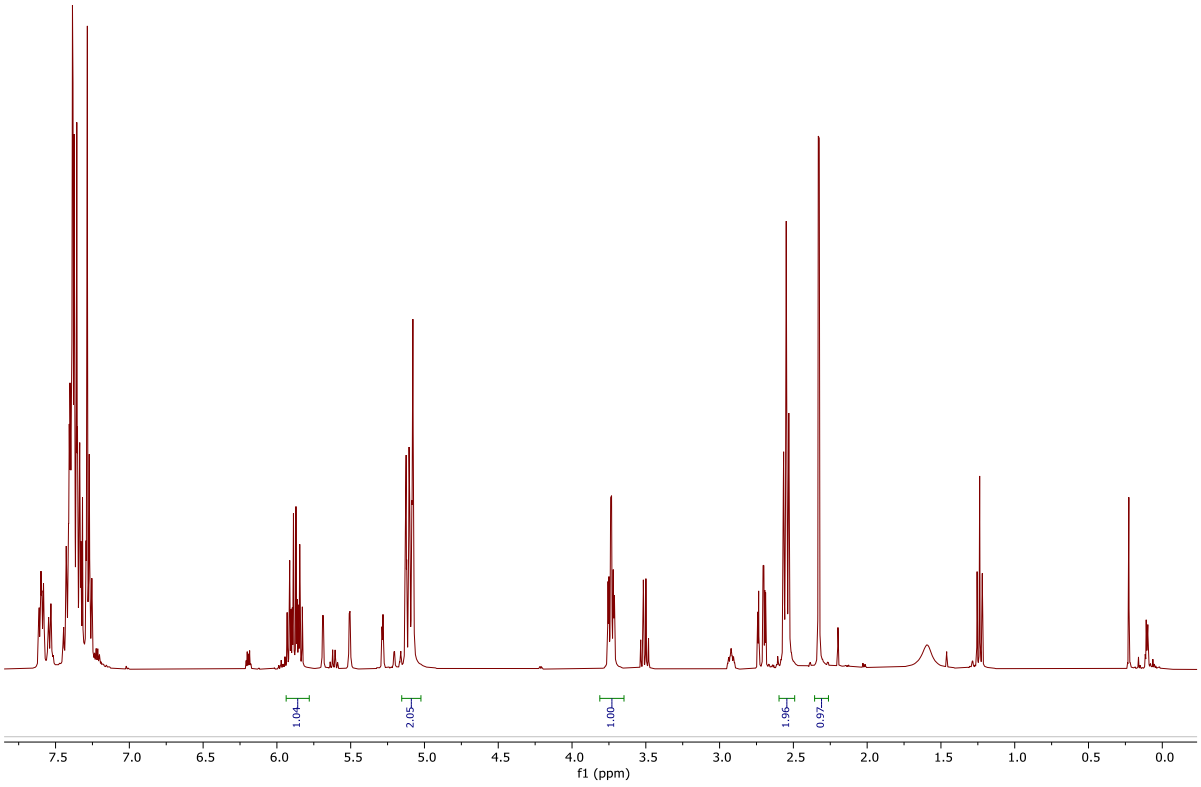

Figure 11. ^{1}H NMR (400 MHz, $CDCl_3$) spectrum of crude product from $FeCl_3$ catalysed synthesis of **R1** using additional work up steps. Impurities can be seen, **R1** signals are integrated.

The crude product was then purified with flash chromatography using distilled hexane as eluent. The isolated product **R1** was collected as a clear oil at a 29% yield (**A 11**). And as a bonus the impurities were also isolated in high purity (**A 26**) as shown in **Figure 12.**

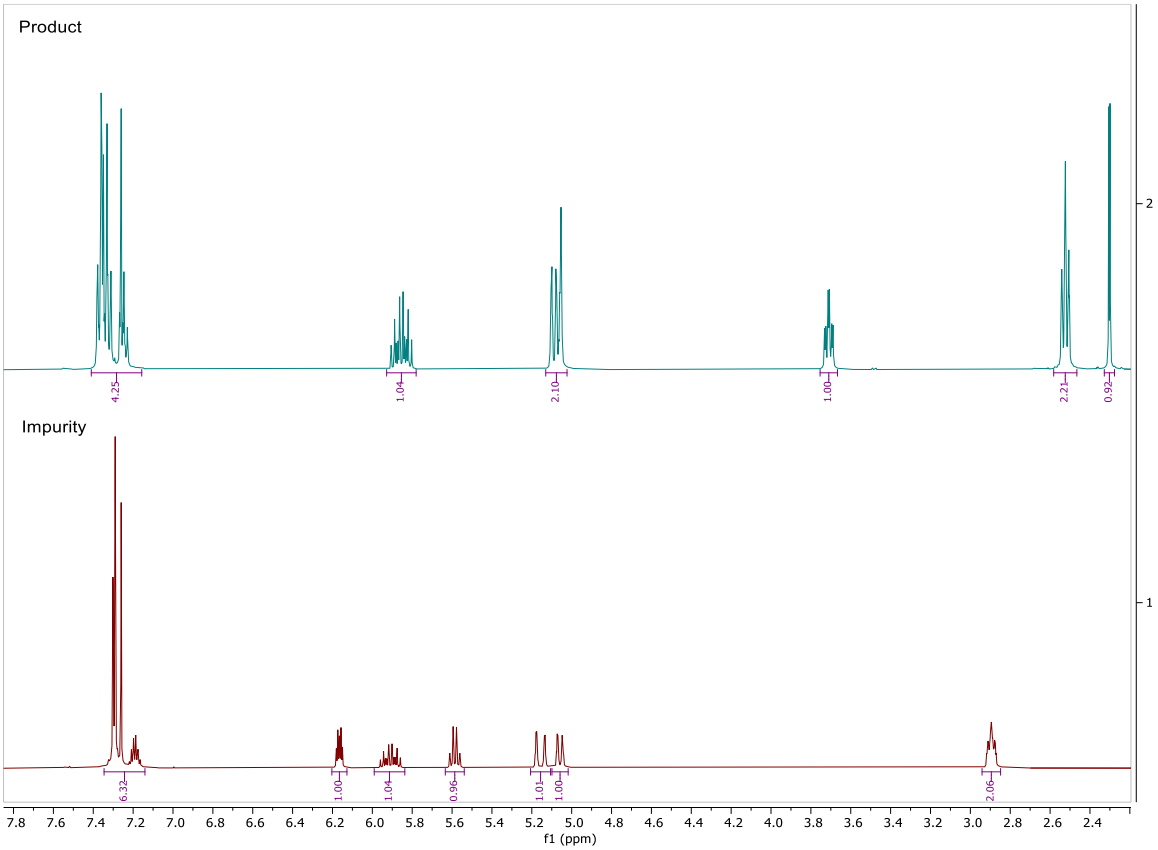

Figure 12. ^{1}H NMR (400 MHz, $CDCl_3$) Isolated product (top) and impurity (bottom) zoomed in on the region of interest.

The signal around 5.9 ppm, the signals between 5.2-5.0 ppm and a total integral of 12 H are features shared between the product and the impurity. This suggested that the impurity might be a by-product in the form of an isomer. Because the impurity was isolated in an unexpected high purity it was also further analysed. A full characterization of the main product as well as the isolated, pure by-product was done by several NMR experiments.

As mentioned above, the ^{1}H NMR spectrum for **R1** is in accordance with the reported data[56] and **R1** was further analysed using ^{13}C, DEPTQ135, HSQC, NOESY and COSY NMR. The ^{13}C spectrum obtained (**A 12**) is in accordance with the reported data[56] and further supported by the DEPTQ135 (**A 13**) as shown in **Figure 13**.

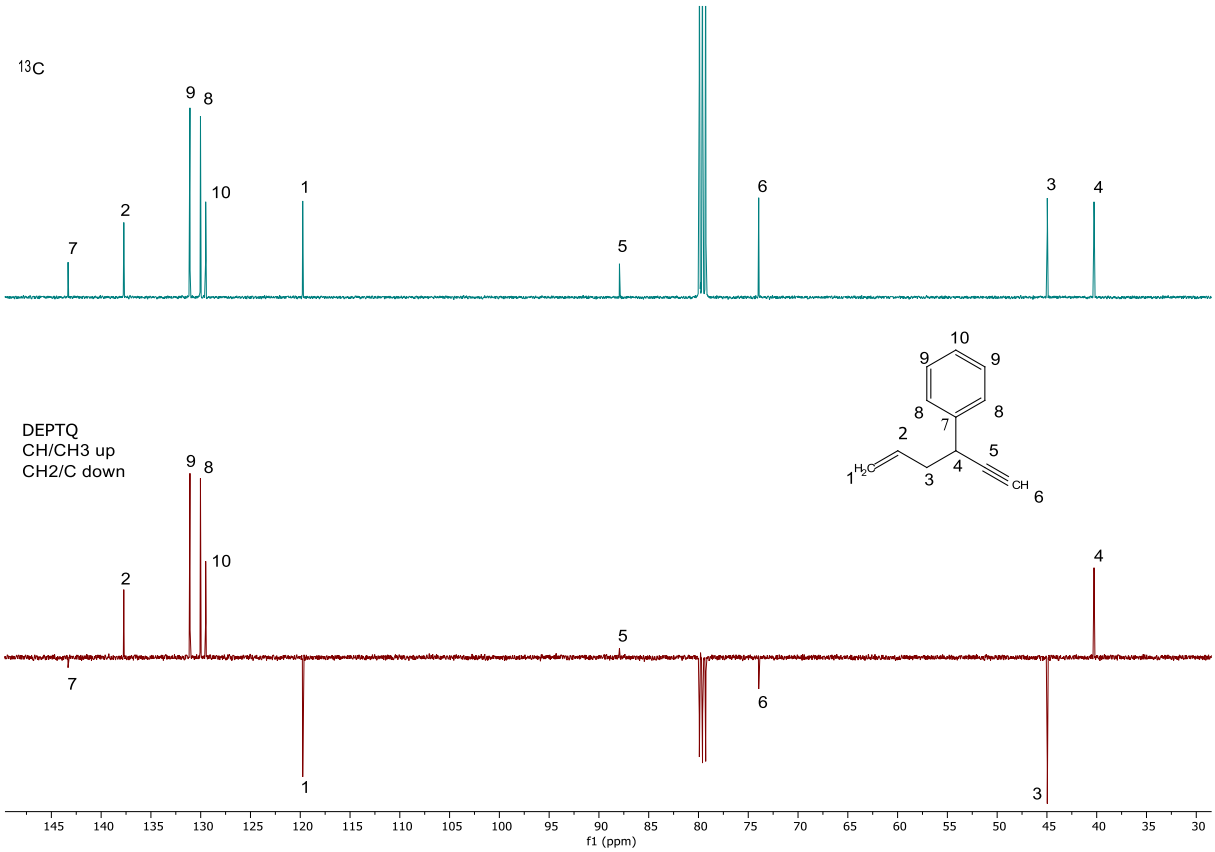

Figure 13. Top: ^{13}C NMR (101 MHz, $CDCl_3$) Isolated **R1** with signals assigned. Bottom: DEPTQ135 NMR (400 MHz, $CDCl_3$) where secondary/quaternary carbon signals are pointing downwards, and primary/tertiary carbon signals are pointed up.

The DEPTQ135 shows the correct phase of connected H to the corresponding C for all signals except the two signals related to the terminal alkyne group (**C^5** 85 ppm and **C^6** 71 ppm). These two signals appear to have their phases reversed. This is a phenomenon that can occur due to the high bond strength of the terminal H-C and poor optimization of the DEPTQ135 experiment[57] and is therefore not counter-indicative of a pure product. The data was further strengthened by the 2D NMR HSQC spectrum (A 14), shown with correlations drawn in Figure 14. The HSQC spectrum shows what proton is bound to which carbon in a molecule.

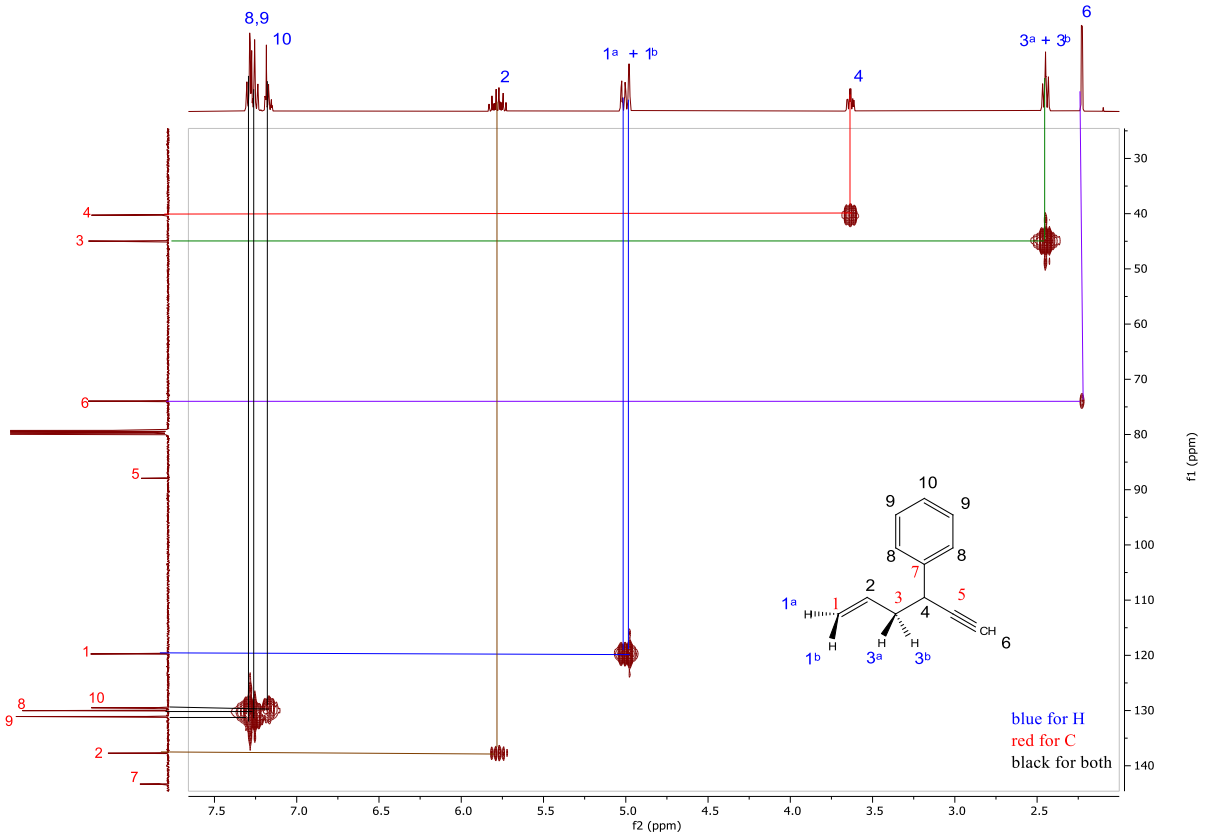

Figure 14. HSQC 2D NMR (400 MHz, $CDCl_3$) spectrum of isolated **R1** with coloured lines showing correlation between ^{1}H spectrum and the ^{13}C spectrum. Protons indicated with blue numbers, carbons with red and black for both carbon and corresponding proton.

As can be observed in the HSQC spectrum the correct number of protons are bound to what was observed in DEPTQ. Most noteworthy correlations are the alkene and alkyne noted 1 and 6, respectively. This shows that the $\mathbf{C^6}$ and $\mathbf{H^6}$ are in fact the terminal alkyne and that the alkene has two protons on its terminal end.

To further strengthen that it was **R1** synthesised two more 2D experiments were conducted. COSY was used to establish that the splitting and couplings were correct and NOESY was used to determine that the position of atoms relative to each other was correct. The COSY spectrum (**A 15**) is shown with correlations drawn in Figure 15.

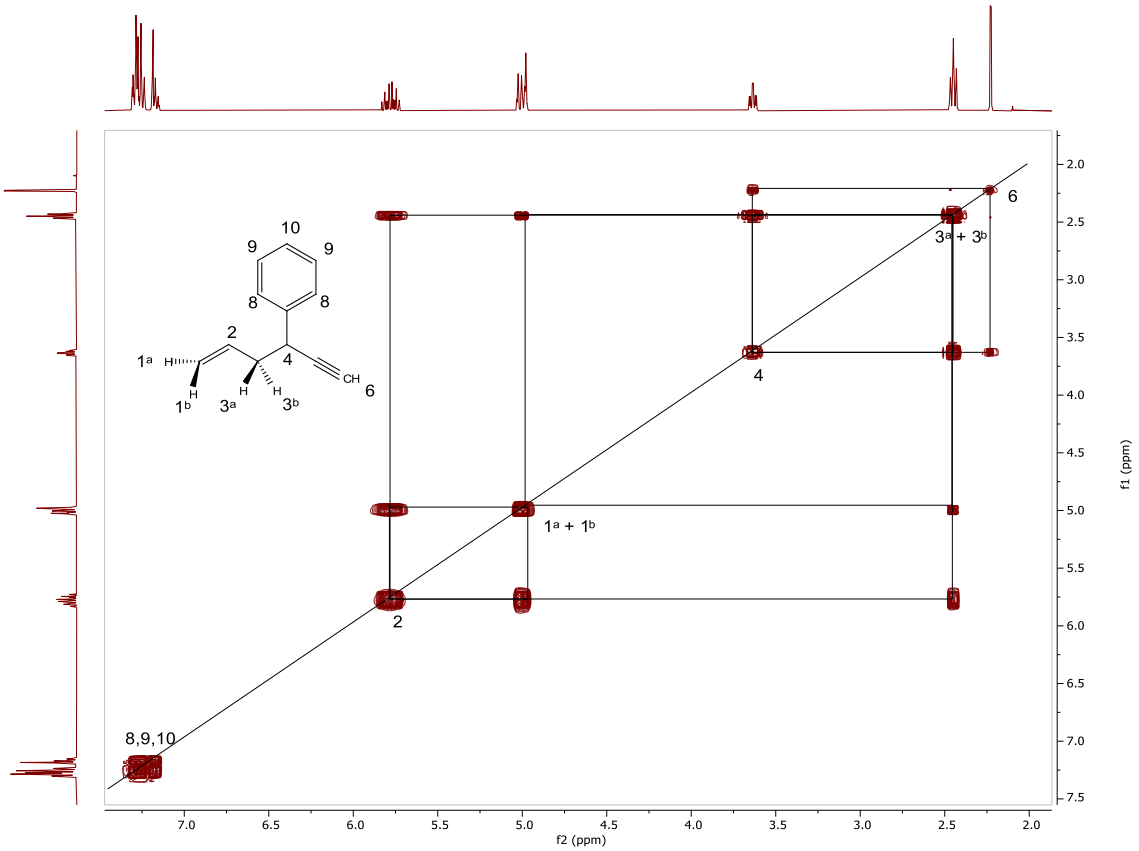

Figure 15. COSY 2D NMR (400 MHz, $CDCl_3$) Isolated **R1** with the diagonal line showing the reference line and correlation between protons are shown with horizontal and vertical lines.

From the COSY spectrum it can be inferred that $\mathbf{H^{2}}$ correlates to $\mathbf{H^{1a+b}}$ and $\mathbf{H^{3a+b}}$ and so forth. This combined with the data from ^{1}H, ^{13}C and HSQC, summarized in **Table 1**, reveals much of the structure of the molecule as is illustrated in **Figure 16**.

Table 1. Summary of coupling data of **R1** from COSY, DEPTQ135, ^{13}C and ^{1}H NMR.

Name	ppm	Correlations	Splitting	Coupling constant	Int.	n-CH_n
$\mathbf{H^{8,9,10}}$	7.33 – 7.13		m		5	5 CH
$\mathbf{H^{2}}$	5.78	1, 3	ddt	J = 17.2, 10.2, 7.0 Hz	1	CH
$\mathbf{H^{1a+b}}$	5.06	2, 3	m		2	CH_2
$\mathbf{H^{4}}$	3.64	3, 6	td	J = 7.2, 2.5	1	CH
$\mathbf{H^{3a+b}}$	2.45	2, 4, 1	tt	J = 7.0, 1.0 Hz	2	CH_2
$\mathbf{H^{6}}$	2.23	4	d	J = 2.5 Hz	1	CH

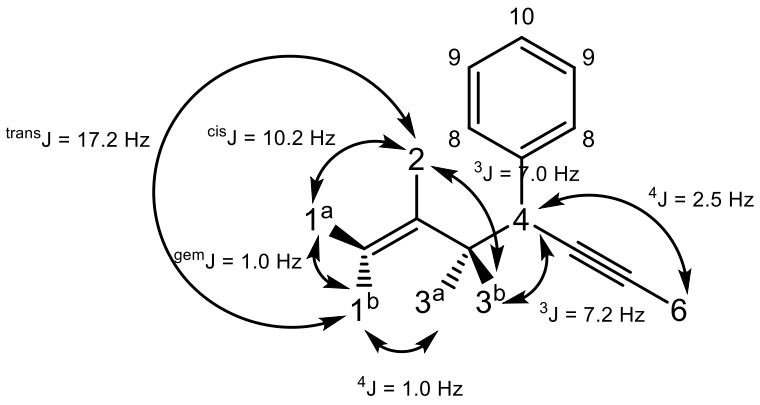

Figure 16. Illustration of coupling pattern of **R1** from 2D NMR data**.**

The splitting pattern was analysed from the data and fitted to the molecule. $\mathbf{H^2}$ shows a typical alkene splitting pattern with a $^{trans}J$ value between 11-18 Hz and a ^{cis}J value between 6-14 Hz[58] to $\mathbf{H^{1a+b}}$. This together with the two neighbouring protons of $\mathbf{H^3}$ adds up to the ddt splitting seen in the ^{1}H NMR spectrum. $\mathbf{H^{1a+b}}$ could probably be analysed to be two separate ddt signals that are overlapping due to the cis trans influence in the alkene. Where one d comes from a geminal coupling due to the inequality of the two protons and should have a coupling constant between 0-3 Hz. The other d stems from coupling to $\mathbf{H^2}$. The t is a long range ^{4}J coupling to $\mathbf{H^{3a+b}}$. $\mathbf{H^{3a+b}}$ protons are not NMR equivalent due to the chiral centre on $\mathbf{C^4}$ making them diastereotopic. However, the difference in the coupling constants is too small to alter the splitting pattern too much and the tt observed rises from the neighbouring $\mathbf{H^2}$ and $\mathbf{H^4}$ ^{3}J coupling and the ^{4}J coupling to $\mathbf{H^{1a+b}}$. The five protons in the phenyl ring should all be split in to 3 signals because of the symmetry exhibiting a AA'BB'C splitting pattern[58]. The signal a bit more up field in the aromatic region is probably the para proton $\mathbf{H^{10}}$ in the ring. But the signals are too intermingled to be interpreted fruitfully, so they have been bunched together under one multiplet.

The NOESY spectrum (**A 16**) further elucidates the molecular structure by showing the actual physical correlations between protons in a molecule. In other words, it does not record correlation through bonds but correlation through relative space between the atoms. These correlations are shown in **Figure 17** and the correlations illustrated on **R1** structure in **Figure 18**.

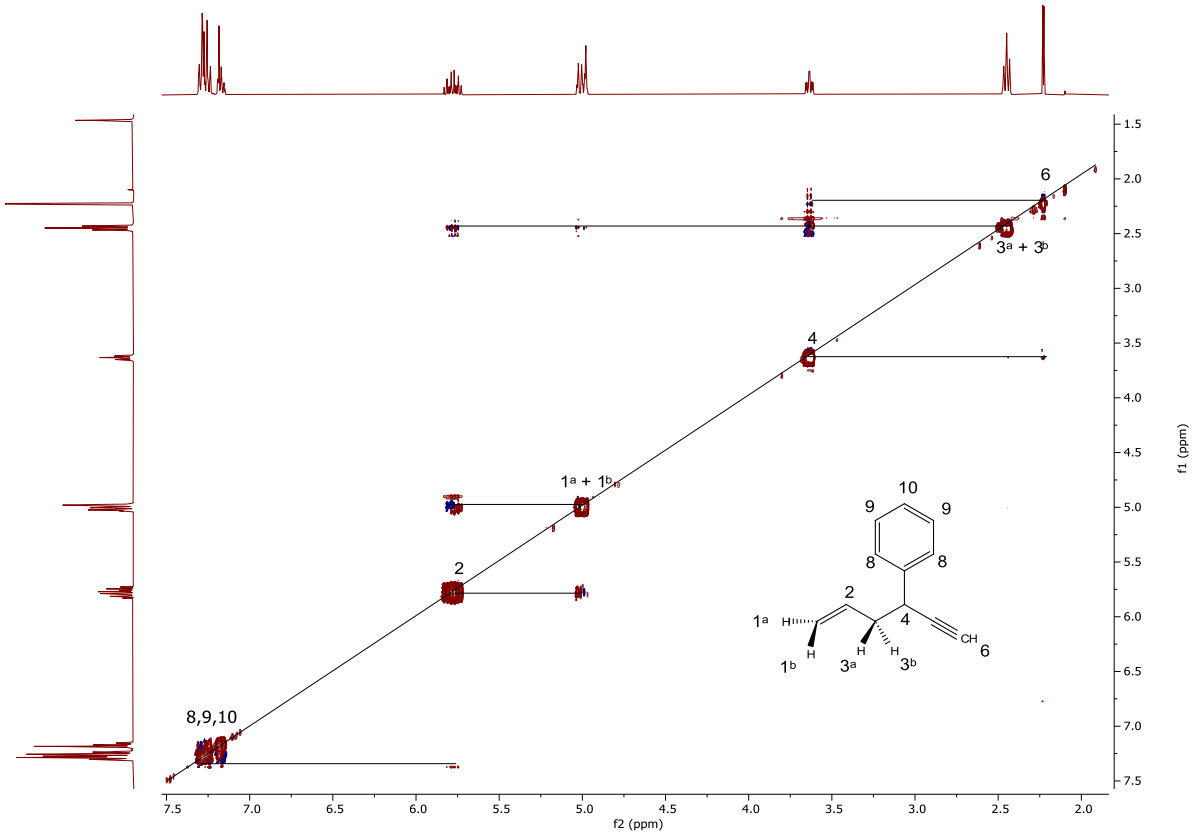

Figure 17. NOESY 2D NMR (400 MHz, $CDCl_3$) of **R1** with the diagonal line showing the reference line and the horizontal lines correlation between protons.

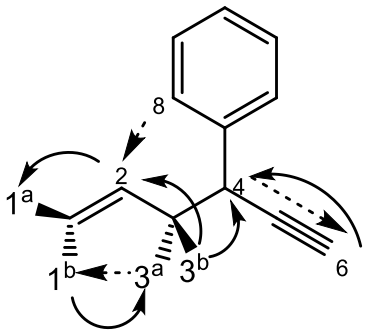

Figure 18. All correlations from NOESY illustrated for **R1**, solid curved arrows indicate a strong signal but dashed straight arrows a weak signal.

The NOESY spectrum support the structure of the molecule as there are no correlations contradicts it. There is a weak signal between a proton on the phenyl ring (noted $\mathbf{H^8}$) and $\mathbf{H^2}$ that is not present in previous NMR experiments, but they are close enough in space to correlate in the NOESY experiment. All the NMR data confirms that it is the desired product **R1** that have been synthesized.

Building on the idea that the isolated impurity is an isomer of **R1**, it was decided that it could be of interest for the catalytic study. With this assumption the difference in the ^{1}H NMR

spectra between the product and the impurity was two additional signals in the alkene region, the CH_2 bridge have shifted up field, no signal of the alkyne proton at 2.30 ppm or the proton sharing carbon with the phenyl. It was therefore speculated that the alkyne undergoes isomerisation into an allene in the catalytic reaction resulting in the structure shown in **Figure 19**.

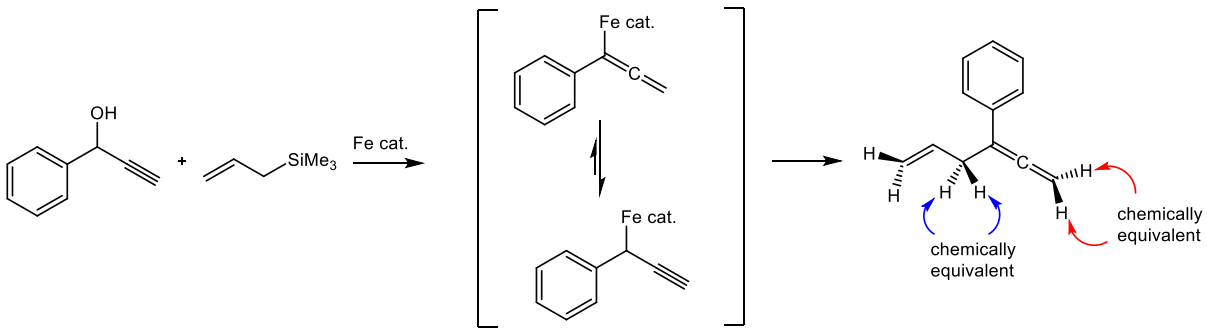

Figure 19. Suggested structure for the isolated impurity hexa-1,2,5-trien-3-ylbenzene.

In retrospective this rearrangement is improbable as the rearrangement does not happen spontaneously as alkynes generally is lower in energy than allenes[59]. It would also make more sense for the metal catalyst to attach to the less sterically hindered side if there was a rearrangement. Although it was found out that the above suggested structure was not the by-product it was investigated at the time with that assumption. From the suggested structure the molecule should have five signals in the alkene/alkane region, as there no longer is a chiral centre on **C[4]** and the protons on the allene are chemically equivalent. As can be observed in the ^{1}H NMR (**A 26**) spectrum there are six signal present in the alkene/alkane region and an attempt to assign them to the suggested molecule is shown in **Figure 20**.

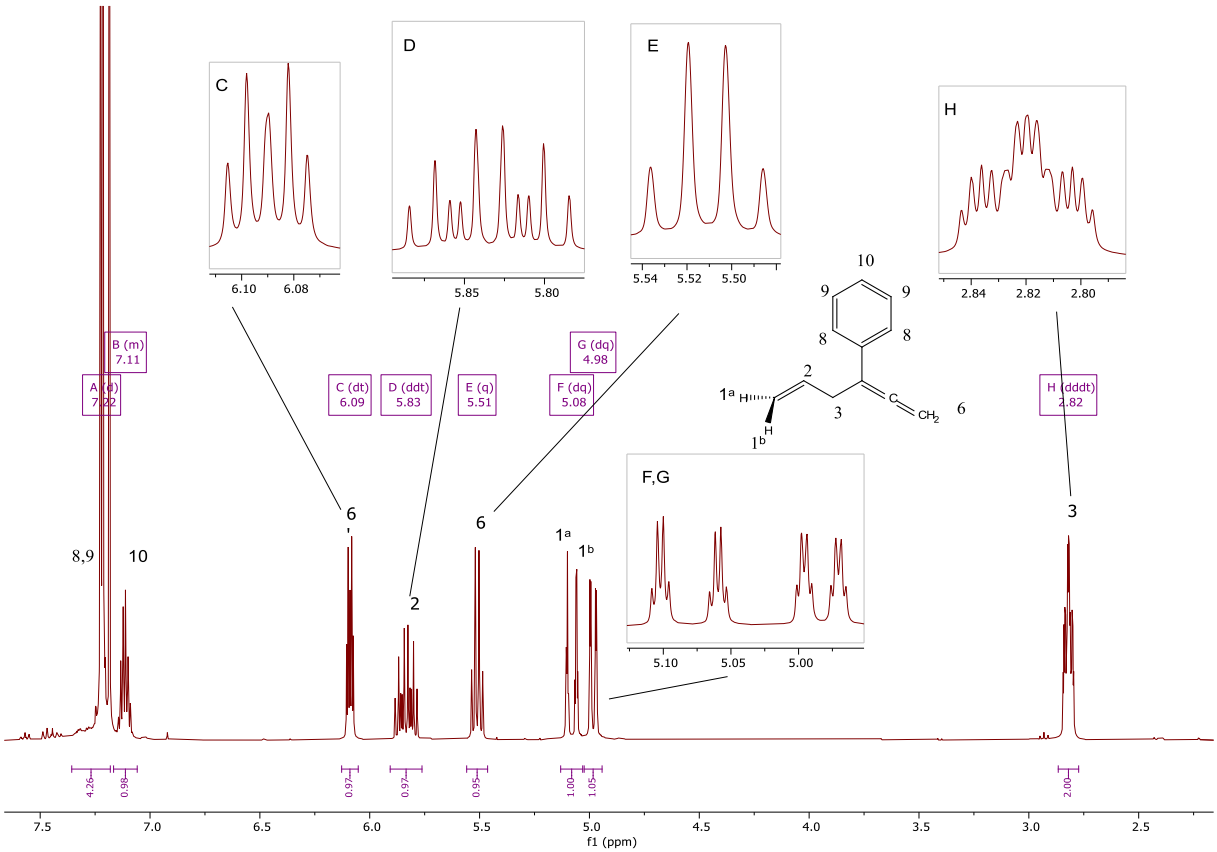

Figure 20. ^{1}H NMR (400 MHz, $CDCl_3$) spectrum of isolated impurity with suggested molecule and assigned signals, with embeded close-up view of the splitting pattern.

Looking at the shift and splitting patterns of the allene (in the spectrum assigned to **H^{6}**) it was quite clear that there was something wrong with the structure as this should have been one signal. The splitting observed for the terminal alkene (assigned to **H^{1a+b}** and **H^{2}**) fits quite well with what is expected. There is a cis/trans coupling to **H^{2}**, a long range ^{4}J coupling to **H^{3}** and a geminal coupling. The three signals in the aromatic region integrate to a total value of five protons (with the solvent signal omitted) suggesting it is the phenyl ring. However, for **H^{3}** the splitting is much more complex than would be expected from the suggested molecule. To further elucidate the structure several NMR experiments were conducted ^{13}C (**A 27**), DEPT135 (**A 28**), NOESY (**A 29**), HSQC (**A 30**), and COSY (**A 31**). The ^{13}C and DEPT135 spectra of the impurity with suggested assignment of signals are shown in **Figure 21**.

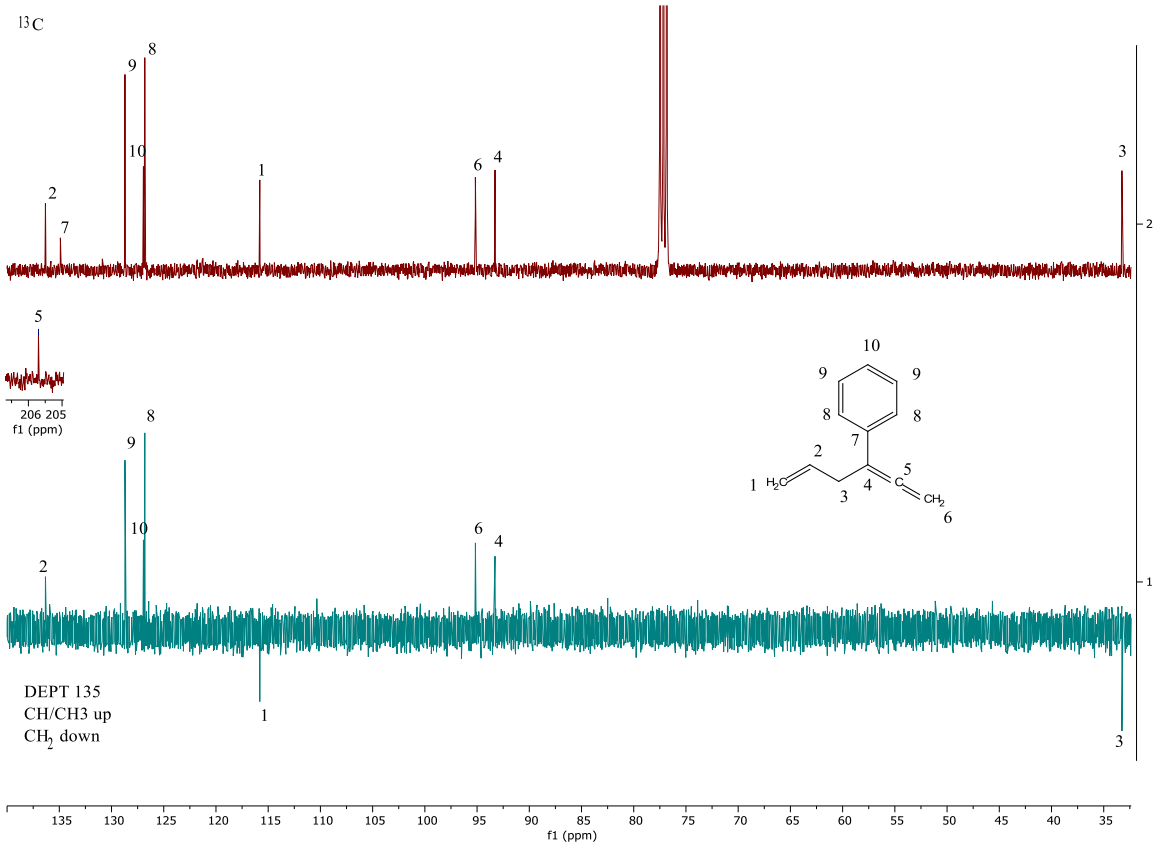

Figure 21. Top: ^{13}C NMR (101 MHz, $CDCl_3$) spectrum of isolated impurity with a signal at 206 ppm embeded, with assigned signals to the suggested molecuele. Bottom: DEPT135 NMR (400 MHz, $CDCl_3$) showing signals for primary and tertiary carbos pointing up and signals for secondary carbons pointing down, with assignments to the suggested molecuele.

From the three spectra it is possible to ascertain with certainty that the suggested molecule structure is incorrect. It a DEPT135 spectrum and not a DEPTQ135 which means that the quaternary carbons do not show up, as can be observed with the solvent signal from $CDCl_3$ and the signal for **C^7**. However, the signals assigned to **C^4** and **C^6** are both pointing up making them in this case primary carbons as there are no signals in the ^1H NMR spectrum integrating to 3 protons.

The C-H ^1J coupling constant of allenes is not as high as that of alkynes, 160-170 Hz compared to 250 Hz. That is to say that the bond strength of allenes is not high enough to reverse the phase as can happen with terminal alkynes. Normally a high ^1J coupling constant will give a weaker signal in the DEPT spectrum[60] however, it will never cause the splitting observed in the ^{13}C and DEPT135 NMR spectra. The two CH could be explained by moving the phenyl to the end of the allene. This would leave the alkene group intact, increase the splitting of the CH_2 bridge and conserve the NMR shifts in the alkene area for the allene. The revised molecule is shown in **Figure 22**.

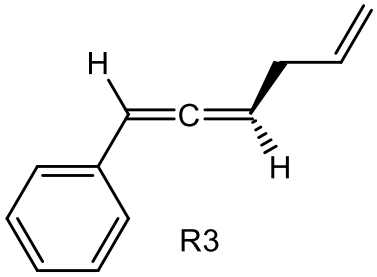

Figure 22. Second suggested structure of the isolated impurity **R3.**

With the new structure in mind the phase sensitive HSQC (**A 30**) NMR was analysed as shown in Figure 23.

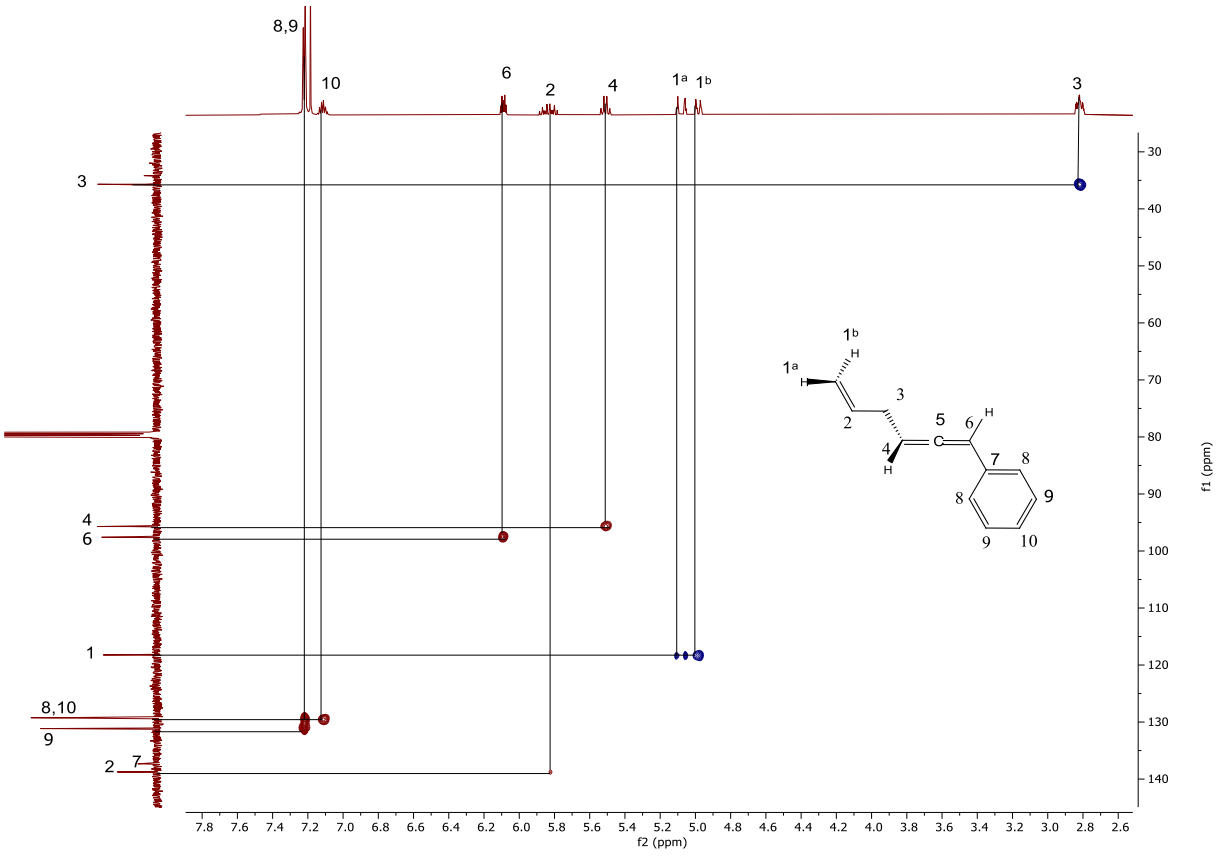

Figure 23. Phase sensitive HSQC NMR (400MHz $CDCl_3$) spectrum of **R3** with lines showing correlation between ^{1}H spectrum and the ^{13}C spectrum. Red colour of the signal indicates CH_3/CH while blue colour indicates CH_2.

The phase sensitive HSQC spectrum gives information of how many protons are bond to each carbon and the correlation between ^{13}C and ^{1}H signals. It is much like a DEPT spectrum but instead of signals pointing up or down depending on phase, the signals are colour coded with red being positive for primary and tertiary carbons and blue being negative for secondary

carbons. The two protons of $\mathbf{H^{1^{a}+1^{b}}}$ are coupled to the same carbon $\mathbf{C^{1}}$ and the signal is blue, this indicates a secondary carbon and fits well with a terminal alkene. The only other signal marked blue is 3 which fits well with the CH_2 bridge. After moving the phenyl to the end of the allene in the new structure the observed signals for 6 and 4 closely match what would be expected from two different CH allene carbons. A very weak signal for 2 further confirms, the new structure. To investigate the coupling and splitting pattern in more detail a COSY spectrum was analysed as shown in **Figure 24**.

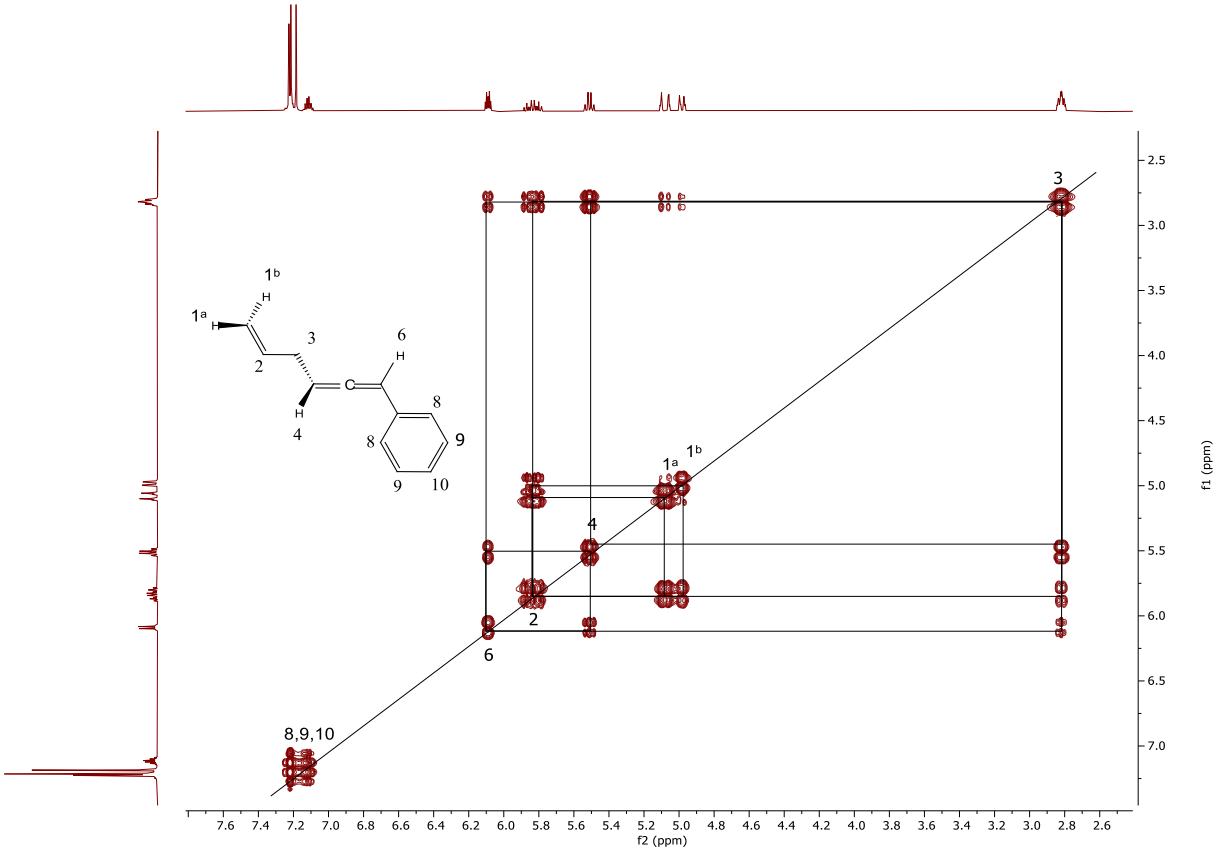

Figure 24. COSY 2D NMR (400 MHz, $CDCl_3$) spectrum of **R3** with the diagonal line showing the reference line correlation between protons are shown with horizontal and vertical lines.

From the couplings seen in the COSY and the previous spectra a summary of the splitting and coupling constants are presented in **Table 2**.

Table 2. Summary of coupling data of isolated impurity from COSY, DEPTQ135, ^{13}C and ^{1}H NMR

Name	ppm	Correlations	Splitting	Coupling constant	Int.	n-CH_n
$H^{8,9,10}$	7.22 – 7.06		m		5	5 CH
H^{6}	6.09	4, 3	dt	J = 6.4, 2.9 Hz	1	CH
H^{2}	5.83	1^{a}, 1^{b}, 3	ddt	J = 16.6, 10.1, 6.4 Hz	1	CH
H^{4}	5.51	6, 3	q	J = 6.7 Hz	1	CH
H^{1a}	5.08	2, 1^{b}, 3	dq	J = 17.1, 1.7 Hz	1	CH_2
H^{1b}	4.98	2, 1^{a}, 3	dq	J = 10.1, 1.5 Hz	1	CH_2
H^{3}	2.82	6, 2, 4, 1^{a}, 1^{b}	dddt	J = 8.1, 6.1, 3.0, 1.5 Hz	2	CH_2

The couplings for **H^{6}** with a ^{4}J coupling constant between 6-7 Hz to **H^{4}** and a ^{5}J coupling constant around 3 Hz to **H^{3}** are indicates that it is an allene[61, 62]. **H^{1a}** and **H^{1b}** is better separated in this spectrum compared to the **R1** showing the splitting pattern for an alkene more clearly. **$H^{1a + 1b}$** couples cis and trans over the double bond to **H^{2}** and a long-range coupling to **H^{3}.** However, the long-range coupling constant between **$H^{1a + 1b}$** and **H^{3}** seems to be very close to the geminal coupling constant that could explain why a dq is observed instead of a ddt. And **H^{2}** shows a ^{3}J coupling to **H^{3}** all indicating that it is an alkene next to a secondary carbon. **H^{4}** couples to **H^{6}** as mentioned and a ^{3}J coupling to **H^{3}** indicating that the assignment for the allene protons is correct. **H^{3}** couples to all other protons in the molecule (excluding the phenyl) explaining the very complex dddt observed. All data support the proposed structure for **R3**. An illustration of all couplings observed in **R3** is shown in **Figure 25**.

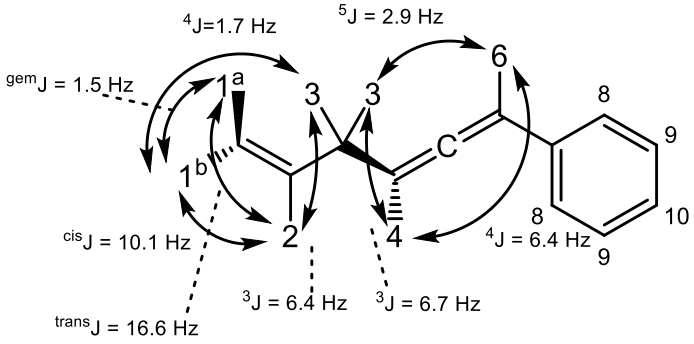

Figure 25. Illustration of couplings from NMR experiments of **R3.**

A NOESY experiment was performed to ensure that the protons also correlate through space in a manner appropriate of the proposed structure. The spectrum is shown in **Figure 26**.

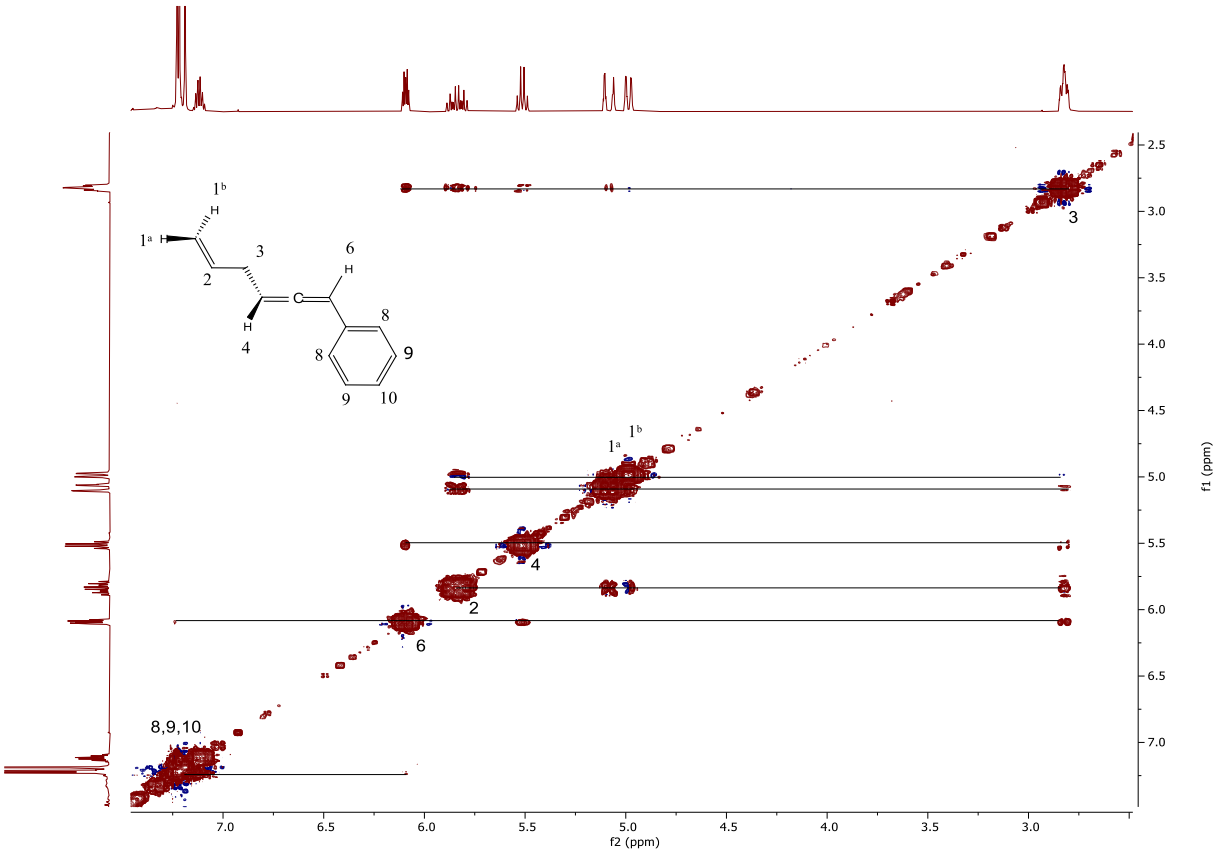

Figure 26. NOESY 2D NMR (400 MHz, $CDCl_3$) spectrum of **R3** with the diagonal line showing the reference line and the horizontal lines correlation between protons, the dashed line an uncertain correlation to the phenyl.

The correlations from the NOESY spectrum for **R3** are illustrated in **Figure 27**.

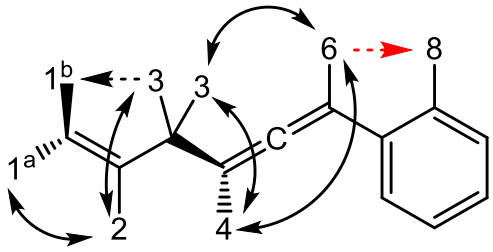

Figure 27. All correlations from NOESY illustrated for **R3**, solid curved double arrows indicate a strong signal both ways, dashed straight arrows a weak signal and dashed red arrow uncertain correlation.

The NOESY spectrum supports the proposed structure for **R3**. The uncertain signal between $\mathbf{H^6}$ and $\mathbf{H^8}$ is probably drowned by the solvent signal. All NMR data supports that the impurity is the proposed structure **R3**.

Huntsman et al.[63] demonstrated that 1-hexen-5-ynes could undergo a Cope-type rearrangement when heated to 340 °C. So, it might be possible that such a rearrangement can take place for substituted 1,5-hexenynes. In this case a rearrangement of **R1** into **R3** during the synthesis as illustrated in **Scheme 20**.

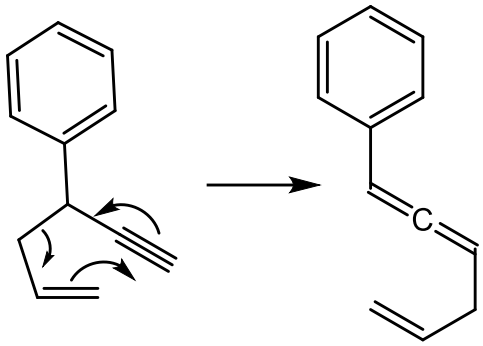

Scheme 20. Illustration of possible cope rearrangement of **R1** to **R3**

Another possibility could be that the isomerisation mentioned above, where the iron catalyst is attached to the less sterically hindered end of the allene is the reason for furnishing **R3**. However, no further investigation was made into the formation of **R3**.

3.1.3 3-phenyl-1-hexen-5-yne

With **R1** successfully synthesized of acceptable purity, the next substituted hexenyne **R2** was synthesized. Only one procedure was found when searching for the molecule on SciFinder (20.09.2021) reported by Morken et al.[64]. The reaction is illustrated in **Scheme 21**.

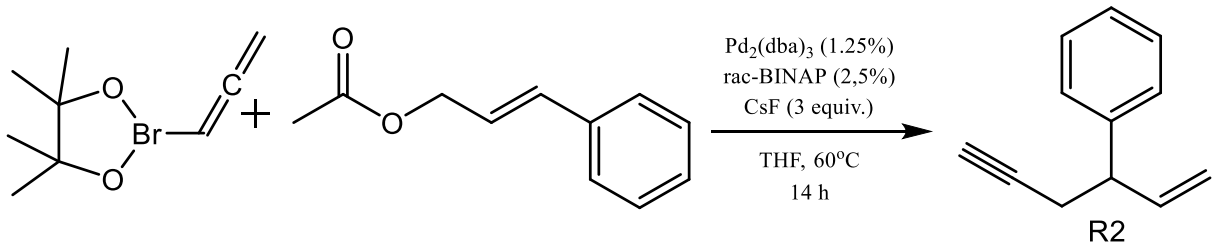

Scheme 21. Synthesis of **R2** following the procedure by Morken et al.[64].

The first attempt followed the above procedure where allenylboronic acid pinacol ester was reacted with cinnamyl acetate in presence of palladium catalyst to produce the crude product. The crude product was analysed with NMR and **R2** could be identified as shown in **Figure 28**.

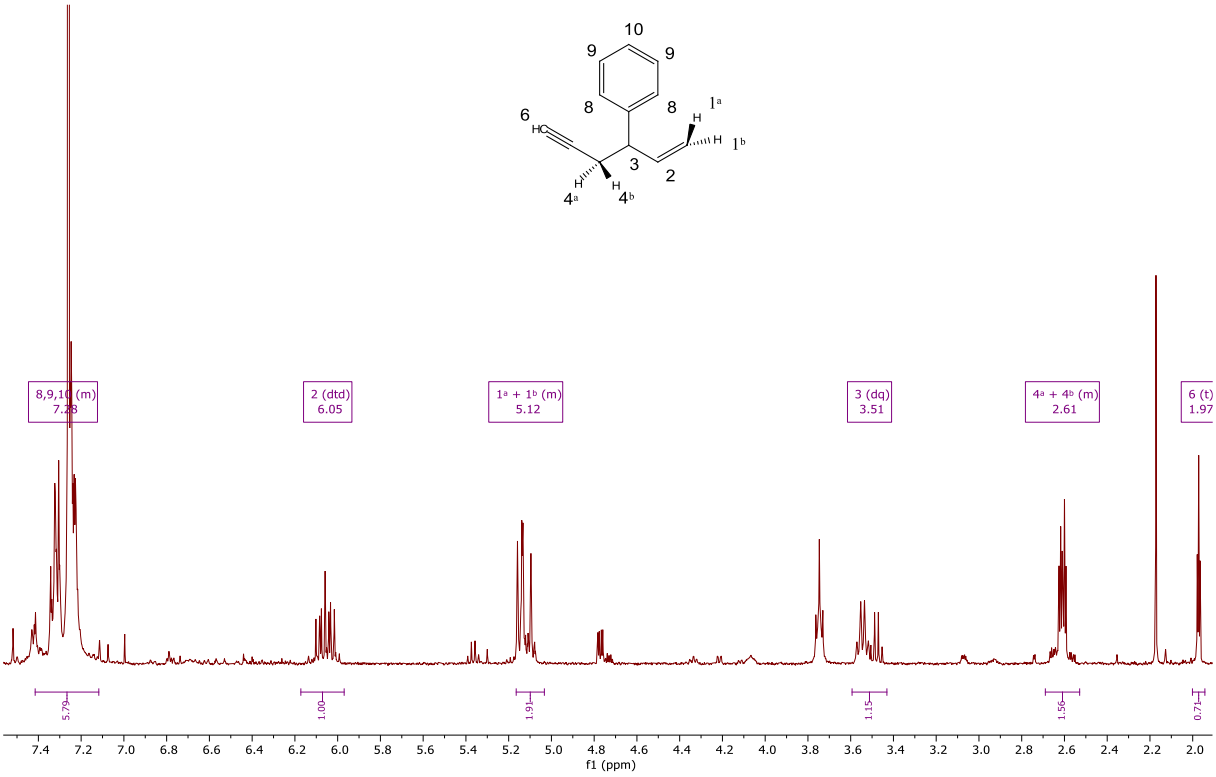

Figure 28. ^{1}H NMR (400 MHz, $CDCl_3$) spectrum of crude in **R2** with signal assign to the molecule from reported data, focused on region of interest.

After purifying the crude product on a column, **R2** was collected as a clear oil at a 42% yield. The product was quite pure with only around 3% of suspected impurities which was promising for a first attempt. The ^{1}H NMR spectrum of isolated **R2** is shown in Figure 29 (**A 17**).

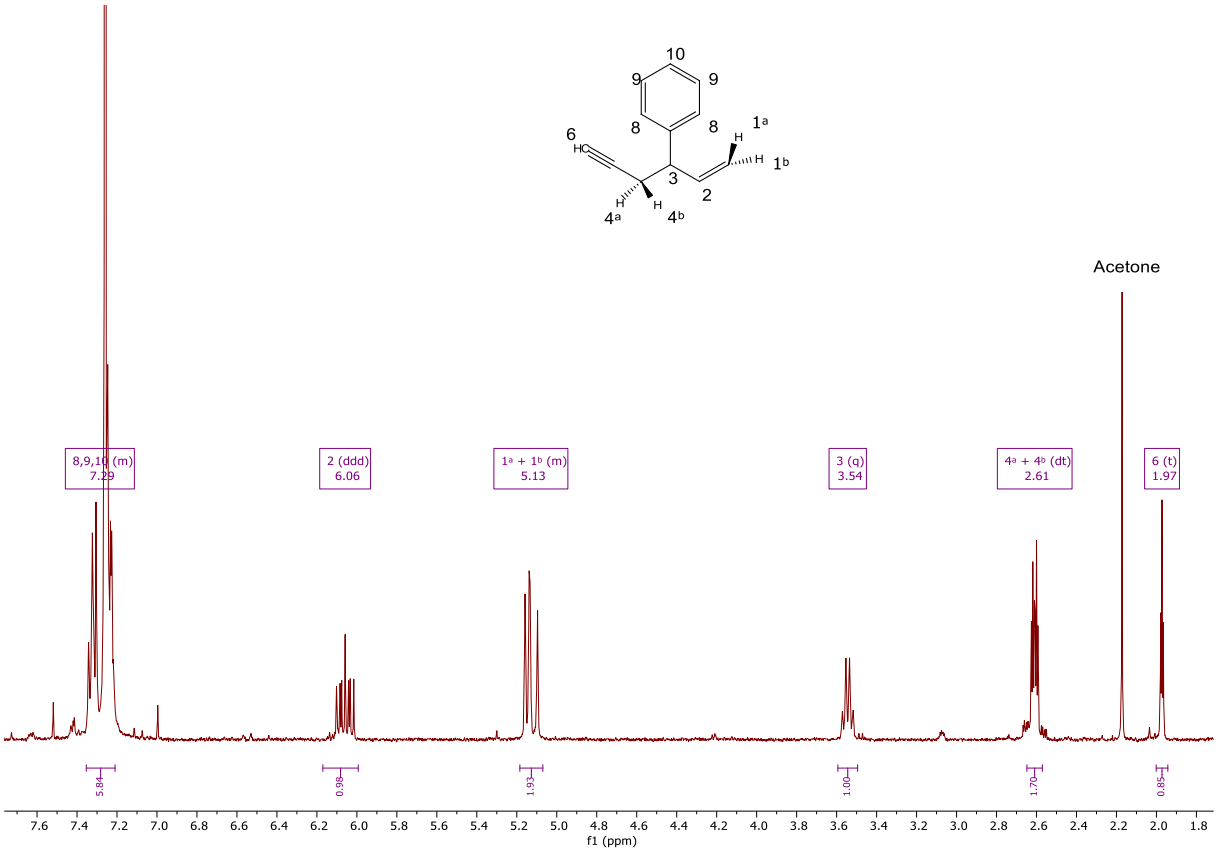

Figure 29. 1H NMR (400 MHz, CDCl3) spectrum focused on region of interest of isolated **R2** with signals assigned to the molecule from reported data. The signal at 2.17 ppm is from acetone used to wash the NMR tube.

The success and ease of the first attempt led to a decision to scale up the second attempt by a tenfold. This was done with the intention of synthesize all product need for the catalytic study in one batch. The same procedure was used as in the first attempt but this time the crude product did not show distinct signals of **R2** when analysed with ^{1}H NMR. An attempt was made to purify the crude product with flash chromatography. However, **R2** was not observed in the ^{1}H NMR analysis as can be seen in spectrum **A 18**. The third attempt was scaled up thrice the original but again **R2** could not be observed in the ^{1}H NMR analysis as can be seen in spectrum **A 19**. The fourth attempt used the same parameters as the first attempt as scaling it up the reaction appeared to be difficult. However, **R2** was still not be observed in the ^{1}H NMR analysis as can be seen in spectrum **A 20**. At the time of the third attempt, the season

had changed to summer and the light conditions in the lab was quite different compared to the conditions during the first two attempts. This could potentially affect the rac-BINAP cocatalyst, as rac-BINAP is listed as an air and light sensitive compound. To counteract this, extra care was made to keep the reaction vial covered with aluminium foil throughout the reaction. The fifth attempt was on the same scale as the first attempt however **R2** could not be observed in the ^{1}H NMR analysis as can be seen in spectrum **A 21**. To rule out light as a problem source all following attempts was also covered with aluminium foil. In the sixth attempt, due to lacking precision of the analytical balance in the glove box, volumetric measurements were used to prepare the catalyst mixture. This was done to rule out the possibility of improper ratio between catalyst and cocatalyst disabling the catalytic activity. By dissolving $Pd_2(dba)_3$ (46 mg, 50 µmol) and rac-BINAP (62 mg, 100 µmol) in THF (2 mL) in separate vials, then transfer 0.1 mL of each to the reaction vial and dilute with 0.6 mL THF the same catalytic mixture as in the procedure was obtained. However, the resulting crude product still showed no **R2** in the ^{1}H NMR analysis as can be observed in spectrum **A 22**. In the seventh attempt the catalytic reactants were weighed in on a high precision scale, outside the glove box then transferred into the inert atmosphere. From there the standard procedure was followed. This increase the risk of air ruining the reaction but ensured all weighing to be precise. However, during reflux the mixture went dry most likely due to a loose screwcap that allowed the solvent to escape. An ^{1}H NMR of crude product was analysed but no **R2** had been produced as can be seen in spectrum **A 23**.

The eighth attempt was a repeat of the seventh, with extra care taken to ensure that the vial was properly sealed. After reflux there was still solvent in the reaction mixture however the ^{1}H NMR of the crude product still showed no **R2** as can be seen in spectrum **A 24**.

In the ninth attempt to rule out any deterioration all chemicals were replaced with newly ordered ones except for THF and $Pd_2(dba)_3$. CsF was the most likely culprit as it is a hygroscopic compound that had been removed out of the glove box and stored unsuitably. The palladium catalyst and THF was used by others in the group without issues and therefore not replaced. However, the resulting crude product still showed no **R2** in the ^{1}H NMR analysis and was very similar to all the other failed reactions as can be seen in spectrum **A 25**. A stacked summary shown in **Figure 30** clearly shows the difference between the first attempt that was successful and all following attempts that failed. Even though there might be traces of **R2** in for example attempt the 6th and 8th attempt it could not be isolated.

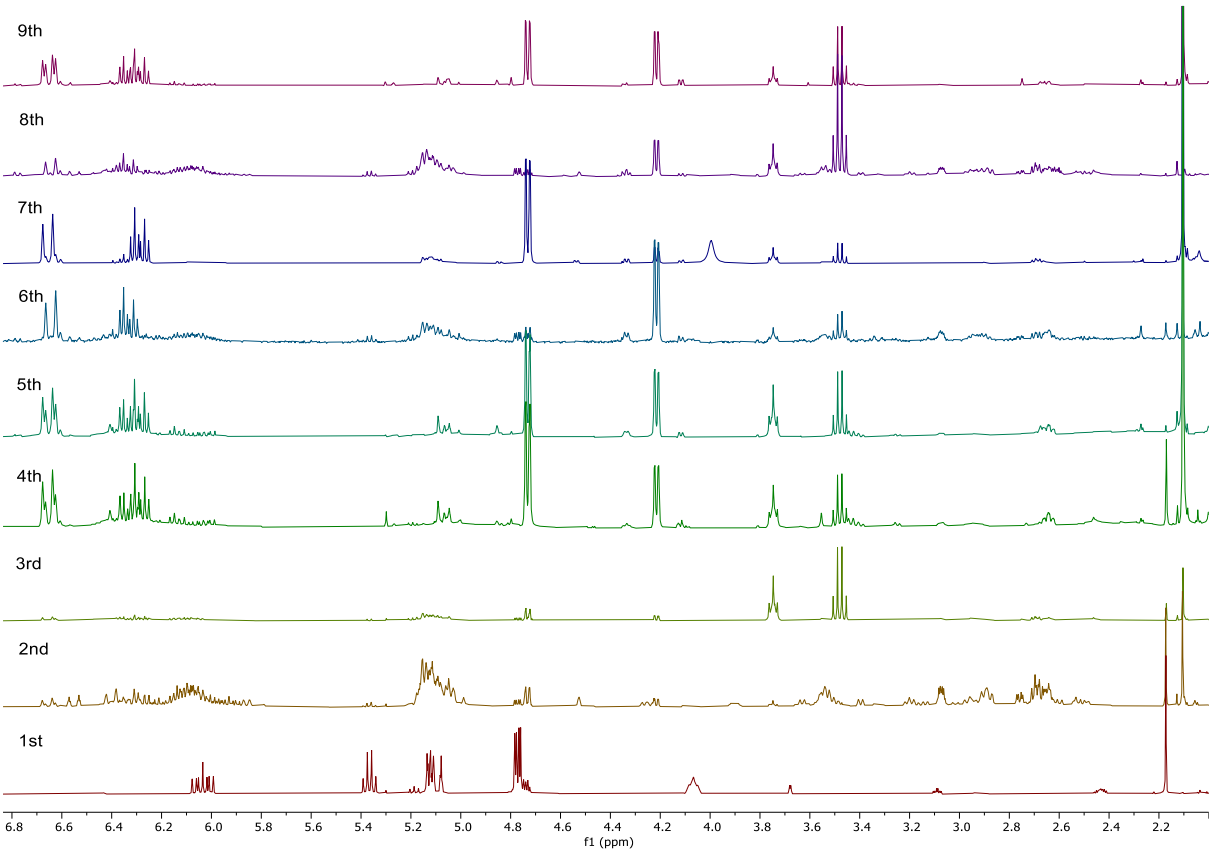

Figure 30. Stacked spectrum of crude from all attempts of synthesizing **R2.** Only the first attempt was successful.

As to why the reaction worked the first time and none of the successive attempts is unknown. As mentioned above lighting conditions, measuring precision, scaling and new chemicals was all tried to mitigate eventual problems with the reaction, without success.

Some reoccurring signals in the failed attempts could indicate that competing side reactions are taking place. For instance, the signal at 4.20 ppm in combination with the splitting of the alkene signals at 6.6 and 6.3 ppm resembles the NMR signals of cinnamyl alcohol. The alcohol could be formed through ester hydrolysis[3] if the CsF was very wet. That idea does not seem likely though, as the same signals are observed in the ninth attempt using fresh CsF, and a signal for acetic acid is never observed. At this point the project was running out of time and no more attempts were done.

3.1.4 (N,C) Au(III) 5-bromo-2-(4-bromophenyl)pyridine complex

As the synthesis of the second substituted hexenyne failed to yield a workable amount for the catalytic studies, the project was pivoted towards the precursor synthesis. The precursors could open ways to synthesis more variants of cyclometalated gold complexes as mentioned in 1.3. It was decided that bromide was going to be the leaving groups on the precursors. As bromide is a good comprise between the cheaper chloride and the better leaving group iodine. Several variants of the ligands, having one or two bromides, were proposed as shown in **Figure 31**.

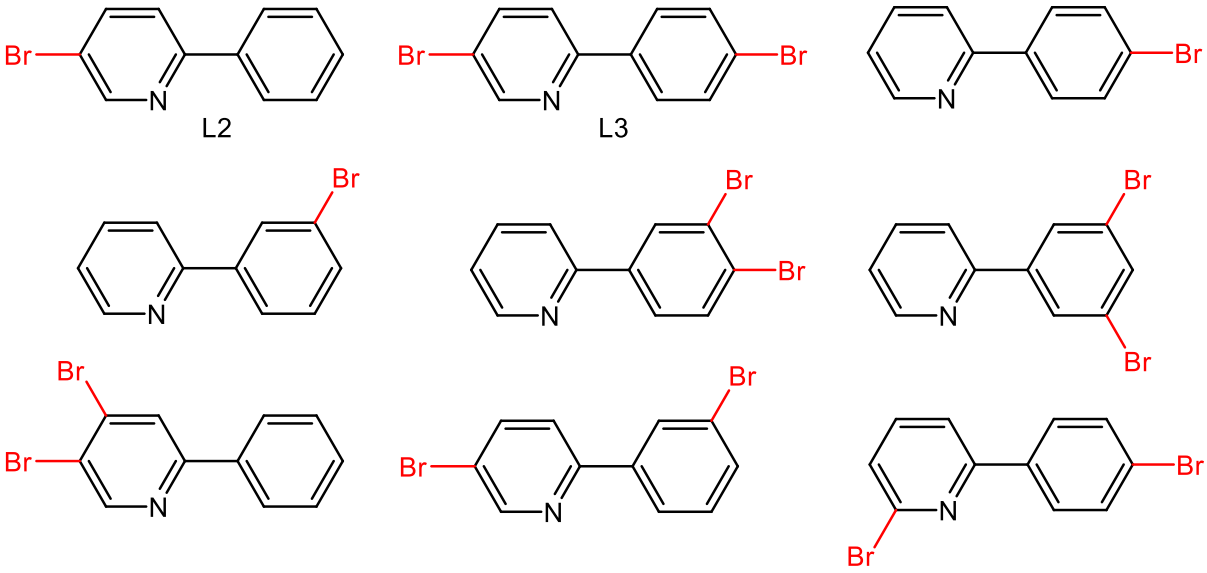

Figure 31. Proposed precursor ligands.

It was decided that **L2** and **L3** would be the first to be synthesised because of their linear structure and that the starting material were readily available. Ligand **L3** was synthesized based on the same Suzuki-Miyaura coupling procedure used for **L1** synthesis developed by the Tilset group[35, 43, 53]The synthesis reaction for **L3** is shown in **Scheme 22**.

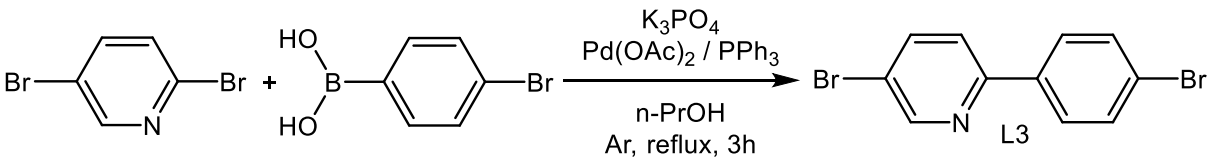

Scheme 22. Synthesis of ligand **L3**.

Reacting 2,5-dibromopyridine with 4-bromophenylboronic acid yielded a yellow brownish powder that was analysed with ^{1}H NMR. In the spectrum **L3** is observed however it also showed a ratio of 11-13% of unreacted pyridine reagent as shown in **Figure 32**.

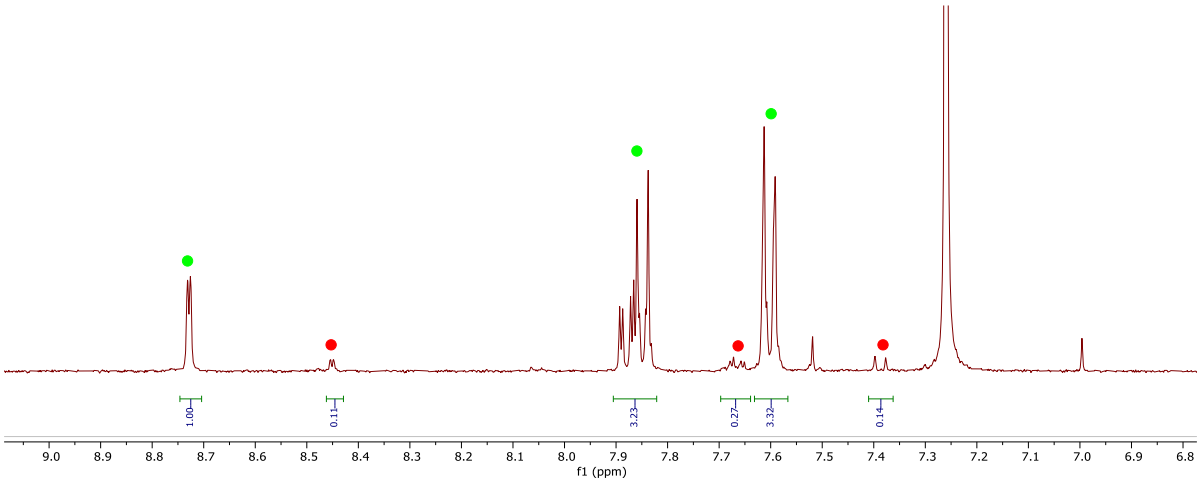

Figure 32. ^{1}H NMR (400 MHz, $CDCl_3$) spectrum, zoomed in on the region of interest of **L3** marked with green circles and unreacted 2,5-dibromopyridine marked with red circles.

To try and separate the unreacted pyridine from **L3**, the mixture was filtered through a silica plug using pure toluene. The idea was to utilize the π-π interactions of the aromatic liquid to achieve separation[65]. This was a partial success as pure product was collected (^{1}H NMR of pure product **A 9**), however a considerable amount of the product was still mixed with the unreacted pyridine and traces of an unknown impurity was significantly more visible (^{1}H NMR of the mix **A 8**). The unknown impurity could potentially be the result of a second Suzuki-Miyaura coupling taking places with the second bromide on the pyridine, but this was never confirmed or investigated. **L3** was successfully synthesized and isolated at a 34% yield. The NMR data are in accordance with the reported values[66]. However, another spectrum was recorded with ^{1}H NMR using a DMSO-d_6 as solvent (**A 10**). As can be observed the signals are much better separated and a better assignment for the signals could be made based on coupling constants as shown in **Figure 33**.

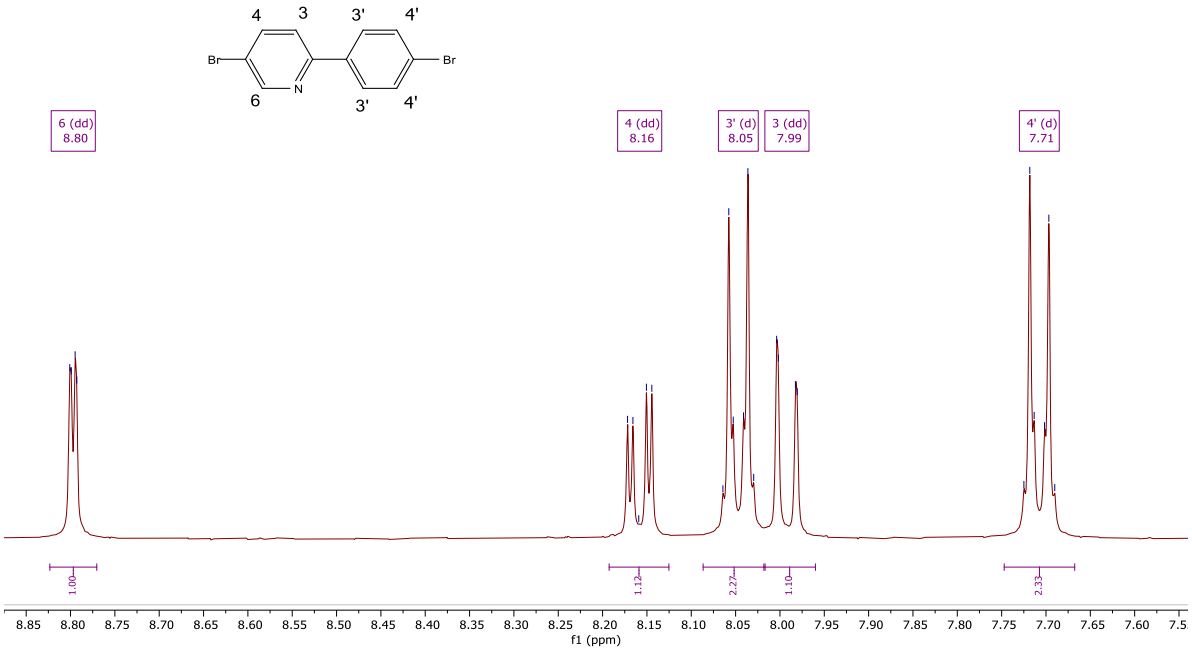

Figure 33. 1H NMR (400 MHz, DMSO-d_6) of the isolated ligand **L3** with assigned signals.

δ 8.79 (dd, *J* = 2.4, 0.7 Hz, 1H, **H^6**), 8.15 (dd, *J* = 8.5, 2.4 Hz, 1H, **H^4**), 8.05 (“d”, *J* = 8.6, 2H; AA’ part of AA’BB’ system, **H$^{3'}$**), 7.98 (dd, *J* = 8.6, 0.8 Hz, 1H, **H^3**), 7.71 (“d”, *J* = 8.6, 2H; BB’ part of AA’BB’ system, **H$^{4'}$**).

In this spectrum it is a clear coupling between the three protons on the pyridine. **H^6** have the highest shift, **H^4** couples to both **H^6** and **H^3** at a coupling constant of 2.4 Hz and 8.5 Hz

respectively. **H^{3}** has the lowest shift of the three protons and shows a long-distance coupling to **H^{6}** at 0.8 Hz. The two signals that integrates to 2 protons each are **H$^{3'}$** and **H$^{4'}$** and the expected AA'BB' coupling pattern due to the symmetry in the phenyl ring are observed.

The **L3** ligand was cyclometalated with gold following the same steps as in the training procedure mention in chapter 3.1.1 shown in **Scheme 23**. However, $NaAuCl_4$ was used instead of $HAuCl_4$ in the hope of reducing the number of free protons of the mixture that might hinder the reaction.

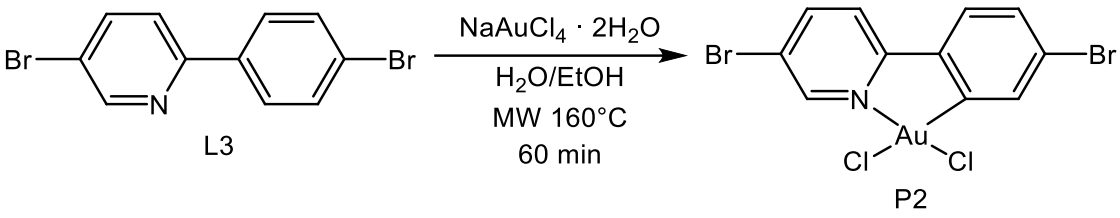

Scheme 23. Microwave assisted synthesis of **P2**.

The first synthesis attempt showed several problems. The ligand was not soluble in water as it floated on top, even with rigorous stirring. After the microwave heating the colour of the water was bright yellow a sign that the gold had not coordinated to the ligand. Nothing precipitated out during the cooling step, even using an ice bath. However, a small amount of solid particles had formed at the bottom of the vessel during the reaction.
The water was carefully decanted and the solids were washed with distilled water and acetonitrile. The solid was then filtrated and dried under air stream. The solids were not soluble in any solvent except DMSO were it dissolved while heated. ^{1}H NMR analysis showed unreacted ligand and something that might be **P2** or N-coordinated gold complex (**A 33**).
In the second attempt ethanol was added to the water mixture drop wise until the ligand started to mix with the water before heating the mixture.
This time a lot of fluffy precipitate formed during the cooling step. But after isolating the precipitate the ^{1}H NMR analysis showed only unreacted ligand (**A 34**).
In the third attempt the time of the microwave heating was increased from 60 min to 120 min. The liquid was colourless after heating but started to darken towards purple and fluffy precipitate was formed during cooling. The ^{1}H NMR spectrum showed only unreacted ligand (**A 35**). The colour change probably was due to free gold nano particles in the mixture. In the fourth attempt acetonitrile was used instead of ethanol to get the ligand to mix with the water.

Acetonitrile reduces the number protons interfering with the coordination towards the nitrogen atom. During addition of acetonitrile, formation of fluffy precipitate was observed in the mixture. This is a sign that N-coordinated complexes was forming. The liquid was clear after heating and some brown precipitate had formed. The precipitate was analysed with ^{1}H NMR (**A 36**) significantly more of the suspected product **P2** was observed compared to the first attempt as is shows in **Figure 34**.

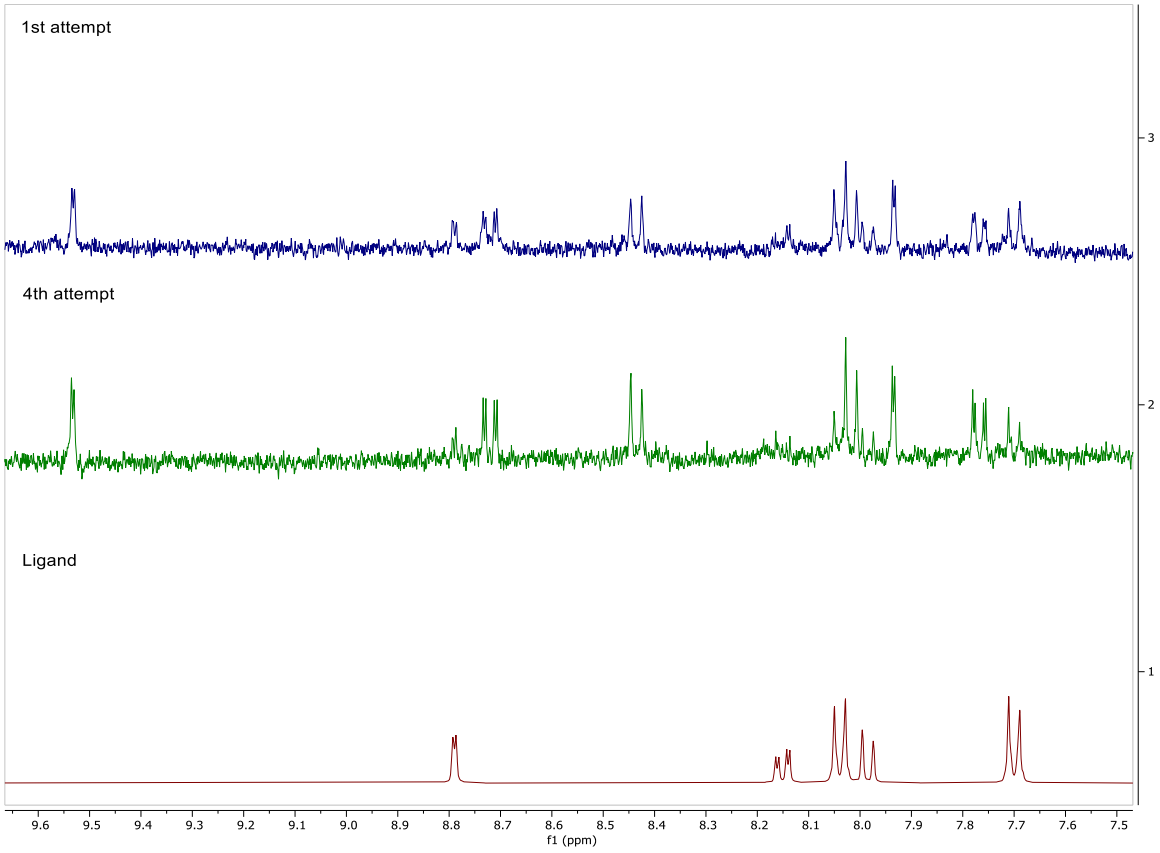

Figure 34. ^{1}H NMR (400 MHz, DMSO-d_6) spectra Top: first attempt of cyclometalation of **P2** Middle: the fourth attempt of cyclometalation of **P2** Bottom: pure **L3** used in the reaction as reference of the unreacted ligand in the cyclometalation attempts.

When subtracting the signals of unreacted pyridine from the ligand spectrum, what is left might be N-coordinated gold complexes or **P2**. A suggested assignment of the signals is shown in **Figure 35**. The splitting and shifts seem to be reasonable for **P2** although nothing conclusive can be derived from the spectrum.

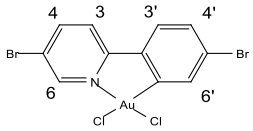

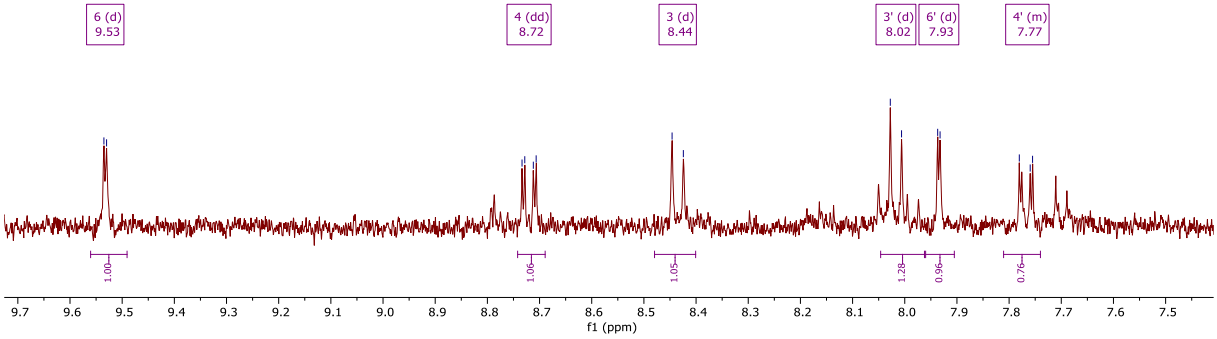

Figure 35. ^{1}H NMR (400 MHz, DMSO-d_6) spectrum, zoomed in on the region of interest, of **P2** with assigned signals, the unmarked signals are unreacted ligand.

^{1}H NMR Data from the spectrum:

^{1}H NMR (400 MHz, DMSO-d_6) δ 9.54 (d, *J* = 2.0 Hz, 1H, **H^{6}**), 8.73 (dd, *J* = 8.7, 2.1 Hz, 1H, **H^{4}**), 8.44 (d, *J* = 8.7 Hz, 1H, **H^{3}**), 8.03 (d, *J* = 8.6 Hz, 1H, **H$^{3'}$**), 7.94 (d, *J* = 1.8 Hz, 1H, **H$^{6'}$**), 7.81 – 7.74 (m, 1H, **H$^{4'}$**).

The signal from **H^{6}**, the proton next to nitrogen, has a shifted downfield compared to the ligand. This is a sign that gold is coordinated to the nitrogen. **H^{4}** couples to **H^{6}** and **H^{3}** with coupling constants ^{3}J = 8.7 Hz and ^{4}J =2.1 Hz respectively, indicates that it is the middle proton in the pyridine. The assignment of **H^{3}** is only based on the coupling constant, as it could also be the signal at 8.03 ppm now assigned to **H$^{3'}$**. The same pattern is shown for the phenyl protons where **H$^{4'}$** is the proton in the middle coupling to **H$^{3'}$** and **H$^{6'}$**. **H$^{6'}$** is the proton by itself as it has the lowest coupling constant. However, no further NMR experiments was conducted to strengthen the assignments. Due to the poor solubility of the complex no good ^{13}C NMR could be obtained therefore no HSQC or HMBC could be run. COSY and NOESY was tried but the resulting spectra were of too poor quality and no further information gained. However, if it were the N-coordinated gold complex seen in the spectrum there should have only been 2 signals with integrating to 2 due to symmetry on the phenyl ring. Even though no pure product could be isolated, the synthesis looks promising as cyclometalation seems to occur.

3.1.5 (N,C) Au(III) 5-bromo-2-phenylpyridine complex

Cyclometalated **L2** into **P1** should be easier because with no bromide on the phenyl, the aromatic π-system is not deactivated and the carbon on the phenyl should be more readily available for cyclometalation to gold.

L2 was synthesized following same Suzuki- Miyaura procedure[35, 43, 53] as previous ligands but using 2,5-dibromopyridine and phenylboronic acid as the reactants. The synthesis is illustrated in **Scheme 24**.

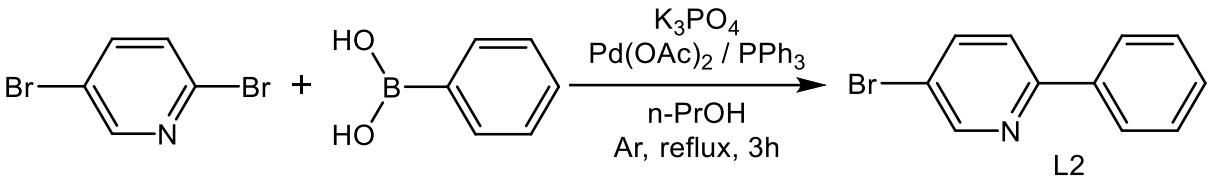

Scheme 24. Synthesis of ligand **L2**

By reacting 2,5-dibromopyridine and benzeneboronic acid a beige tinted powder was furnished at a 63% yield. The product was analysed with ^{1}H NMR (**A 7**) shown in **Figure 36**.

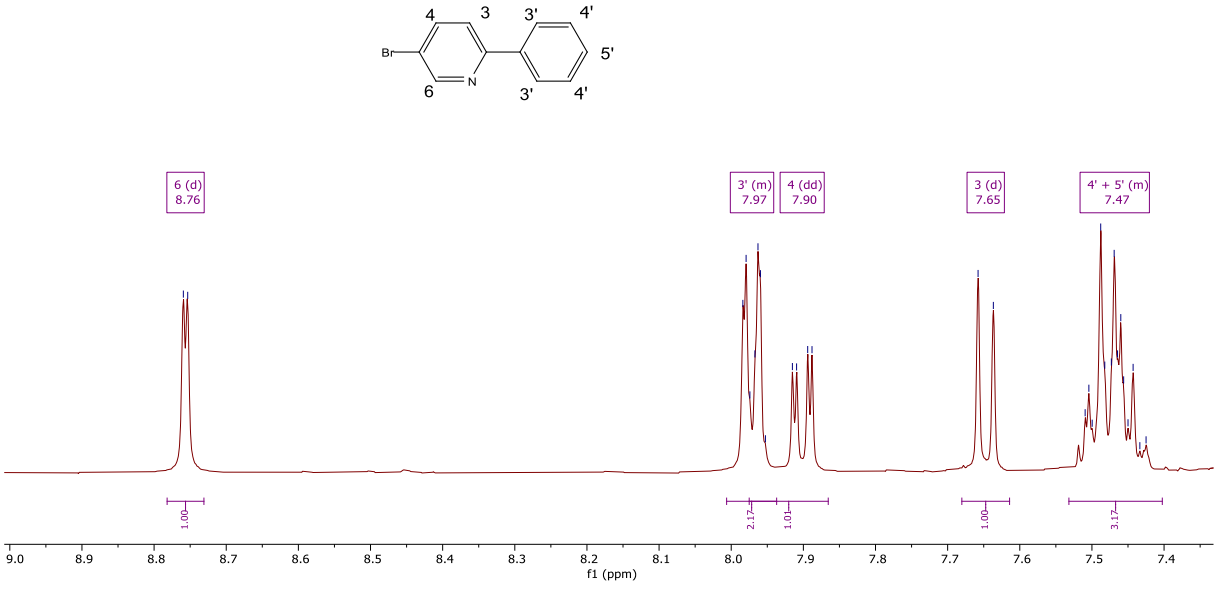

Figure 36. ^{1}H NMR (400 MHz, $CDCl_3$) of the isolated ligand **L2** with assigned signals, focused on the aromatic region.

^{1}H NMR (400 MHz, $CDCl_3$) δ 8.76 (d, J = 2.4 Hz, 1H. **H^{6}**), 8.01 – 7.94 (m, 2H, **H$^{3'}$**), 7.90 (dd, J = 8.5, 2.4 Hz, 1H, **H^{4}**), 7.65 (d, J = 8.5 Hz, 1H, **H^{3}**), 7.53 – 7.40 (m, 3H, **H$^{4'}$**+ **H$^{5'}$**)

From the molecule six signals in the aromatic region are expected. Three from the pyridine and three from the phenyl with two signals integrating to 2 due to symmetry. The three pyridine protons show the same pattern as with **L3**. Where **H^{6}** signal is a d furthest down field at 8.76 ppm coupling to **H^{4}** with a coupling constant ^{4}J = 2.4 Hz. **H^{4}** signal is a dd that couples to **H^{3}** with a coupling constant ^{3}J= 8.5 Hz. and the **H^{3}** signal is a d furthest up field of the three. On the phenyl side the remaining two signals integrates to five protons. Where the signal furthest down field integrating to 2 is most likely **H$^{3'}$** and the remaining signal furthest up field integrating to 3 is **H$^{4'}$** and **H$^{5'}$** intermingled. The ligand was also analysed with ESI-MS where the main peak at m/z 234 corresponds to [M+H] and the expected isotope peak from the bromide at m/z 236 [M+H] was observed. The ^{1}H NMR analysis is in accordance with previously reported data[67], and it was established that the desired product **L2** was isolated.

The ligand was cyclometalated with gold using the same microwave heated procedure as the **Au(tpy)Cl$_2$** synthesis. The $NaAuCl_4$ had run out so $HAuCl_4$ was used instead with the concern of adding more free protons in solution that could compete with the pyridine's free electron pair. The **L2** ligand was as poorly soluble in water as previous attempts with **L3** ligand. To try and reduce the number of free protons in the solution, acetonitrile was used instead of ethanol to get the ligand to mix with the water. Otherwise following the same steps as the **Au(tpy)Cl$_2$** synthesis. The reaction is shown in **Scheme 25**.

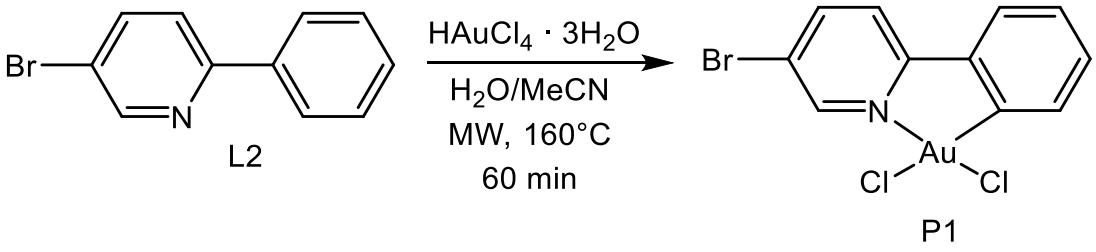

Scheme 25. Microwave assisted synthesis of **P1**.

By reacting **L2** with $HAuCl_4$ a beige powder was furnished at a 53% yield. The product was analysed with ^1H NMR (**A 32**) the spectrum is shown in **Figure 37**.

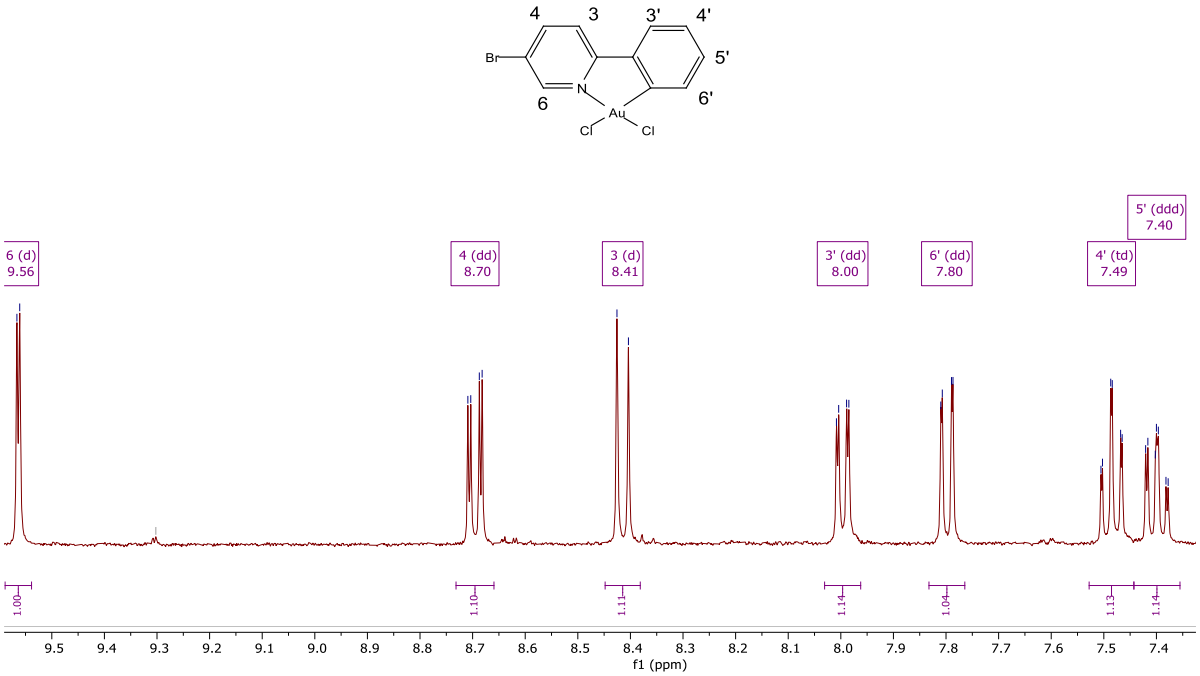

Figure 37. ^1H NMR (400 MHz, DMSO-d_6) spectrum, zoomed in on the region of interest, of **P1** with assigned signals.

^1H NMR (400 MHz, DMSO) δ 9.56 (d, J = 2.1 Hz, 1H, **H^6**), 8.70 (dd, J = 8.7, 2.2 Hz, 1H, **H^4**), 8.41 (d, J = 8.7 Hz, 1H, **H^3**), 8.00 (dd, J = 7.7, 1.7 Hz, 1H, **H$^{3'}$**), 7.80 (dd, J = 8.1, 1.1 Hz, 1H, **H$^{6'}$**), 7.49 (td, J = 7.5, 1.2 Hz, 1H, **H$^{4'}$**), 7.40 (ddd, J = 8.0, 7.4, 1.7 Hz, 1H, **H$^{5'}$**).

From the molecule structure seven signals is expected as all protons should have a unique resonance. All proton signals in the pyridine have shifted down field, a sign that gold have coordinated to the N-atom. The pattern for those three atoms is similar to what was observed for **L2**. The d furthest down field at 9.56 ppm is assigned to **H^6** the proton next to the nitrogen and couples to **H^4** with a coupling constant ^4J= 2.1 Hz. The dd at 8.70 ppm for **H^4** also couples to **H^3** with a coupling constant ^3J = 8.7 Hz and the **H^3** signal being furthest up field of the three at 8.41 ppm. The phenyl side have bit more complex coupling pattern than what **L2** showed. With four different signals integrating to 4 protons indicates that the symmetry is broken, and that gold have cyclometalated to the phenyl ring. The four signals observed consists of two dd, a td and a ddd where the two dd should be **H$^{3'}$** and **H$^{6'}$**. To determine which signal belongs to what proton more NMR experiments would be needed. However, based on the shifts from **Au(tpy)Cl$_2$ H$^{3'}$** signals should have a higher shift than **H$^{6'}$** signal.

With this assumption the two remaining signals could be determined by the coupling constants. Where the signal at 7.49 ppm should be **H$^{4'}$** that couples to **H$^{3'}$** and **H$^{5'}$** with a coupling constant ^{3}J = 7.5 Hz, and to **H$^{6'}$** with a coupling constant ^{4}J = 1.2 Hz. The signal at 7.40 ppm would then be **H$^{5'}$** coupling to **H$^{6'}$** with a coupling constant ^{3}J = 8.0 Hz and a long-range coupling ^{4}J = 1.7 Hz to **H$^{3'}$**. Judging from the NMR analysis the product **P2** was successfully synthesised and isolated.

Because **P2** is poorly soluble in DMSO, other solvents were evaluated. However, none of DCM, TFA, Benzene, pentane, toluene, hexane, or chloroform shoved any better solubility. This hindered NMR analysis as no good ^{13}C NMR could be obtained and the COSY, NOESY spectra recorded was of too poor quality to be used.
The more time requiring 2D NMR experiments were conducted the day after the synthesis using the same NMR sample, and it was observed that some decomposing had occurred, as can be observed in **Figure 38**.

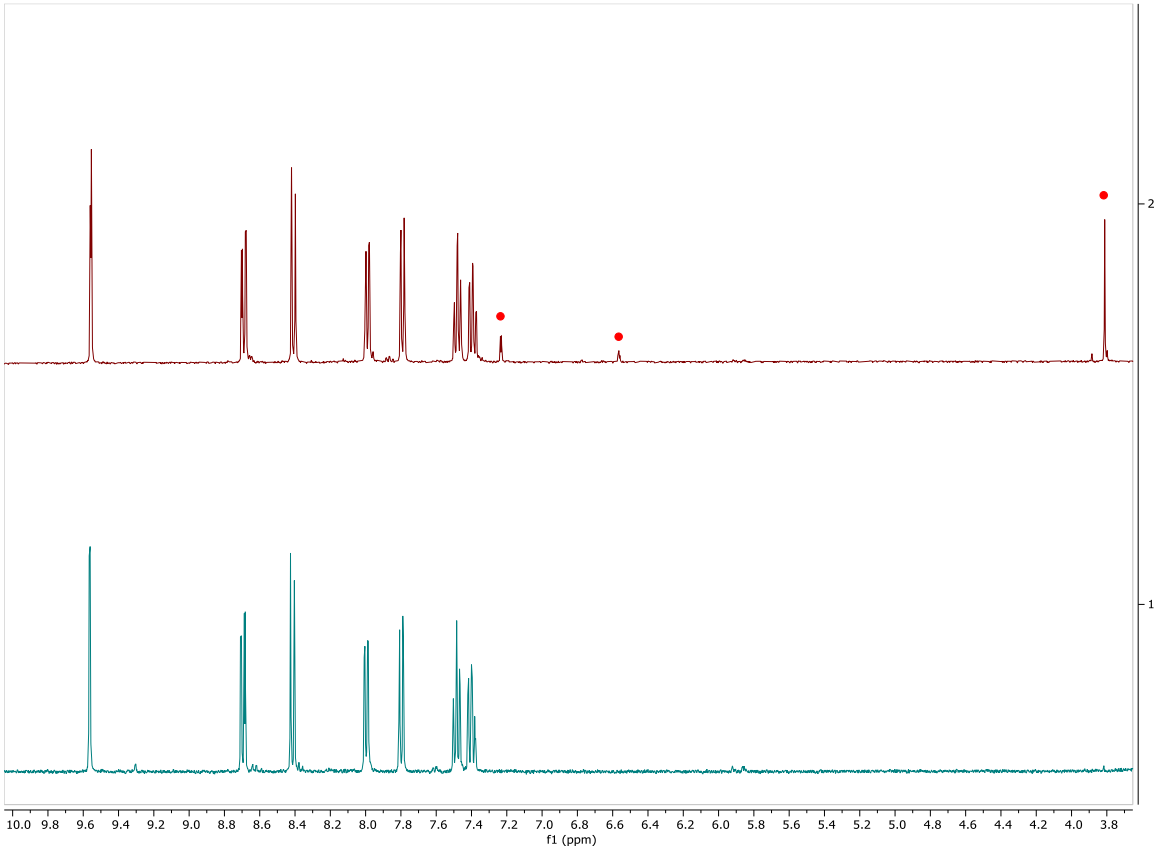

Figure 38. ^{1}H NMR (400 MHz, DMSO-d_6) spectrum, zoomed in on the region of interest, of **P1** Top: NMR spectrum showing signals suspected to be decomposed material marked with red dot taken the 1 day after the synthesis spectrum. Bottom: NMR spectrum directly after product synthesized.

The sample had been heated with a heat gun to try and dissolve the precipitated gold complex, so it was of interest to see if the decomposition was due to the aggressive heating or decomposition over time in the solvent. So, the same sample was reheated with the heat gun until the DMSO was boiling in the NMR-tube and then analysed. After leaving it another 24h an ^{1}H NMR experiment of the same sample was run. The four different ^{1}H NMR spectra are shown in **Figure 39**.

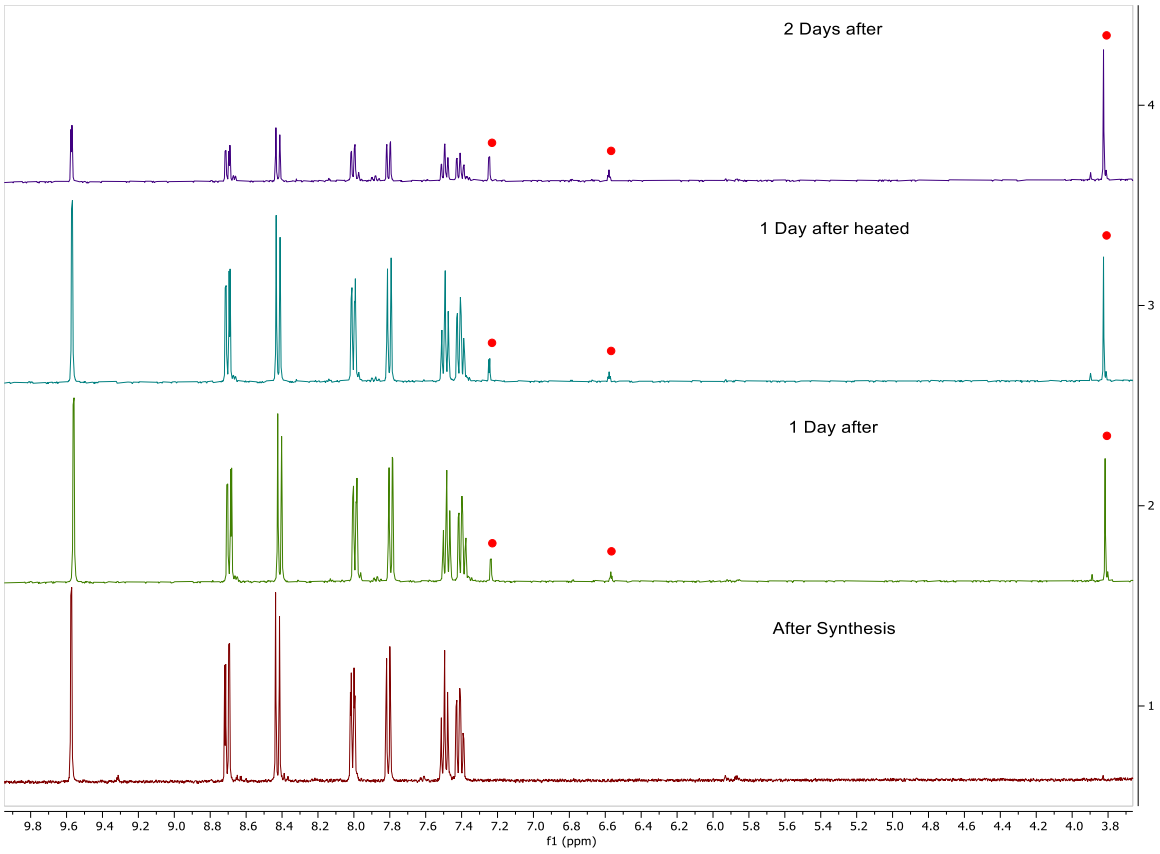

Figure 39. ^{1}H NMR (400 MHz, DMSO-d_6) spectrum of **P1** zoomed in on the region of interest**.** Signals suspected to be decomposed material are marked with red dot Top: NMR spectrum taken the two days after the synthesis Top middle: NMR spectrum taken the 1 day after the synthesis spectrum reheated with heat gun. Bottom middle: NMR spectrum taken the 1 day after the synthesis spectrum. Bottom: NMR spectrum directly after product synthesized.

From these tests it looks like heating does not decompose the gold complex, however over time it decomposes in DMSO. No investigation was made as to the nature of the decomposed material.

3.2 Catalysis

The catalysis experiments were split into three parts. First control experiments were setup to ensure that catalytic activity observed derives from the catalyst, to monitor potential decomposition or unwanted side reactions. The second part consists of recreation of previous catalytic experiments done in the Tilset group[21] and expands on them with substituted hexenyne. And lastly explore milder conditions for the reactions that shows promising catalytic activity. However, the final part was never conducted in this project due to failed synthesis of **R2** and lack of time.

All reactions presented in this chapter were on a small scale (typically 5 - 10 mg) and monitored in situ by ^{1}H NMR spectroscopy unless stated otherwise. The general procedure for reactions was to add the Au(III) complex into relevant solvent in an NMR tube, take a reference spectrum, then add the organic reagent. The reaction was monitored with ^{1}H NMR spectroscopy in 5- or 10-min intervals until no further changes in the spectrum could be observed.

3.2.1 Control experiments

Controls were planned for all catalytic experiments usually with the absence of **AuPincOAc^{F}**. Stability controls were only conducted with TFA and DCM due to time constraints. All compounds seemed stable for at least 24h in the solvents and no unwanted reaction was observed. However, some decomposition of **AuPincOAc^{F}** might have occurred over the duration of seven days. See 6.2.13 for more detailed description of the control experiments.

3.2.2 Reactivity of (N,C,C) AuPincOAc^{F} toward hexenynes

Experiments previously conducted by the Tilset group, have shown catalytic activity of **AuPincOAc^{F}** towards unsubstituted hexenynes. Catalysing the formation of the **C2** intermediate and **C1**[22] . These experiments were recreated as a reference point.

To confirm the presence of the **C2** intermediate the procedure reported by Schmidtke[21] was followed. By dissolving **AuPincOAc^{F}** (5 mol%) in TFE-d_3 a reference ^{1}H NMR spectrum was recorded before **R4** (1 equiv.) was added to the mixture and monitored with ^{1}H NMR every 5 min over 180 min. The resulting NMR spectra was compared to the reported spectra at the same time intervals, the data from recreation are shown in **Figure 40**.

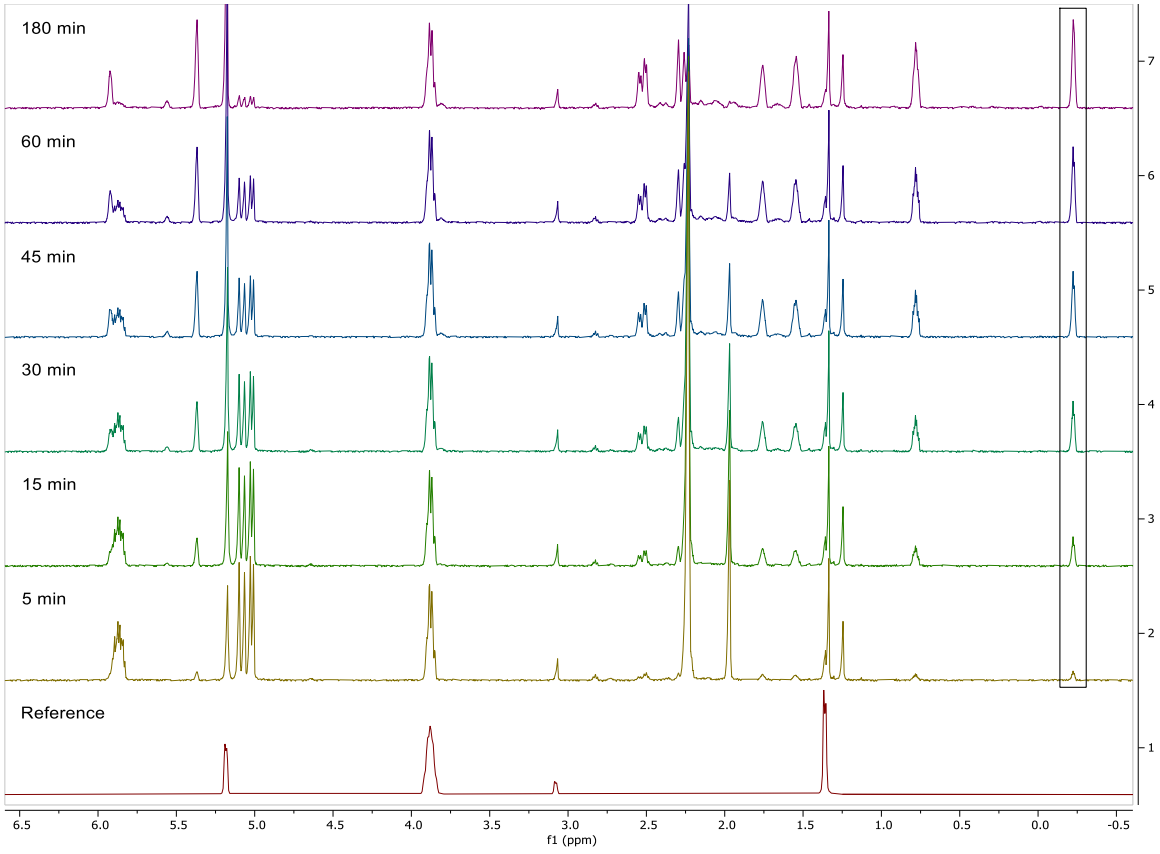

Figure 40. Stacked ^{1}H NMR (500 MHz, TFE-d_3) spectra showing the reaction progress of **AuPincOAc^{F}** with **R4** over 180 minutes. The spectra is focused on the vinylic and aliphatic regions. A characteristic resonance at -0.23 ppm is highlighted with a dashed box. The reference spectrum shows **AuPincOAc^{F}** in solvent.

The characteristic resonance of the methylene bridge in the cyclopropane at -0.23 ppm increases over time indicating the formation of **C2**. Additionally, the decreasing alkene signals at 5.8 and 5.0 ppm belong to the starting material indicating that **C2** is generated and **R4** is consumed. These observations correspond with the trends reported by Schmidtke[21]. The

signal at 3.2 ppm from **AuPincOAc^{F}** does not decrease over time indicating that the catalyst does not decompose in the monitored time frame shown in **Figure 41**.

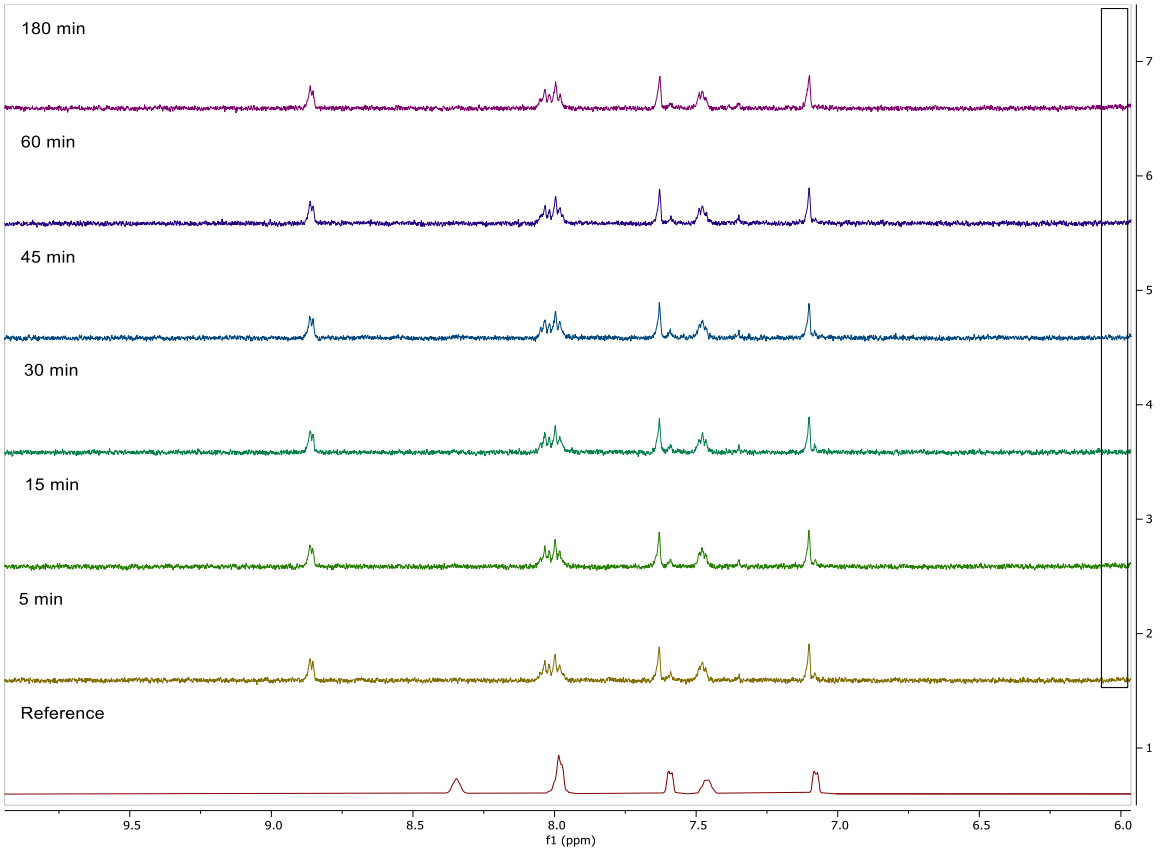

Figure 41. Stacked ^{1}H NMR (500 MHz, TFE-d_3) spectra showing the reaction progress of **AuPincOAc^{F}** with **R4** over 180 minutes focused on the aromatic region. The reference spectrum shows **AuPincOAc^{F}** in solvent.

The signal at 8.3 ppm in the reference spectrum shifts to 8.8 ppm in the reaction. This suggests that the trifluoroacetate ligand on the gold complex has been exchanged, a sign that it might be partaking in the reaction. Although **C2** was never isolated, examination of the last spectrum at 3h, shows signals and splitting that are in agreement with the reported data for **C2**[68]. The assignment of signals to **C2** is shown in **Figure 42**.

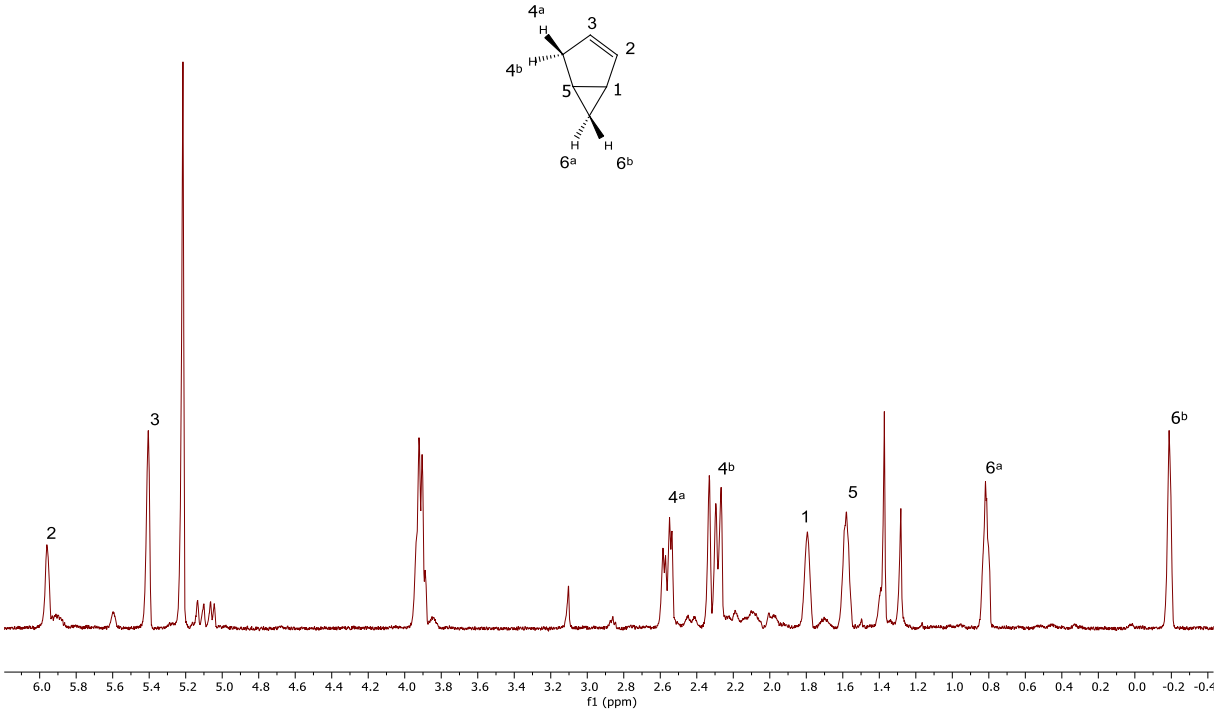

Figure 42. ^{1}H NMR (500 MHz, TFE-d_3) spectra showing **C2** from reaction of **AuPincOAc^{F}** with **R4** after 180 minutes.

To recreate the synthesis of **C1** from **R4** the procedure reported by Schmidtke[21] was followed. **AuPincOAc^{F}** (1 equiv.) was dissolved in CD_2Cl_2:TFA (5:1) and a reference spectrum was recorded before **R4** (1.2 equiv.) was added to the solution. When **R4** was added a yellow tint was observed in the solution. ^{1}H NMR monitoring of the reaction was started immediately and followed up every 5 min over the course of 180 min. The experiment deviated from the reported procedure in two important aspects. Firstly, the internal standard was not added to the mixture. Secondly, the reaction was conducted at room temperature instead of 273K as reported. The recorded ^{1}H NMR spectra is shown in **Figure 43**.

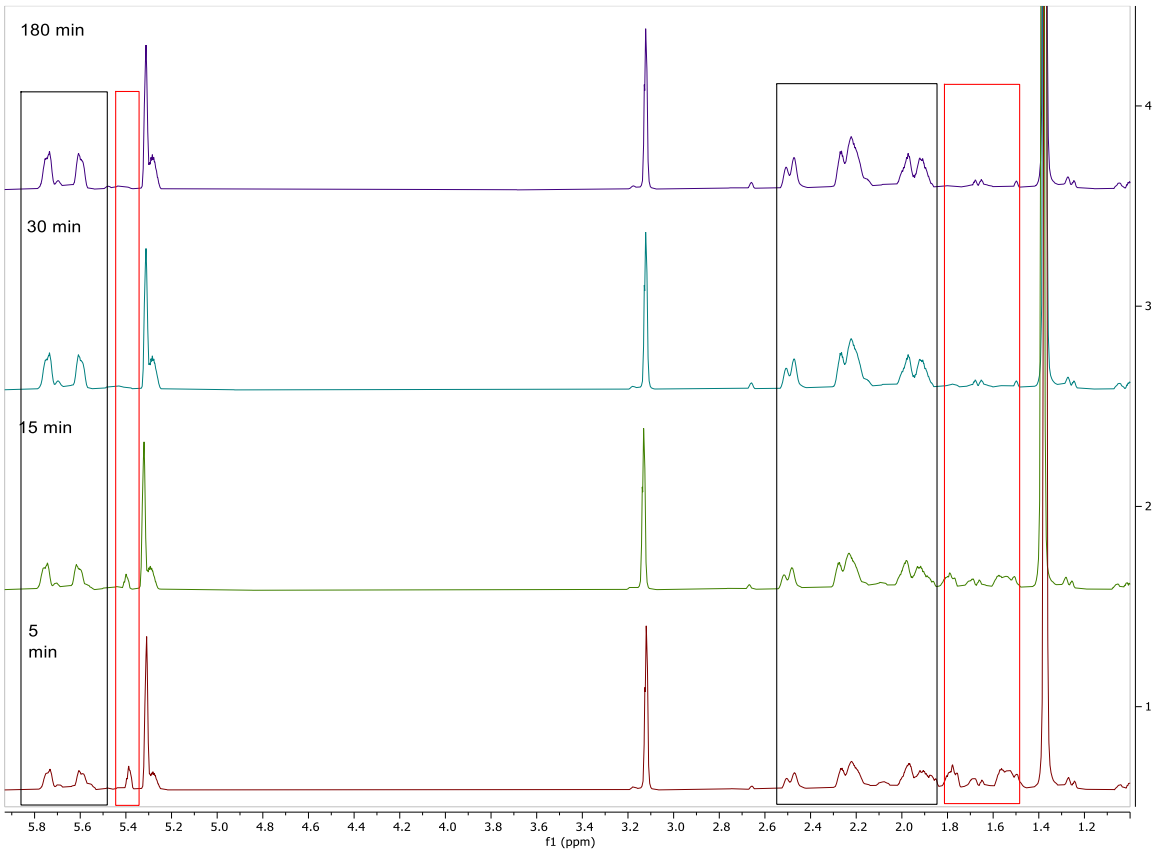

Figure 43. ^{1}H NMR (500 MHz, CD_2Cl_2) stacked spectra showing the reaction of **AuPincOAc^{F}** with **R4** in presence of TFA over 180 minutes. **C1** marked with black dashed rectangles and **R4** is marked with red dashed rectangles.

Due to the difference in temperature the reaction was completed much faster, and the bicyclic intermediate **C2** was not observed. No real comparison to the reported experiment could therefore be done. However, it was observed that **R4** was consumed and **C1** is formed. The assignment of signals for C1 can be found in 6.2.10 where the observed signals form ^{1}H NMR are in accordance with previously reported data[21].

3.2.3 Reactivity of AuPincOAc^{F} toward substituted hexenynes

The catalytic reactivity of **AuPincOAc^{F}** towards **R1** was recreated following the procedure reported by Schmidtke [21]. **AuPincOAc^{F}** (1 equiv.) was dissolved in CD_2Cl_2:TFA (5:1) and a reference spectrum was recorded with ^{1}H NMR before **R1** (1.2 equiv.) was added to the solution. The reaction was monitored with ^{1}H NMR every 10 min for 180 min. The resulting NMR spectra of selected times is shown in **Figure 44**.

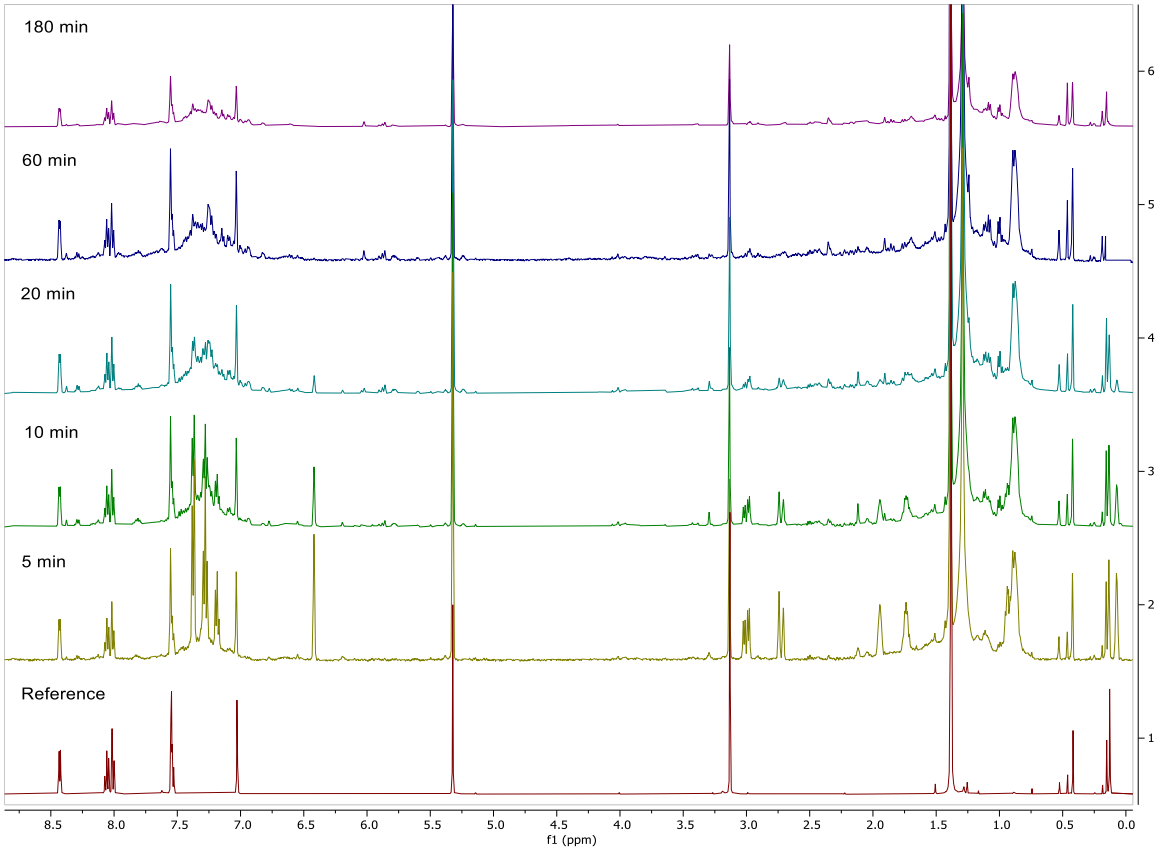

Figure 44. ^{1}H NMR (500 MHz, CD_2Cl_2) spectra showing the progress of the reaction of **AuPincOAc^{F}** with **R1** over 180 minutes. Reference spectrum shows **AuPincOAc^{F}** in solvent.

The results are in accordance with the reported data. The reaction seems to be very fast as no signals from **R1** can be observed in the first spectrum recorded. It is probable that all **R1** was converted into what is suspected to be **C3**. It was suggested in the previous experiment[21] that **C3** further converts into an NMR silent compound. A decrease in the **C3** signals is observed in this experiment as well. Decomposition of the gold catalyst is observed during the experiment as indicated by the decrease of signals in the aromatic region belonging to **AuPincOAc^{F}**. There are signals between 0.08-0.5 ppm that are most likely plasticizers as the DCM/TFE/TFA were all added with a plastic syringe and should be disregarded. Focusing on the spectrum at 5 min, the signals correspond well with the reported data of **C3** as are shown in **Figure 45**.

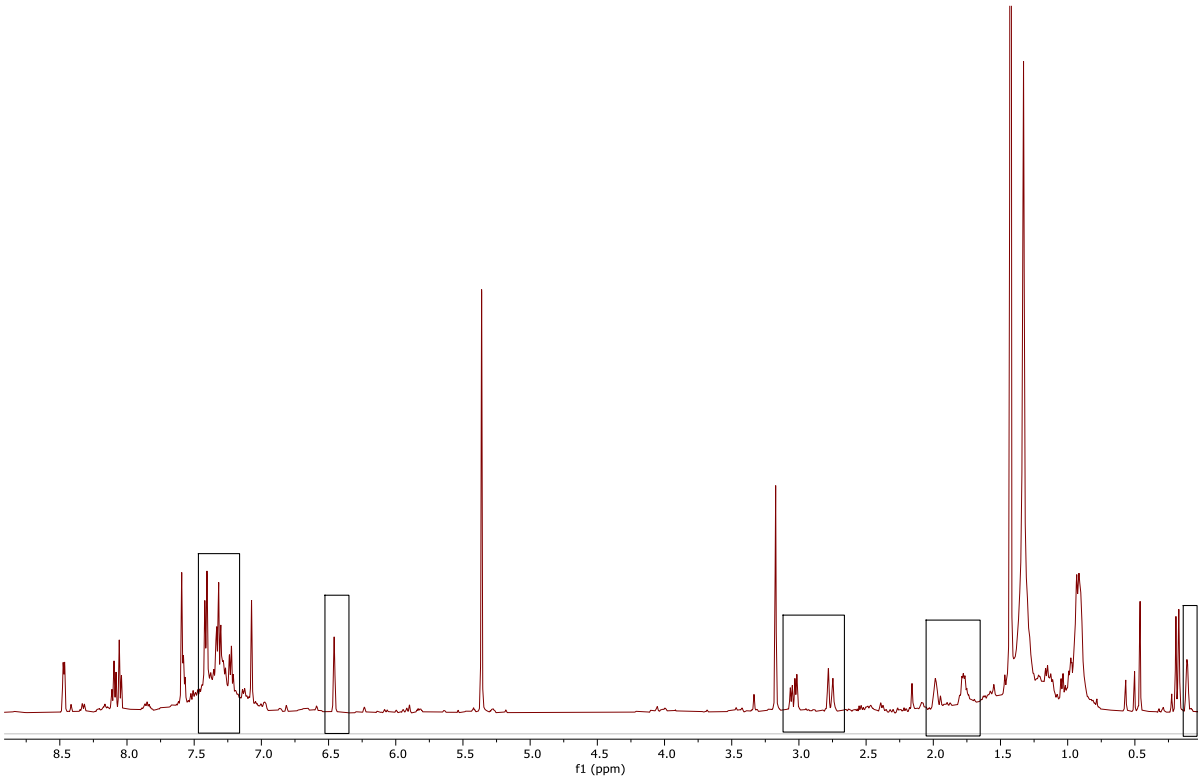

Figure 45. ^{1}H NMR (500 MHz, CD_2Cl_2) spectrum showing suspected signals originating from **C3** marked with dashed rectangles.

Catalytic experiments for **R2** were never conducted as there was not enough compound synthesized to run an experiment.

4 Conclusion

The aim of this thesis has been to explore the role of **AuPincOAc^{F}** in catalysing the cycloisomerization of hexenynes. To this end two hexenynes were synthesized. These include **R1** that has previously shown cycloisomerization activity and **R2** that was deemed a potential candidate for such a reaction.

The first part of this thesis covers the synthesis, purification, and purification optimization of **R1** and **R2**. Previously reported synthesis of **R1** yielded a product with significant impurities. A workup step was incorporated into the previously established protocol to increase purity. This also made it possible to isolate a by-product. That by-product was extensively investigated by NMR using both 1D and 2D experiments and it was determined to be **R3**. **R3** could be of interest as another species to include in the catalytic studies of the **AuPincOAc^{F}**. The synthesis of **R2** was shown to be possible and a tiny amount of the substance was synthesized. The synthesis was never successfully repeated in this project. This might imply that the reaction is extremely sensitive and needs specific conditions to successfully synthesis the product. Several attempts were made to control for different error sources; however, it was never established exactly what caused the synthesis to fail. As there was not enough **R2** synthesis for catalytic studies, the project was pivoted to creating precursors of cyclometalated Au(III) complexes this is presented in the second part.

The precursors were synthesized following earlier established procedures, creating a ligand with a Suzuki-Miyaura coupling, followed by a microwave assisted cyclometalation. The products of each reaction were analysed with NMR and MS to confirm that the desired product was synthesized. One new precursor, **P1**, was synthesized and isolated. Different solvents were evaluated with DMSO showing the best solvent ability. However, DMSO was only able to achieve partial solubilisation possibly limiting further reactions.
The second precursor **P2** was synthesized but not isolated. NMR and MS analysis both showed promising data indicating that it was in fact the desired product though a definite identification was not achieved. The species showed the same insolubility as **P1**.
Due to time restrictions no substitution reactions were attempted on the precursors.

Both species show promise as precursors for future Au(III) complex synthesis. The procedure to synthesis the precursors is uncomplicated and with some optimization should give better

yields. Brominated phenyls and pyridines have shown to readily partake in a Suzuki-Miyaura couplings so the precursors should be a suitable reactant for this purpose. But the solubility may be a hinderance for the substitution reactions.

5 Future work

Catalytic studies involving the Au(III) pincers complex reactivity towards substituted hexenynes should conducted as they will assist in elucidating the gold complex's role in the cycloisomerization of hexenynes. It was shown that the reactants of interest are synthesizable, although the **R2** procedure needs to be optimized. The isolated by-product should be included in further catalytic studies to determine whether allenes also undergo cycloisomerization.

The precursors show a promising future that could lead to entirely new, interesting gold(III) complexes. Initially the Suzuki-Miyaura coupling should be examined to see if the substitution of bromide is achievable and if yields and purity are acceptable. The leaving groups on the ppy-ligand may be further explored with different halogens and functional groups that can support other coupling reactions for example a mild Heck reaction or as a Grignard reagent. Schemes for these examples are shown in **Scheme 26**.

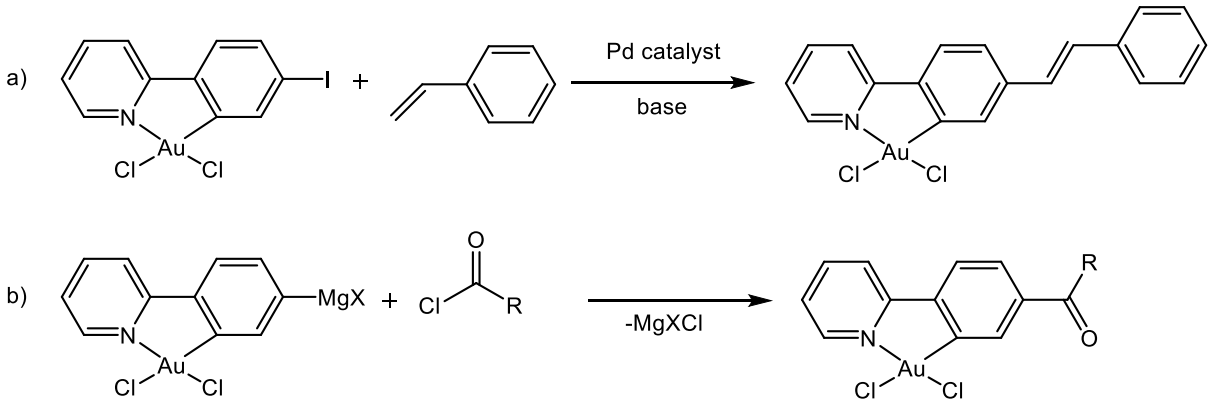

Scheme 26. Two examples of potential reactions with precursor Au(III) complexes with a) showing a general Heck reaction with an iodide on the precursor, and b) showing the precursor acting as a Grignard reagent with a magnesium halide attached to the phenyl.

6 Experimental

6.1 General procedures

Chemicals were purchased from ABCR, TCI, AK Scientific, Fluorochem, Alpha Aesar and Sigma Aldrich, they were used as received. Distilled water (Type II water) was used in the syntheses of Au(III) complexes and for workups. All solvents (including deuterated solvents) were purchased from Sigma Aldrich, VWR, Merck, Cambridge Isotope Laboratories or Eurisotope and used as received. CD_2Cl_2 was dried over molecular sieves prior to use. CH_2Cl_2, acetonitrile and THF used in reactions were purified using a MB SPS-800 solvent purifying system from MBraun. All reactions were conducted in air and at ambient temperature, unless stated otherwise. Microwave assisted reactions were performed with a Milestone MicroSYNTH microwave reactor with a SK-10 rotor or, for reaction volumes smaller than 10 mL, in an Anton Paar GmbH Monowave 300 synthesis reactor equipped with an internal IR probe calibrated with a Ruby thermometer. NMR spectra were recorded on Bruker Avance AVII400 and DRX500 instruments at ambient temperature, unless stated otherwise.

^{1}H and ^{13}C NMR spectra have been referenced relative to residual solvent signals (CD_2Cl_2: $\delta(^{1}H)$ 5.32, $\delta(^{13}C)$ 54.0; $CDCl_3$: $\delta(^{1}H)$ 7.26, $\delta(^{13}C)$ 77.2; TFA-d: $\delta(^{1}H)$ 11.50; TFE-d: $\delta(^{1}H)$ 3.88), $\delta(^{13}C)$ 61.5. Multiplicities are abbreviated as: s - singlet, d - doublet, t- triplet, q - quartet, qn - quintet, sx - sextet, sp - septet, m - multiplet, br. - broad, the ^{13}C resonances are proton decoupled.

6.2 Synthesis and catalytic experiments

6.2.1 Synthesis of $Au(tpy)Cl_2$

The title compound was synthesized following the procedure reported by Shaw et al.[33]. 2-(p-tolyl)pyridine (0.0860 g, 0.508 mmol, 1 equiv.) and $HAuCl_4 \cdot H_2O$ (0.1754 g, 0.445 mmol, 1 equiv.) dissolved in 15 ml of distilled water was added to a microwave vessel. The vessel was transferred into a microwave and heated to 160°C for 30 min. The mixture was then cooled to rt. During cooling precipitate formed that was then collected by vacuum filtering. The solids were washed with 2×2.5 mL of distilled water followed by 2×2.5 mL acetonitrile then one last time with distilled water. The washed solids were dried in an oven, covered with foil for 60 min yielding the product as a white powder (0.1314 g, 0.302 mmol, 68% yield). The product was confirmed by ^{1}H NMR and ESI-MS analysis. (**A 1** and **A 37**).

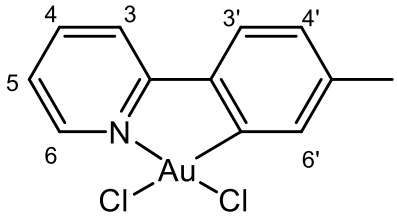

$Au(tpy)Cl_2$

^{1}H NMR (400 MHz, DMSO-d_6) δ 9.49 (dt, J = 6.1, 1.1 Hz, 1H, **H^6**), 8.39 – 8.33 (m, 2H, **H^4** + **H^3**), 7.85 (d, J = 7.9 Hz, 1H, **H$^{3'}$**), 7.72 (td, J = 6.0, 3.2 Hz, 1H, **H^5**), 7.62 (s, 1H, **H$^{6'}$**), 7.31 (d, J = 7.9 Hz, 1H, **H$^{4'}$**), 2.40 (s, 3H, **CH$_3$**).

MS (ESI, Acetonitrile): m/z (rel. %): 458/460 ([M + Na], 16/10), 400/402 ([M - Cl), 100/32))

The analytical results were in agreement with previously reported data for $Au(tpy)Cl_2$[33].

6.2.2 Synthesis of 2-(3,5-di-tert-butylphenyl) pyridine

The title compound was synthesized following the procedure reported by Holmsen[43]. 2-bromopyridine (0.7857 g, 4.97 mmol, 1 equiv.) and (3,5-di-tert-butylphenyl)boronic acid (1.1687 g, 4.99 mmol, 1 equiv.) solved in propanol (10 mL) was added to a round flask equipped with a stir bar. A solution of 1M K_3PO_4 (2.1242 g, 10 mmol dissolved in 10 mL distilled water) was prepared on the side and then added to the flask. The flask then was sealed, and the mixture degassed for 5 min with argon gas, creating an inert atmosphere in the flask. To the mixture $Pd(OAc)_2$ (0.0253 g, 0.11 mmol, 2 mol%) and PPh_3 (0.0792 g, 0.30 mmol, 6 mol%) was added followed by another 5 min of degassing with argon. The mixture was then heated to reflux for 3h. The mixture was then cooled down to rt and transferred to a separatory funnel. To the funnel DCM (50 mL) and distilled water (50 mL) was added. The organic phase was extracted and washed 2 times with 2M NaOH (50 mL), one time with distilled water (50 mL) and finally brine (50 mL). The washed organic phase was dried with $NaSO_4$ filtered and reduced under vacuum to obtain the crude product. The crude product was purified with flash chromatography using 5% ethyl acetate: 95% distilled hexane as eluent. The solvent was removed under vacuum to yield the product (1.1792 g, 4.416 mmol, 89% yield). The product was confirmed by ^{1}H NMR and ESI-MS analysis (**A 6** and **A 39**).

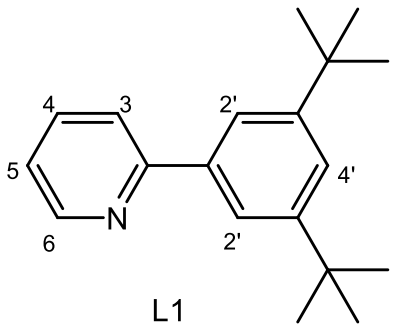

L1

^{1}H NMR (400 MHz, $CDCl_3$) δ 8.74 (d, J = 4.7 Hz, 1H, **H^6**), 7.85 (d, J = 2.0 Hz, 2H, **H$^{2'}$**), 7.81 – 7.71 (m, 2H, **H^3 + H^4**), 7.55 (t, J = 1.8 Hz, 1H, **H$^{4'}$**), 7.24 (ddd, J = 5.9, 4.8, 2.6 Hz, 1H, **H^5**), 1.44 (d, J = 1.7 Hz, 18H, **2(CH_3)$_3$**).

MS (ESI, Acetonitrile): m/z (rel. %): 268/269 ([M + H], 100/21)

The analytical results were in agreement with previously reported data for **L1**[43].

6.2.3 Synthesis of AuPincOAc^F

The title compound was synthesized following the procedure reported by Holmsen[43]. $Au(OAc)_3$ (0.1880 g, 0.5025 mmol, 1.00 equiv.) and **L1** (0.1831 g, 0.6847 mmol, 1.36 equiv.) dissolved in a mixture of TFA (7.5 mL) and distilled water (7.5 mL) was added to a microwave vessel. The vessel was then heated to 120 °C for 30 min and afterwards cooled down to rt. During cooling precipitate formed. To the mixture TFA was added one pipette at the time while stirring until all precipitates had dissolved (10 times in total). The mixture was then gravity filtered through filter paper and the filtrate set in an ice bath. Distilled water (20 mL) was added to the chilled filtrate and the product precipitated out. The product was collected and washed with distilled water (3×5 mL).The title compound was obtained as a white powder (0.2371 g, 0.412 mmol, 82% yield). The product was confirmed by ^{1}H NMR and ESI-MS analysis (**A 2** and **A 38**).

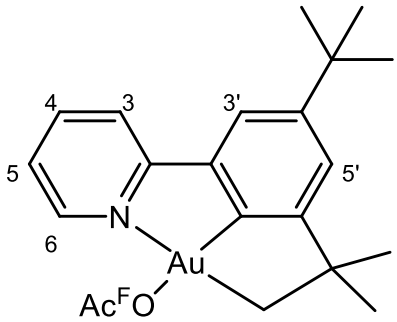

AuPincOAc^F

^{1}H NMR (400 MHz, CD_2Cl_2) δ 8.52 (d, J = 5.4 Hz, 1H, **H^6**), 8.06 – 7.95 (m, 2H, **H^3 + H^4**), 7.54 – 7.49 (m, 2H, **H^5 + H$^{3'}$**), 7.00 (d, J = 1.8 Hz, 1H, **H$^{5'}$**), 3.15 (s, 2H, CH_2), 1.38 (s, 6H, **$(CH_3)_2$**), 1.37 (s, 9H, **$(CH_3)_3$**)

MS (ESI, Acetonitrile): m/z (rel. %): 520/522 ([M - OAc^F + Cl + Na], 100/33), 463 ([M - OAc^F], 85)

The analytical results were in agreement with previously reported data for **AuPincOAc^F** [21, 43].

6.2.4 Synthesis of 4-phenyl-1-hexen-5-yne

The title compound was synthesized after a combination of reported procedures[21, 50, 54, 56]. The reaction was conducted under inert gas in a 100 mL round-bottom flask equipped with a septum. 1-phenylprop-2-yn-1-ol (0.625 mL, 5.13 mmol, 1.00 equiv.) and allyl trimethylsilane (2.50 mL, 15.7 mmol, 3.00 equiv.) were dissolved in 10 mL dry acetonitrile (MeCN) and added to the flask. To the reaction mixture anhydrous $FeCl_3$ solution (1.25 mL in dry MeCN, 41.5 mg, 0.50 mmol, 5 mol%) was added drop wise. The solution was stirred for 2 h at room temperature. Afterwards another 1.25 mL of $FeCl_3$ solution (in dry MeCN, 41.5 mg, 0.50 mmol, 5 mol%) were added drop wise. After stirring the solution for 1 h at room temperature, $NaHCO_3$ 2 mL was added to the solution. The remaining material was extracted three times with ethyl acetate (20 mL) and the organic layer was dried with Na_2SO_4 and filtered through a silica plug. The organic phase was removed under reduced pressure yielding the crude product as a yellow–brown oil. The crude product was purified by flash chromatography using distilled hexane as eluent to furnish **R1** as a clear oil (0.2245 g, 1.44 mmol, 28% yield). The product was confirmed by ^{1}H and ^{13}C NMR analysis (**A 11** and **A 12**).

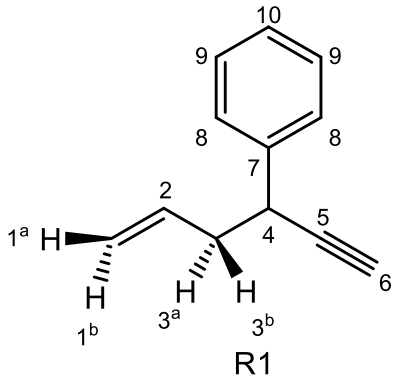

R1

^{1}H NMR (400 MHz, $CDCl_3$): δ 7.39–7.30 (m, 4H, $\mathbf{H^{8+9}}$), 7.27–7.21 (m, 1H, $\mathbf{H^{10}}$), 5.86 (ddt, 1H, J = 17.2, 10.3, 7.0 Hz, $\mathbf{H^{2}}$), 5.11–5.02 (m, 2H, $\mathbf{H^{1a+1b}}$), 3.71 (td, 1H, J = 7.2, 2.5 Hz, $\mathbf{H^{4}}$), 2.53 (tt, 2H, J = 7.0, 1.4 Hz, $\mathbf{H^{3a+3b}}$), 2.30 (d, 1H, J = 2.5 Hz, $\mathbf{H^{6}}$). The resonance at δ 1.54 arises from water in the solvent.

^{13}C-NMR (101 MHz, $CDCl_3$): δ 140.9 ($\mathbf{C^{7}}$), 135.3 ($\mathbf{C^{2}}$), 128.6 ($\mathbf{C^{9}}$), 127.6 ($\mathbf{C^{8}}$), 127.1 ($\mathbf{C^{10}}$), 117.3 ($\mathbf{C^{1}}$), 85.5 ($\mathbf{C^{5}}$), 71.5 ($\mathbf{C^{6}}$), 42.5 ($\mathbf{C^{3}}$), 37.8 ($\mathbf{C^{4}}$).

The analytical results were in agreement with previously reported data for **R1**[21, 50, 54, 56].

6.2.5 Synthesis of 3-phenyl-1-hexen-5-yne

The title compound was synthesized after a procedure reported by Morken et al.[64]. An oven dried vial equipped with a stir bar was transferred into a glovebox. To the vial $Pd_2(dba)_3$ (0.005 g, 5.4 µmol, 1.25 mol%) and rac-BINAP (0.007 g, 11.2 µmol, 2.7 mol%) dissolved in THF (0.8 mL) was added and stirred for 5 min. Then cinnamyl acetate (70 µL, 0.42 mmol, 1 equiv.), caesium fluoride (0.184 g, 1.2 mmol, 2.9 equiv.) and allenylboronic acid pinacol ester (85 µL, 0.47 mmol, 1.1 equiv.) was added to the mixture. The vial was sealed and removed from the glovebox. The vial was heated in an oil bath to 60 °C while stirring for 14h. The reaction mixture was then cooled down to room temperature diluted with diethyl ether and filtered through a silica plug. The filtrate was concentrated under reduced pressure yielding the crude product. The crude product was then purified with flash chromatography using distilled hexane as eluent and **R2** was obtained as a clear oil (27.2 mg, 0.153 mmol, 42% yield). The product was confirmed by ^{1}H NMR analysis (**A 17**)

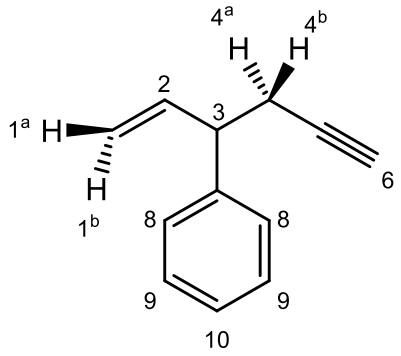

R2

^{1}H NMR (400 MHz, $CDCl_3$): δ 7.33 (2H, m, **H^9**), 7.25-7.22 (3H, m, **H^8 + H^{10}**), 6.06 (1H, ddd, J = 17.25 Hz, 10.35 Hz, 7.05 Hz, **H^2**), 5.14 (2H, m **H$^{1a + 1b}$**), 3.54 (1H, q, J = 7.15 Hz, 7.15 Hz, 7.17 Hz, **H^3**), 2.61 (2H, dt, J = 7.0 Hz, 2.89 Hz, 2.89 Hz, **H$^{4a + 4b}$**), 1.97 (1H, t, J = 2.63 Hz, 2.63 Hz, **H^6**);

The analytical results were in agreement with previously reported data for **R2**[64].

6.2.6 Synthesis of 5-bromo-2-phenylpyridine

The title compound was synthesized following the procedure reported by Holmsen[43]. 2,5-dibromopyridine (0.5002 g, 2.11 mmol, 1 equiv.) and phenylboronic acid (0.2598 g, 2.13 mmol, 1 equiv.) dissolved in propanol (5 mL) was added to a round flask equipped with a stir bar. A solution of K_3PO_4 (0.9003 g, 4.24 mmol, 2 equiv.) dissolved in 5 mL distilled water was prepared on the side and then added to the flask. The flask was sealed, and the mixture was then degassed for 5 min with argon gas creating an inert atmosphere. $Pd(OAc)_2$ (0.0095 g, 42 µmol, 2 mol%) and PPh_3 (0.0336 g, 128 µmol, 6 mol%) was added to the mixture followed by another 5 min degassing with argon. The mixture was then heated to reflux for 4h. The mixture was cooled down to rt and transferred to a separatory funnel. To the funnel DCM (25 mL) and distilled water (25 mL) was added. The organic phase was extracted and then washed two times with 2M NaOH (25 mL), one time with distilled water (25 mL) and finally brine (25 mL). The washed organic phase was dried with Na_2SO_4, filtered and the organic phase removed under vacuum. The crude product was purified with flash chromatography using 50% DCM: 50% distilled hexane as eluent furnishing **L2** as a beige powder (0.312 g, 1.33 mmol, 63% yield). The product was confirmed by ^{1}H NMR and ESI-MS analysis (**A 7** and **A 40**, **A 41**).

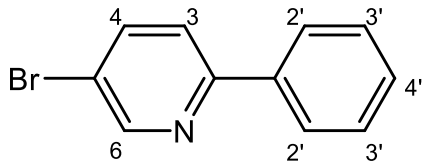

L2

^{1}H NMR (400 MHz, $CDCl_3$) δ 8.75 (d, *J* = 2.2 Hz, 1H, **H^6**), 8.00 – 7.93 (m, 2H, **H$^{2'}$**), 7.88 (dd, *J* = 8.5, 2.4 Hz, 1H, **H^4**), 7.64 (dd, *J* = 8.5, 0.8 Hz, 1H, **H^3**), 7.59 – 7.38 (m, 3H, **H$^{3'}$+H$^{4'}$**)

MS (ESI, Acetonitrile): m/z (rel. %): 234/236 ([M + H], 100/98)

The analytical results were in agreement with previously reported data for **L2**[67].

6.2.7 Synthesis of 5-bromo-2-(4-bromophenyl) pyridine

The title compound was synthesized following the procedure reported by Holmsen[43]. 2,5-dibromopyridine (0.5024 g, 2.12 mmol, 1 equiv.) and 4-bromophenylboronic acid (0.4592 g, 2.29 mmol, 1.1 equiv.) dissolved in propanol (5 mL) was added to a round flask equipped with a stir bar. A solution of K_3PO_4 (0.9034 g, 4.25 mmol, 2 equiv.) dissolved in 5 mL distilled water was prepared on the side and then added to the flask. The flask was sealed, and the mixture was degassed for 5 min with argon gas creating an inert atmosphere. $Pd(OAc)_2$ (0.0096 g, 43 µmol, 2 mol%) and PPh_3 (0.0336 g, 127 µmol, 6 mol%) was added to the mixture followed by another 5 min degassing with argon. The mixture was then heated to reflux for 3h. The mixture was cooled down to rt and transferred to a separatory funnel. To the funnel DCM (25 mL) and distilled water (25 mL) was added. The organic phase was extracted and then washed two times with 2M NaOH (25 mL), one time with distilled water (25 mL) and finally brine (25 mL). The washed organic phase was dried with Na_2SO_4, filtered and the organic phase removed under vacuum. The crude product was purified with flash chromatography using 50% DCM: 50% distilled hexane as eluent furnish **L3** as a white powder (0.2242 g, 0.72 mmol, 34% yield). The product was confirmed by ^{1}H NMR and ESI-MS analysis (**A 9** and **A 42**).

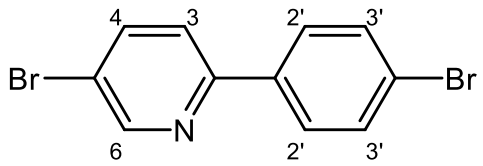

L3

^{1}H NMR (400 MHz, $CDCl_3$) δ 8.75 (d, J = 2.4 Hz, 1H, **H^6**), 7.92 – 7.85 (m, 3H, **H$^{2'}$+H^3**), 7.63 (dd, J = 8.3, 1.2 Hz, 3H, **H$^{3'}$+H^4**).

MS (ESI, Acetonitrile): m/z (rel. %): 312/314/316 ([M + H], 51/100/48)

The analytical results were in agreement with previously reported data for **L3**[66].

6.2.8 Synthesis of (N,C) Au(III) 5-bromo-2-phenylpyridine complex

The title compound was synthesized following the procedure reported by Shaw et al[33]. **L2** (0.0348 g, 0.15 mmol, 1 equiv.) and $HAuCl_4 \cdot H_2O$ (0.0587 g, 0.15 mmol, 1 equiv.) was added to a microwave vessel followed by 5 ml of distilled water. Acetonitrile was added dropwise until **L2** started mixing with the water, fluffy precipitate was observed. The vessel was transferred into a microwave and heated to 160°C for 30 min. The mixture was cooled to rt and precipitate formed. The precipitate was washed with 2×2.5 mL of distilled water followed by 2×2.5 mL acetonitrile then finally with distilled water 2.5 mL. The washed precipitate was dried under an air stream for 60 min furnishing the product **P1** as a beige solid (0.0401 g, 0.08 mmol, 53% yield). The product was confirmed by ^{1}H NMR and ESI-MS analysis (**A 32** and **A 43**,**A 44**).

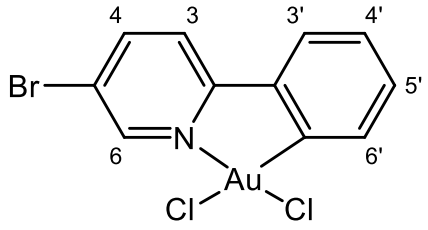

P1

^{1}H NMR (400 MHz, DMSO-d_6) δ 9.56 (d, *J* = 2.1 Hz, 1H, **H^6**), 8.70 (dd, *J* = 8.7, 2.2 Hz, 1H, **H^4**), 8.41 (d, *J* = 8.7 Hz, 1H, **H^3**), 8.00 (dd, *J* = 7.7, 1.7 Hz, 1H, **H$^{6'}$**), 7.80 (dd, *J* = 8.1, 1.1 Hz, 1H, **H$^{3'}$**), 7.49 (td, *J* = 7.5, 1.2 Hz, 1H, **H$^{5'}$**), 7.40 (ddd, *J* = 8.9, 7.4, 1.7 Hz, 1H, **H$^{4'}$**).

MS (ESI, Acetonitrile): m/z (rel. %): 522/524/526 ([M + Na], 11/18/8)

From the analytical results it was established that **P1** was synthesised.

6.2.9 Synthesis of (N,C) Au(III) 5-bromo-2-(4-bromophenyl)pyridine complex

The title compound was synthesized after a reported procedure[33]. **L3** (0.0471 g, 0.15 mmol, 1 equiv.) and $HAuCl_4 \cdot H_2O$ (0.0588 g, 0.15 mmol, 1 equiv.) was added to a microwave vessel followed by 5 ml of distilled water. Acetonitrile was added dropwise until **L3** started mixing with the water, fluffy precipitate was observed. The vessel was transferred into a microwave and heated to 160 °C for 60 min. Brown solid had formed and liquid turned clear during heating. The mixture was cooled to rt no precipitate was formed. The solids were washed with distilled water approximately 2 mL followed by acetonitrile approximately 2 mL, then one last time with distilled water approximately 2 mL. The washed solids were dried under air stream for 60 min yielding impure **P2** as a brown solid. As the product could not be isolated no yield was established. The product was confirmed by ^{1}H NMR and ESI-MS analysis (**A 36**, **A 45** and **A 46**).

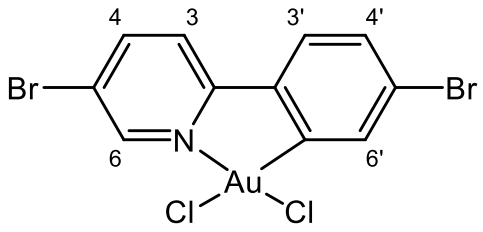

P2

^{1}H NMR (400 MHz, DMSO-d_6) δ 9.54 (d, *J* = 2.0 Hz, 1H, **H^6**), 8.73 (dd, *J* = 8.7, 2.1 Hz, 1H, **H^4**), 8.44 (d, *J* = 8.7 Hz, 1H, **H^3**), 8.03 (d, *J* = 8.6 Hz, 1H, **H$^{3'}$**), 7.94 (d, *J* = 1.8 Hz, 1H, **H$^{6'}$**), 7.81 – 7.74 (m, 1H, **H$^{4'}$**).

MS (ESI, Acetonitrile): m/z (rel. %): 541/543/545 ([M - Cl], 46/100/70)

From the analytical results it was established that **P2** was probably synthesised but not isolated.

6.2.10 Reactivity of AuPincOAc^{F} toward R4 in the presence of TFA

Recreation of catalytic experiment previously reported in the Tilset group[21]. **AuPincOAc^{F}** (7.60 mg, 0.013 mmol, 1.00 equiv.) was dissolved in CD_2Cl_2 (0.5 mL) and 0.1 mL of TFA were added. The colourless solution was transferred to an NMR tube. In another NMR tube a reference sample of **R4** (0.002 mL) in CD_2Cl_2 (0.5 mL) was prepared. Reference spectra of both samples were recorded. Afterwards **R4** (1.8 µL, 0.017 mmol, 1.25 equiv.) was added to the solution of **AuPincOAc^{F}** and the reaction was monitored by ^{1}H-NMR spectroscopy every 5 minutes for 180 min. The formation of **C1** was indicated by two new sets of signals consisting of three multiplets each between δ 5.84 to 5.28 ppm and δ 2.49 to 1.85 ppm. The product was confirmed by the ^{1}H NMR spectrum after 180 min (**A 3**).

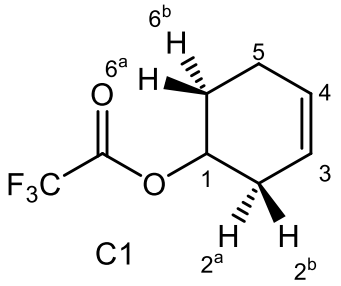

^{1}H NMR (500 MHz, CD_2Cl_2) δ 5.84 – 5.70 (m, 1H, **H^{4}**), 5.60 (d, *J* = 9.8 Hz, 1H, **H^{3}**), 5.28 (td, *J* = 5.7, 2.9 Hz, 1H, **H^{1}**), 2.49 (d, *J* = 17.8 Hz, 1H, **H^{2a}**), 2.33 – 2.09 (m, 3H, **H$^{2b + 5}$**), 2.03 – 1.85 (m, 2H, **H$^{6a + 6b}$**).

AuPincOAc^{F} are visible in the aromatic region between δ 8.45−7.00 ppm and a signal at δ 1.44-1.33 ppm. The resonance between δ 0.53−0.09 ppm are impurities that might arise from grease.

The analytical results were in agreement with previously reported data for **C1**[21].

6.2.11 Reactivity of AuPincOAc^{F} toward R4 in TFE-d_3

Recreation of catalytic experiment previously reported in the Tilset group[21]. **AuPincOAc^{F}** (2.70 mg, 4.5 μmol, 5 mol%) was suspended in TFE-d_3 (ca. 0.75 mL). The solution was transferred to an NMR tube and a reference ^{1}H-NMR spectrum was recorded. Then **R4** (9.75 μL, 90 μmol, 1 equiv.) was added to the solution via a syringe and the reaction was monitored by ^{1}H-NMR spectroscopy every 5 min over 180 min. Almost full conversion of **R4** into **C2** was observed after 180 minutes. The product was confirmed by the ^{1}H NMR spectrum after 180 min (A 4**)**

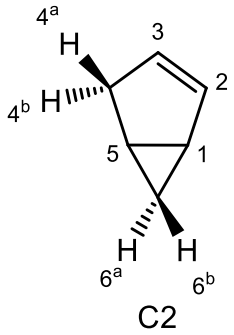

C2

^{1}H NMR (500 MHz, TFE-d_3) δ 5.93 (1H, **H^{2}**), 5.37 (1H, **H^{3}**), 2.53 (1H, **H^{4a}**), 2.23 (1H, **H^{4b}**), 1.76 (1H, **H^{1}**), 1.55 (1H, **H^{5}**), 0.78 (1H, **H^{6a}**), -0.23 (1H, **H^{6b}**).

The analytical results were in agreement with previously reported data for **C2**[21].

6.2.12 Reactivity of AuPincOAc^{F} toward R1 in the presence of TFA

Recreation of catalytic experiment previously reported in the Tilset group[21]. **AuPincOAc^{F}** (7.7 mg, 0.013 mmol, 1.00 equiv.) was dissolved in CD_2Cl_2 (0.5 mL) and 0.1 mL of TFA were added. The solution was transferred to an NMR tube and a reference spectrum was recorded. Then **R1** (3.3 µL, 0.020 mmol, 1.53 equiv.) was added to the **AuPincOAc^{F}** solution and the reaction was monitored every 10 min over 180 min. After 60 minutes no signal from **R1** or **C3** were observed. The solution had turned a purple colour during the 180 min NMR monitoring. **C3** was confirmed by the first ^{1}H NMR spectrum recorded of the experiment (**A 5**)

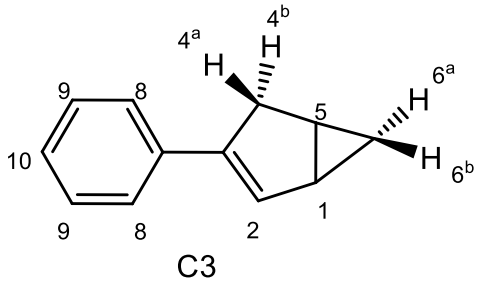

C3

^{1}H NMR (500 MHz, CD_2Cl_2) δ 7.41 – 7.14 (5H, **H^{8,9,10}**), 6.40 (1H, **H^{2}**), 2.97 (1H, **H^{4a}**), 2.71 (1H, **H^{4b}**), 1.92 (1H, **H^{1}**), 1.71 (1H, **H^{5}**), 0.91 (1H, **H^{6a}**), 0.5 (1H, **H^{6b}**).

The analytical results were in agreement with previously reported data for **C3**[21].

6.2.13 Catalytic control experiments

An NMR tube was loaded with approximately 1.00 µL (approximately 0.9 mmol) of the hexenyne starting materials or **AuPincOAc^{F}** 2 mg (0.0035 mmol) dissolved in the desired deuterated NMR solvent (0.5 mL). The experiment was monitored by ^{1}H NMR spectroscopy over a period of seven days.

Reactivity and stability of R4 in TFA-d in absence of AuPincOAc^{F}.

No changes were observed over a period of seven days.

Reactivity and stability of R1 in TFA-d in absence of AuPincOAc^{F}.

Upon dissolving **R1** in TFA-d the solution gradually turned a light pink colour.
No changes were observed over a period of seven days other than a darkening of the pink to a more purple colour.

Reactivity and stability of R2 in TFA-d in absence of AuPincOAc^{F}.

Upon dissolving **R2** in TFA-d the solution gradually turned a light-yellow colour. No changes were observed over a period of seven days.

Reactivity and stability of AuPincOAc^{F} in TFA-d.

No changes were observed over a period of seven days other than a darkening of the pink colour.

Reactivity and stability of R4 in CD_2Cl_2 in absence of AuPincOAc^{F}.

No changes were observed over a period of seven days.

Reactivity and stability of R1 in CD_2Cl_2 in absence of AuPincOAc^{F}.

No changes were observed over a period of seven days.

Reactivity and stability of R2 in CD_2Cl_2 in absence of $AuPincOAc^F$.

No changes were observed over a period of seven days.

Reactivity and stability of $AuPincOAc^F$ in CD_2Cl_2.

Over a period of seven days the mixture started to turn purple, likely decomposition of **$AuPincOAc^F$**.

Bibliography

1. C. Louis and O. Pluchery, *Gold Nanoparticles for Physics, Chemistry and Biology*, ICP, 2011.
2. S. Löffelsender, P. Schwerdtfeger, S. Grimme and J.-M. Mewes, *J. Am. Chem. Soc*, 2022, **144**, 485-494.
3. R. Chang and K. Goldsby, *Chemistry*, McGraw Hill, 12th edn., 2016.
4. Y. Okinaka and M. Hoshino, *Gold Bull.*, 1998, **31**, 3-13.
5. C. F. Shaw, *Chem. Rev*, 1999, **99**, 2589-2600.
6. A. Oskarsson, *j. EFSA*, 2016, **14**, 4362.
7. N. R. Panyala, E. M. Peña-Méndez and J. Havel, *J. Appl. Biomed.*, 2009, **7**, 75-91.
8. G. Hermann, V. Wilhelm and S. Kurt,*Germany Pat.*, DE1244766B, 1967.
9. Y. Huang, X. Dong, Y. Yu and M. Zhang, *Appl. Surf. Sci.*, 2016, **387**, 1021-1028.
10. G. C. Bond and P. A. Sermon, *Gold Bull.*, 1973, **6**, 102-105.
11. M. Haruta, T. Kobayashi, H. Sano and N. Yamada, *Chem. Lett.*, 1987, **16**, 405-408.
12. B. Nkosi, N. J. Coville and G. J. Hutchings, *J. Chem. Soc., Chem. Commun.*, 1988, 71-72.
13. J. C. Fierro-Gonzalez and B. C. Gates, *Chem. Soc. Rev.*, 2008, **37**, 2127-2134.
14. Y. Fukuda and K. Utimoto, *J. Org. Chem.*, 1991, **56**, 3729-3731.
15. L. Prati and M. Rossi, *J. Catal.*, 1998, **176**, 552-560.
16. J. K. Edwards, B. E. Solsona, P. Landon, A. F. Carley, A. Herzing, C. J. Kiely and G. J. Hutchings, *J. Catal.*, 2005, **236**, 69-79.
17. E. E. Stangland, K. B. Stavens, R. P. Andres and W. N. Delgass, *J. Catal.*, 2000, **191**, 332-347.
18. Q. Fu, H. Saltsburg and M. Flytzani-Stephanopoulos, *Science*, 2003, **301**, 935-938.
19. S. Carrettin, J. Guzman and A. Corma, *Angew. Chem. Int. Ed.*, 2005, **44**, 2242-2245.
20. M. S. M. Holmsen, Ph.D. Dissertation, University of Oslo, Faculty of Mathematics and Natural Sciences, Department of Chemistry, 2019.
21. I. Schmidtke, Master Thesis, University of Oslo, 2020.
22. I. Schmidtke, Erasmus project, University of Oslo/University of Hamburg, 2019.
23. F. Mohr, *Gold Bull.*, 2004, **37**, 164-169.
24. H. Schmidbaur and K. C. Dash, *Adv. Inorg. Chem.*, 1982, **25**, 239-266.
25. A. S. K. Hashmi, J. P. Weyrauch, M. Rudolph and E. Kurpejović, *Angew. Chem. Int. Ed.*, 2004, **43**, 6545-6547.
26. G. O. Spessard and G. L. Miessler, *Organometallic Chemistry*, OUP, 3rd edn., 2016.
27. H. Schmidbaur and A. Schier, *Arab. J. Sci. Eng.*, 2012, **37**, 1187-1225.
28. D. Aguilar, M. Contel, R. Navarro and E. P. Urriolabeitia, *Organometallics*, 2007, **26**, 4604-4611.
29. M. Albrecht, *Chem. Rev.*, 2010, **110**, 576-623.
30. M. Bachmann, J. Terreni, O. Blacque and K. Venkatesan, *Chemistry*, 2017, **23**, 3837-3849.
31. J. A. Garg, O. Blacque and K. Venkatesan, *Inorg. Chem.*, 2011, **50**, 5430-5441.
32. E. C. Constable and T. A. Leese, *J. Organomet. Chem.*, 1989, **363**, 419-424.
33. A. P. Shaw, M. Tilset, R. H. Heyn and S. Jakobsen, *J. Coord. Chem.*, 2011, **64**, 38-47.
34. J. Martín, E. Gómez-Bengoa, A. Genoux and C. Nevado, *Angew. Chem. Int. Ed.*, 2022, **61**, e202116755.
35. K. Hylland, I. Schmidtke, D. S. Wragg, A. Nova and M. Tilset, *Dalton Trans.*, 2022, **51**, 582-597.
36. E. Peris and R. H. Crabtree, *Chem. Soc. Rev.*, 2018, **47**, 1959-1968.

37. G. van Koten, *Top. Organomet. Chem.*, 2013, **40**, 1-20.
38. M. E. O'Reilly and A. S. Veige, *Chem. Soc. Rev.*, 2014, **43**, 6325-6369.
39. R. Kumar and C. Nevado, *Angew. Chem. Int. Ed. Engl.*, 2017, **56**, 1994-2015.
40. J. Grajeda, A. Nova, D. Balcells, Q. J. Bruch, D. S. Wragg, R. H. Heyn, A. J. M. Miller and M. Tilset, *Eur. J. Inorg. Chem.*, 2018, **2018**, 3113-3117.
41. R. Kumar, A. Linden and C. Nevado, *Angew. Chem. Int. Ed*, 2015, **54**, 14287-14290.
42. M. A. Cinellu, A. Zucca, S. Stoccoro, G. Minghetti, M. Manassero and M. Sansoni, *J. Chem. Soc.*, 1996, , 4217-4225.
43. M. S. M. Holmsen, A. Nova, K. Hylland, D. S. Wragg, S. Øien-Ødegaard, R. H. Heyn and M. Tilset, *Chem. Commun.*, 2018, **54**, 11104-11107.
44. H. Schmidbaur and A. Schier, *Organometallics*, 2010, **29**, 2-23.
45. J. P. Genet, L. Leseurre, V. Michelet and P. Y. Toullec, *Org. Lett.*, 2007, **9**, 4049-4052.
46. E. Jimenez-Nunez and A. M. Echavarren, *Chem. Rev*, 2008, **108**, 3326-3350.
47. C. Obradors and A. M. Echavarren, *Acc. Chem. Res*, 2014, **47**, 902-912.
48. M. Marín-Luna, O. Nieto Faza and C. Silva López, *Front. Chem.*, 2019, **7**, 296.
49. M. R. Luzung, J. P. Markham and F. D. Toste, *J. Am. Chem. Soc*, 2004, **126**, 10858-10859.
50. J. P. Reeds, A. C. Whitwood, M. P. Healy and I. J. S. Fairlamb, *Organometallics*, 2013, **32**, 3108-3120.
51. P. K. Freeman, M. F. Grostic and F. A. Raymond, *J. Org. Chem.*, 1965, **30**, 771-777.
52. J. A. C. Broekaert, *Analytical and Bioanalytical Chemistry*, 2015, **407**, 8943-8944.
53. K. T. Hylland, S. Øien-Ødegaard and M. Tilset, *Eur. J. Org. Chem.*, 2020, **2020**, 4208-4226.
54. Z.-p. Zhan, J.-l. Yu, H.-j. Liu, Y.-y. Cui, R.-f. Yang, W.-z. Yang and J.-p. Li, *J. Org. Chem*, 2006, **71**, 8298-8301.
55. D. C. Harris and C. A. Lucy, *Quantitative chemical analysis*, Macmillan International Higher Education, New York, 9th edn., 2016.
56. S.-S. Weng, K.-Y. Hsieh and Z.-J. Zeng, *Tetrahedron*, 2015, **71**, 2549-2554.
57. J. B. Maria-Magdalena Cid, *Structure Elucidation in Organic Chemistry: The Search for the Right Tools*, Beaverton: Ringgold, Inc, Beaverton, 2015.
58. D. L. Pavia, *Introduction to spectroscopy*, Cengage Learning, Stamford, Conn, 5th edn., 2015.
59. N. Krause and A. S. K. Hashmi, *Modern Allene Chemistry*, Wiley-VCH, 1st edn., 2004.
60. S. Loss, *Basic 1D and 2D Experiments*, Bruker Biospin AG, 2005.
61. M. Barfield and B. Chakrabarti, *Chem. Rev*, 1969, **69**, 757-778.
62. E. I. Snyder and J. D. Roberts, *J. Am. Chem. Soc*, 1962, **84**, 1582-1586.
63. W. D. Huntsman, J. A. De Boer and M. H. Woosley, *J. Am. Chem. Soc.*, 1966, **88**, 5846-5850.
64. M. J. Ardolino and J. P. Morken, *J. Am. Chem. Soc.*, 2012, **134**, 8770-8773.
65. T. F. Headen, C. A. Howard, N. T. Skipper, M. A. Wilkinson, D. T. Bowron and A. K. Soper, *J. Am. Chem. Soc.*, 2010, **132**, 5735-5742.
66. M. Lepeltier, F. Appaix, Y. Y. Liao, F. Dumur, J. Marrot, T. Le Bahers, C. Andraud and C. Monnereau, *Inorg. Chem.*, 2016, **55**, 9586-9595.
67. G. St-Pierre, S. Ladouceur, D. Fortin and E. Zysman-Colman, *Dalton Trans.*, 2011, **40**, 11726-11731.
68. G. Dumartin, J.-P. Quintard and M. Pereyre, *J. Organomet. Chem.*, 1983, **252**, 37-46.

Appendix

NMR spectra

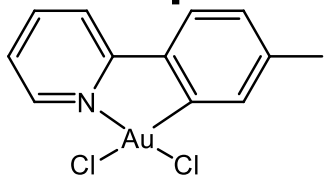

Au(tpy)

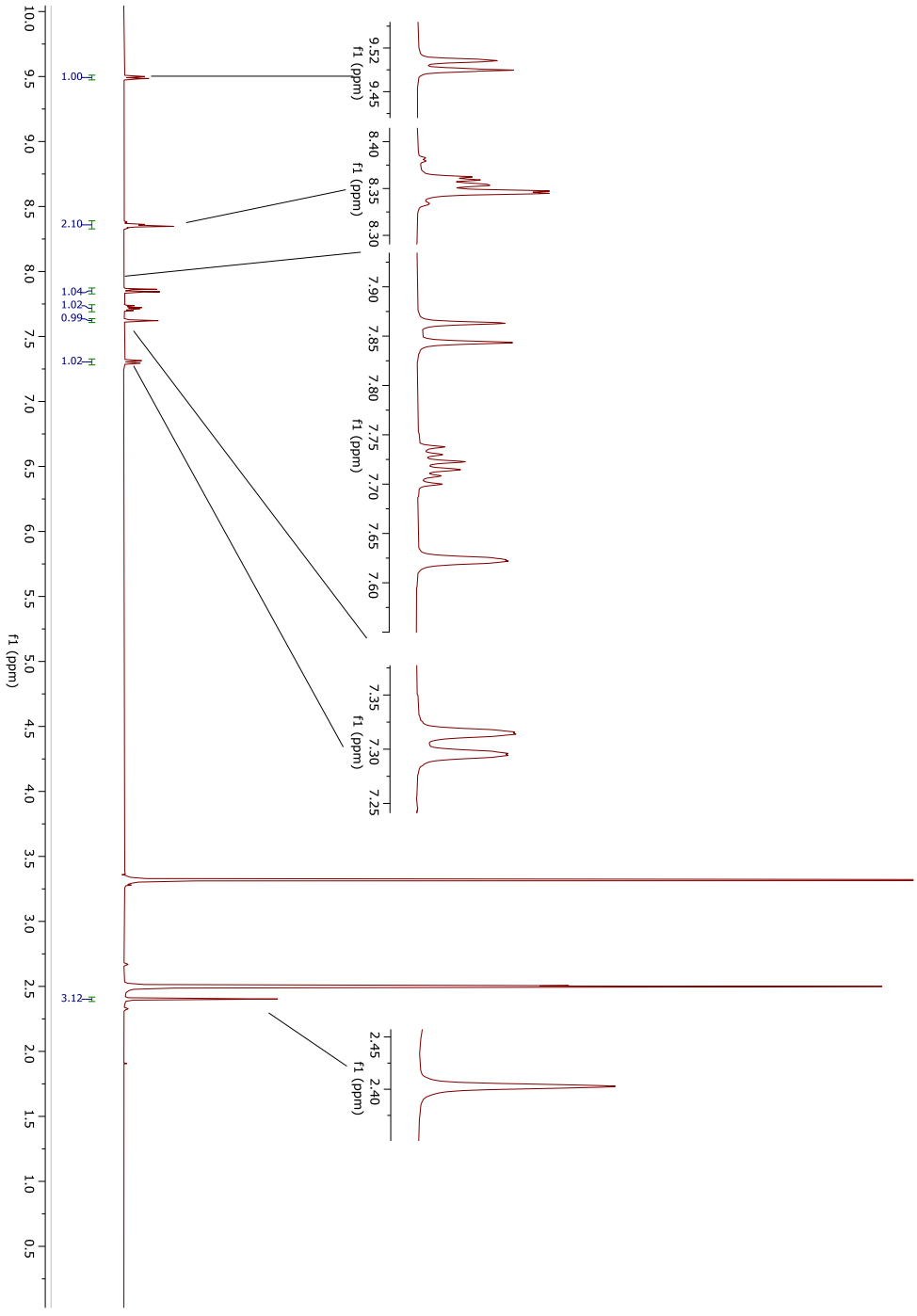

A 1. ^{1}H NMR (400 MHz, DMSO-d_6) spectrum of **Au(tpy)Cl$_2$** with embedded close-up view.

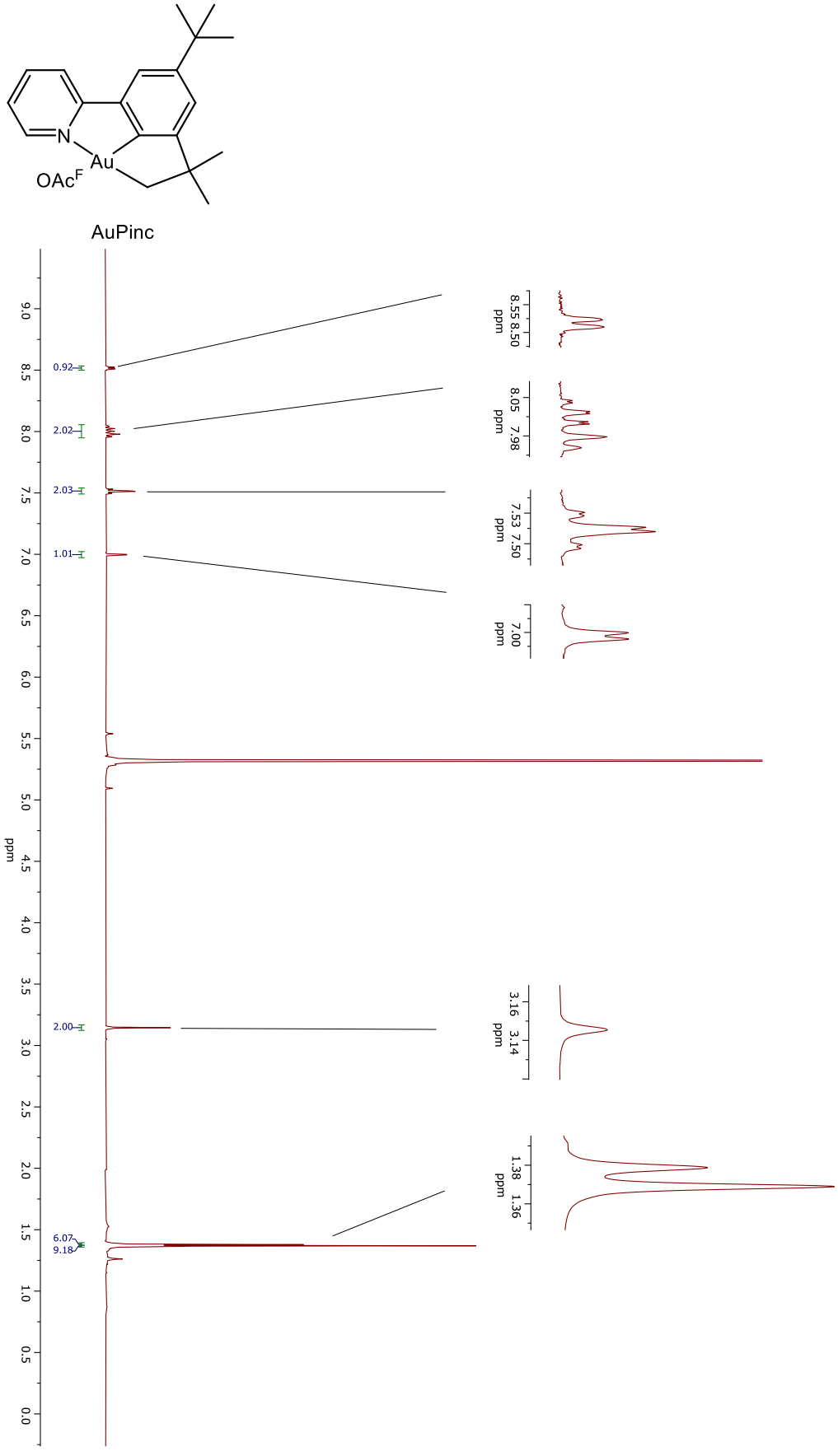

A 2. ^{1}H NMR (400 MHz, CD_2Cl_2) spectrum of **AuPincOAc^{F}** with embedded close-up view.

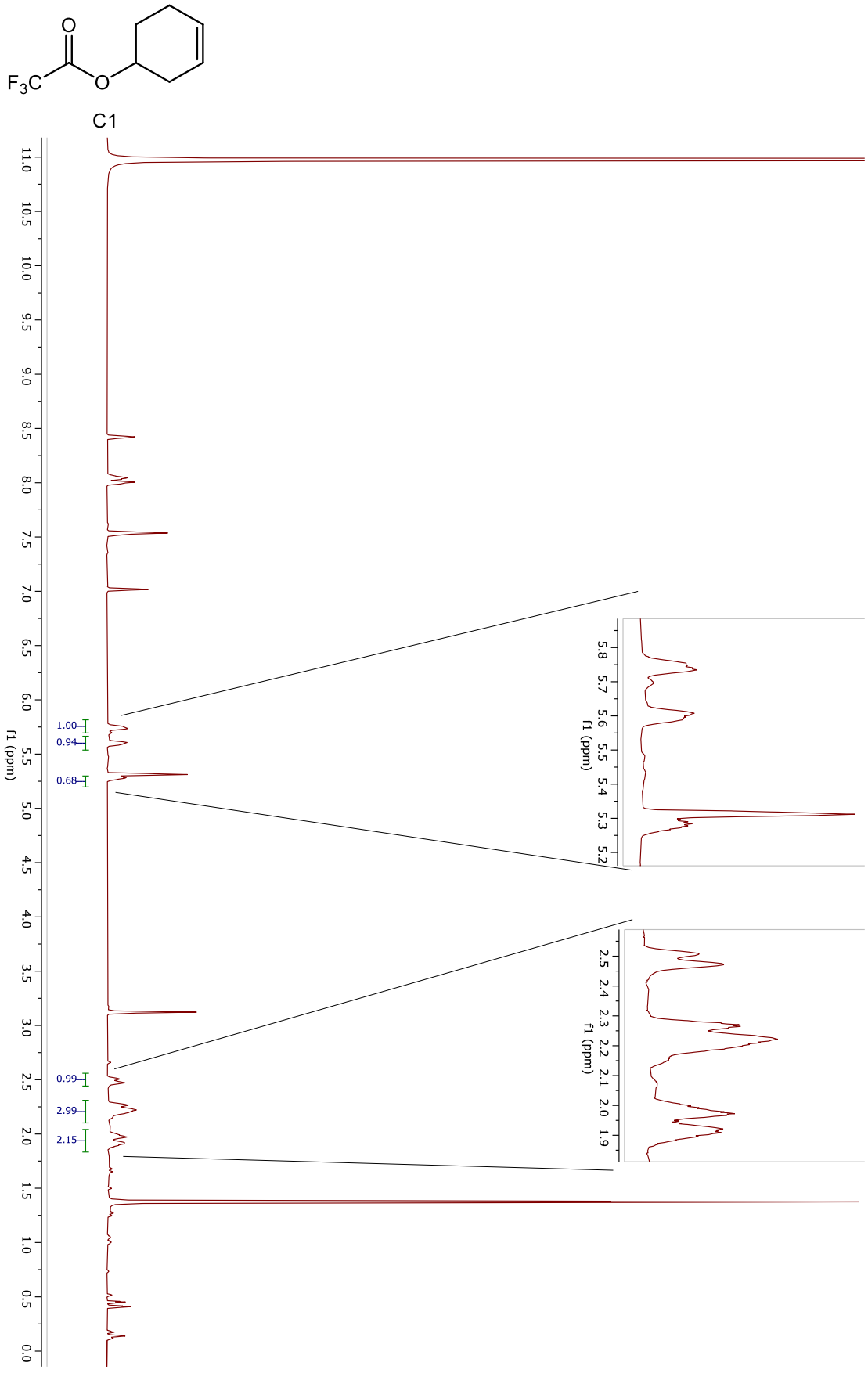

A 3. ^{1}H NMR (500 MHz, CD_2Cl_2) spectrum of **C1** from catalytic reaction after 180 min, with embedded close-up view.

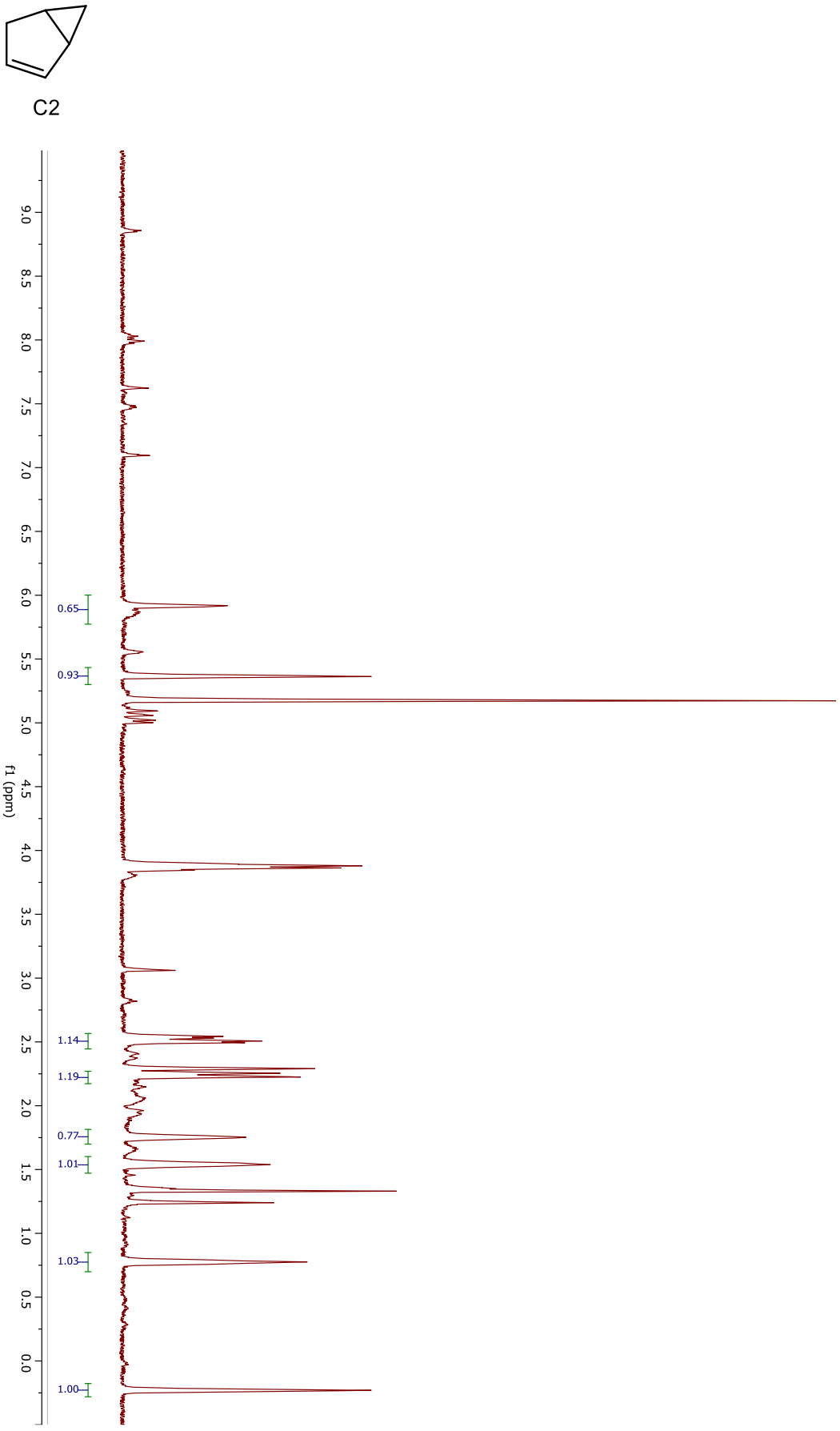

A 4. 1H NMR (500 MHz, TFE-d_3) spectrum of **C2** from catalytic reaction after 180 min.

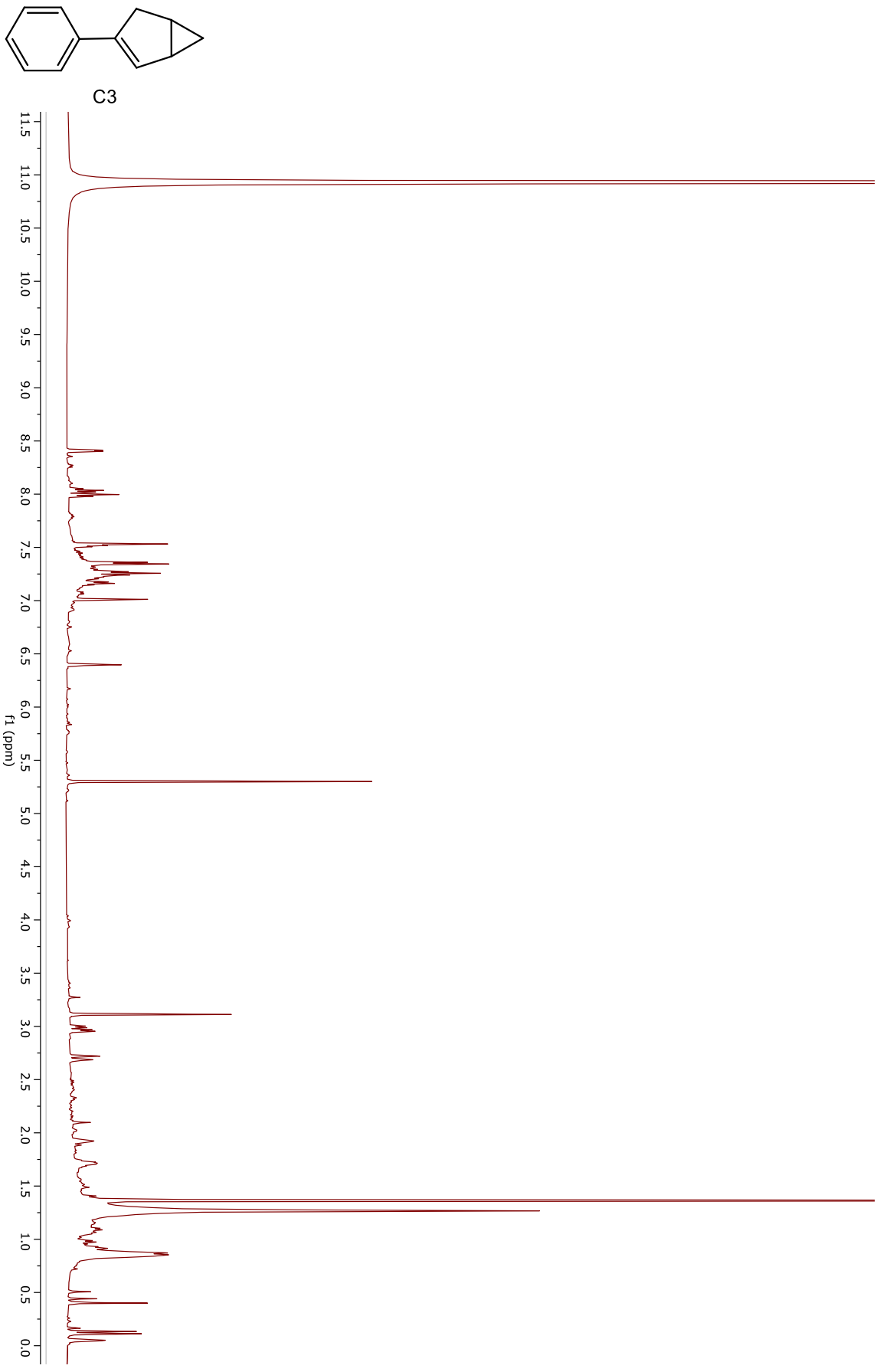

A 5. ^{1}H NMR (500 MHz, CD_2Cl_2) spectrum of **C3** from catalytic reaction after 10 min.

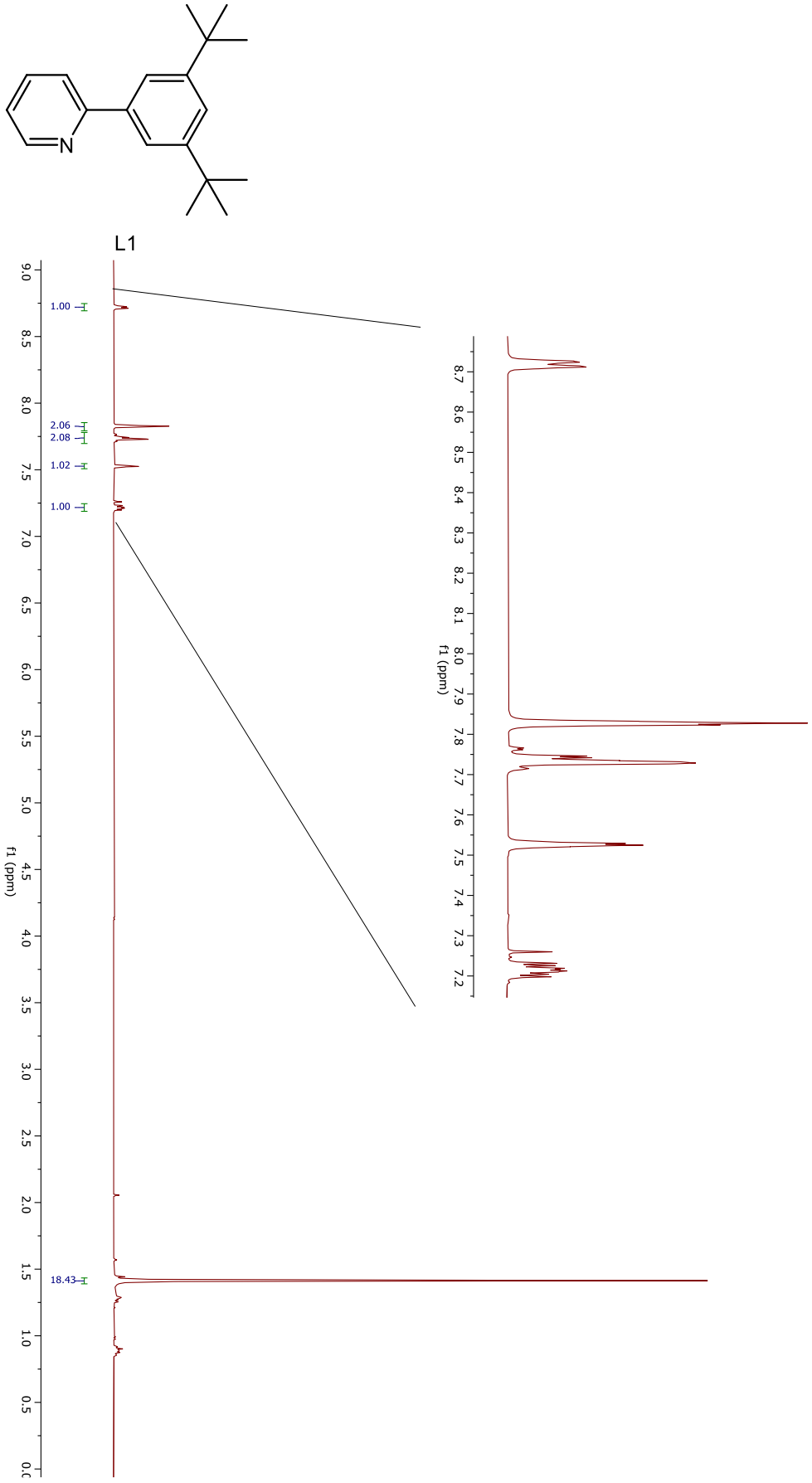

A 6. ^{1}H NMR (400 MHz, $CDCl_3$) spectrum of **L1** with embedded close-up view.

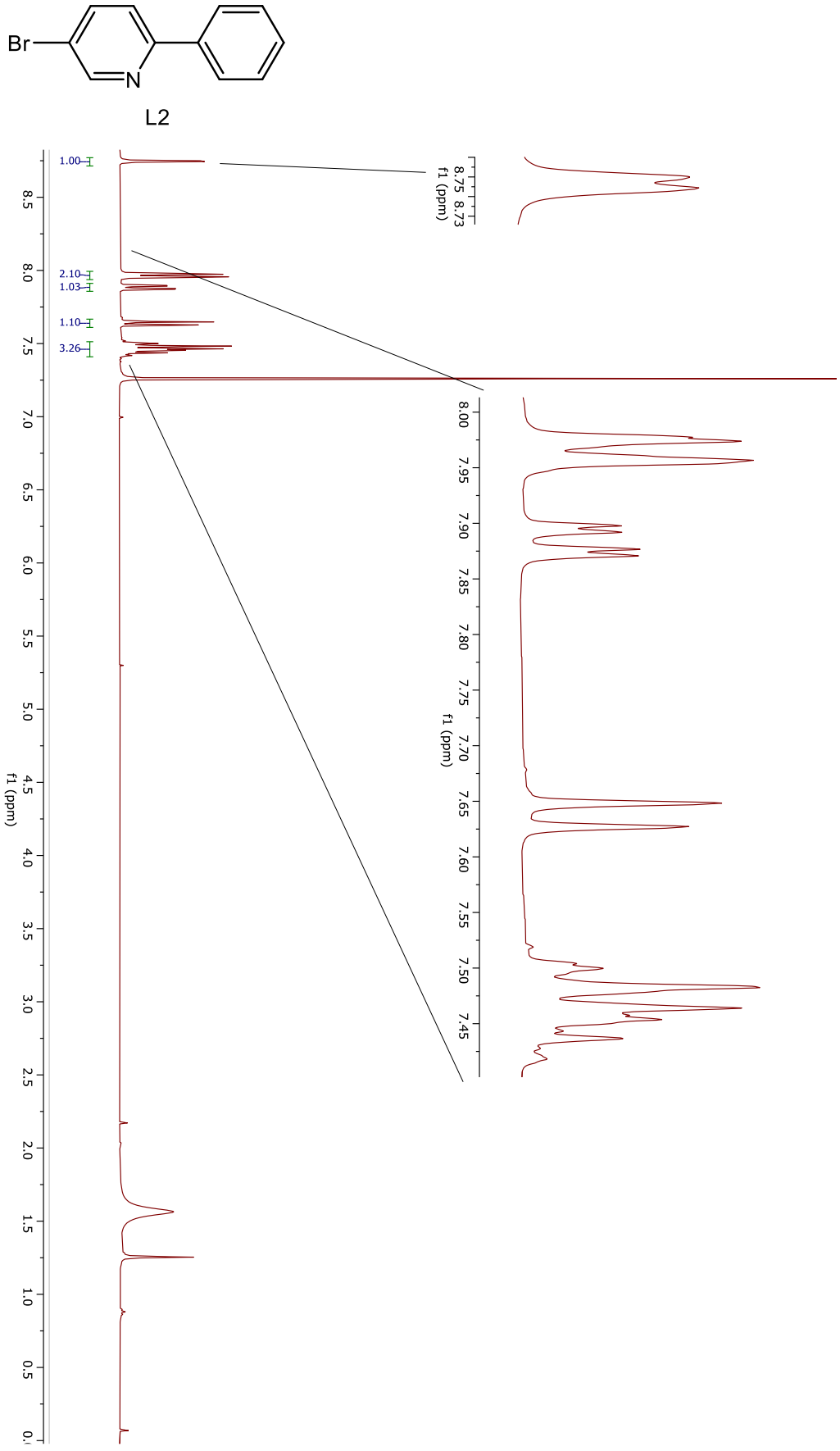

A 7. ^{1}H NMR (400 MHz, $CDCl_3$) spectrum of **L2** with embedded close-up view.

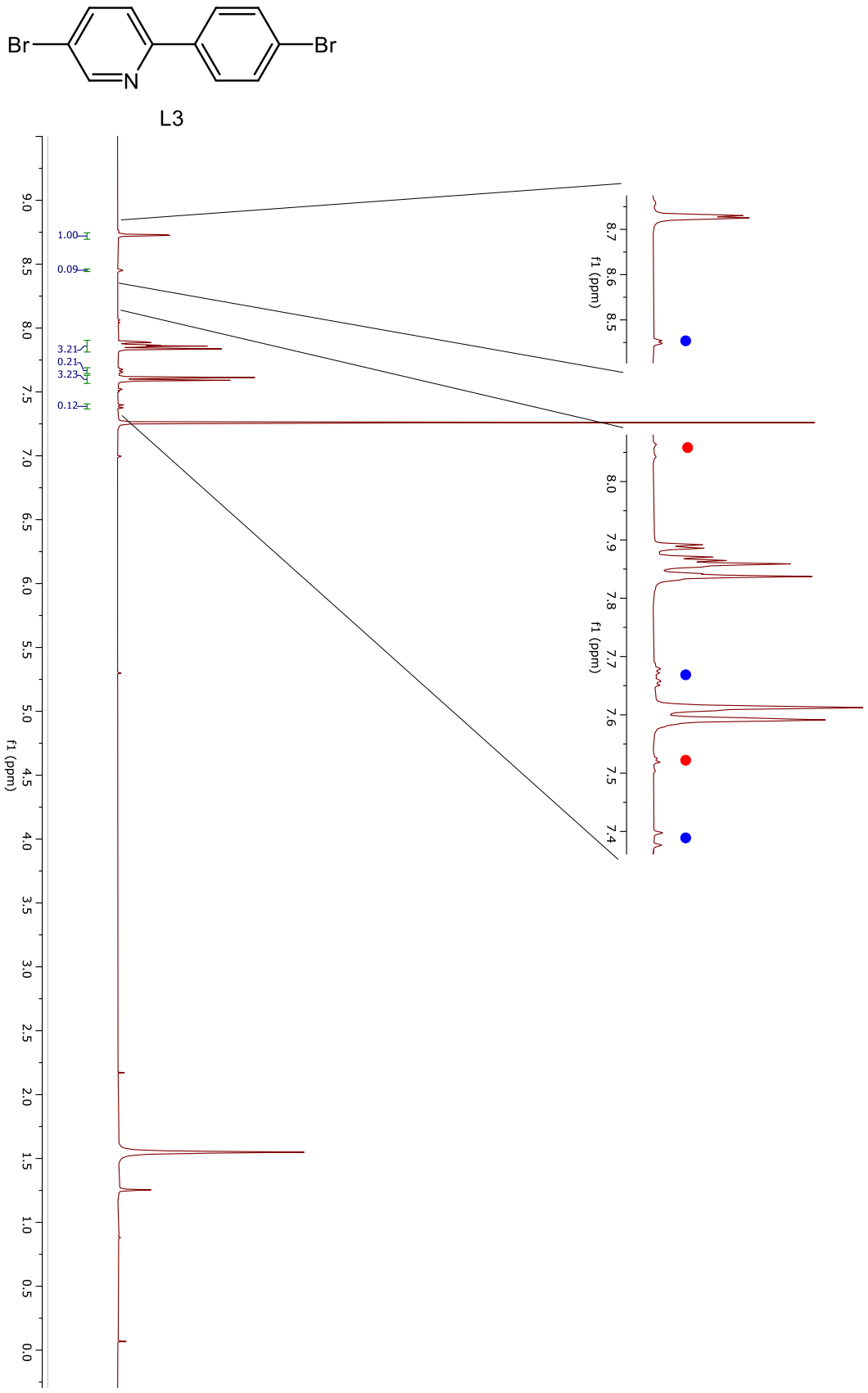

A 8. ^{1}H NMR (400 MHz, $CDCl_3$) spectrum of **L3**, unreacted pyridine (marked with blue dots) and unknown impurity (marked with red dots) with embedded close-up view. The signal at 5.3 ppm is DCM solvent not fully evaporated. The signal at 1.54 ppm is H_2O from solvent. The signal at 1.25 ppm is grease.

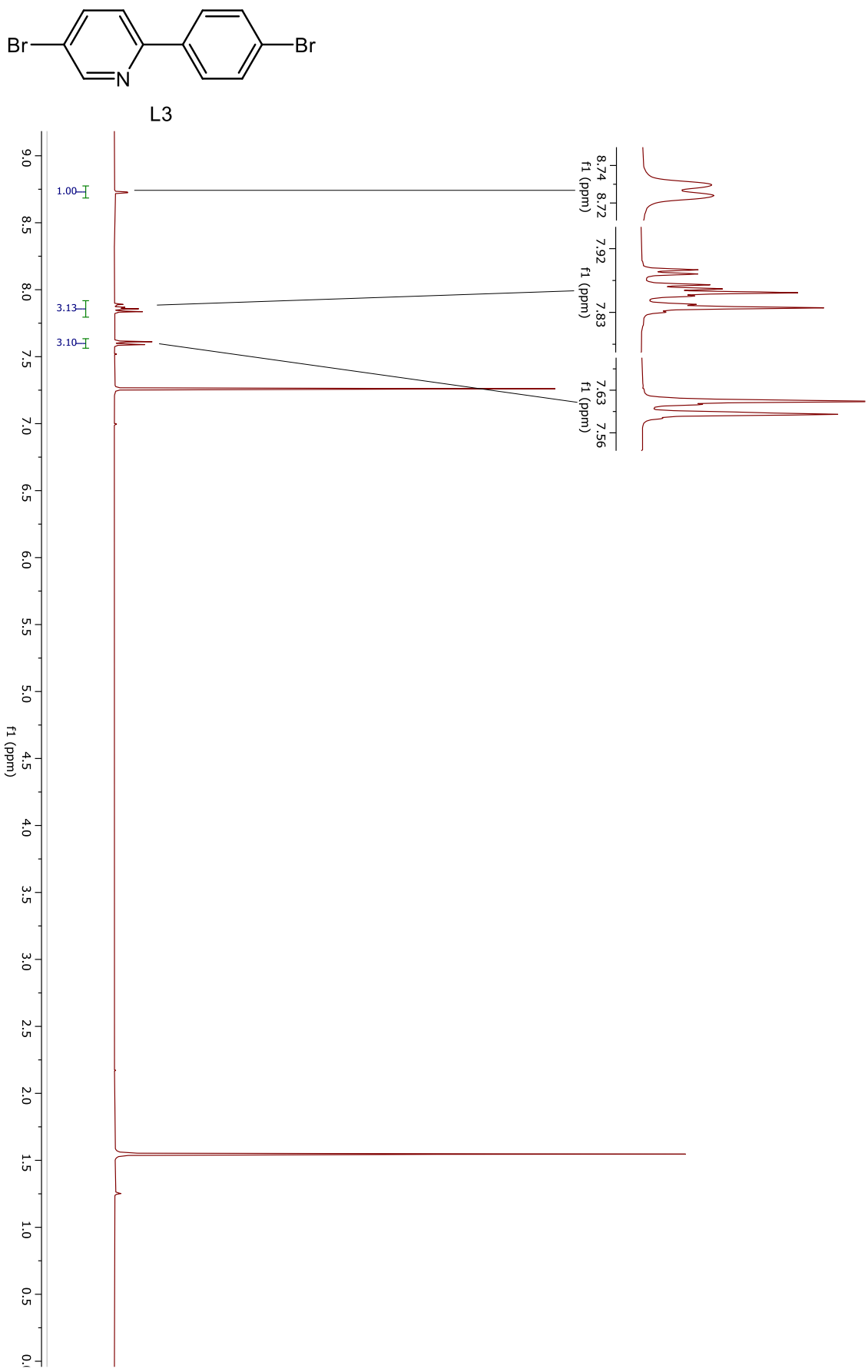

A 9. ^{1}H NMR (400 MHz, $CDCl_3$) spectrum of **L3** with embedded close-up view.

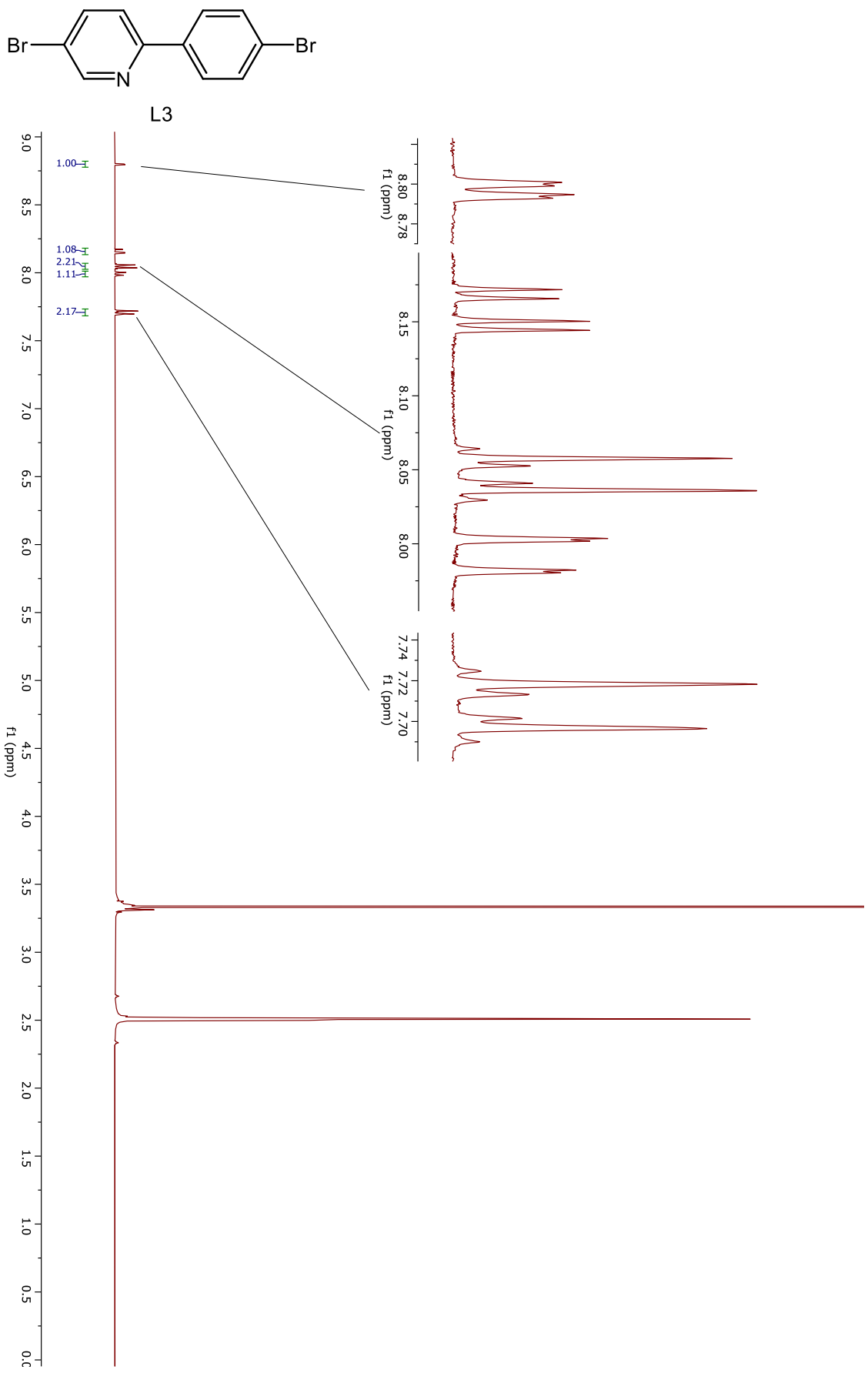

A 10. ^{1}H NMR (400 MHz, DMSO-d_6) spectrum of **L3** with embedded close-up view.

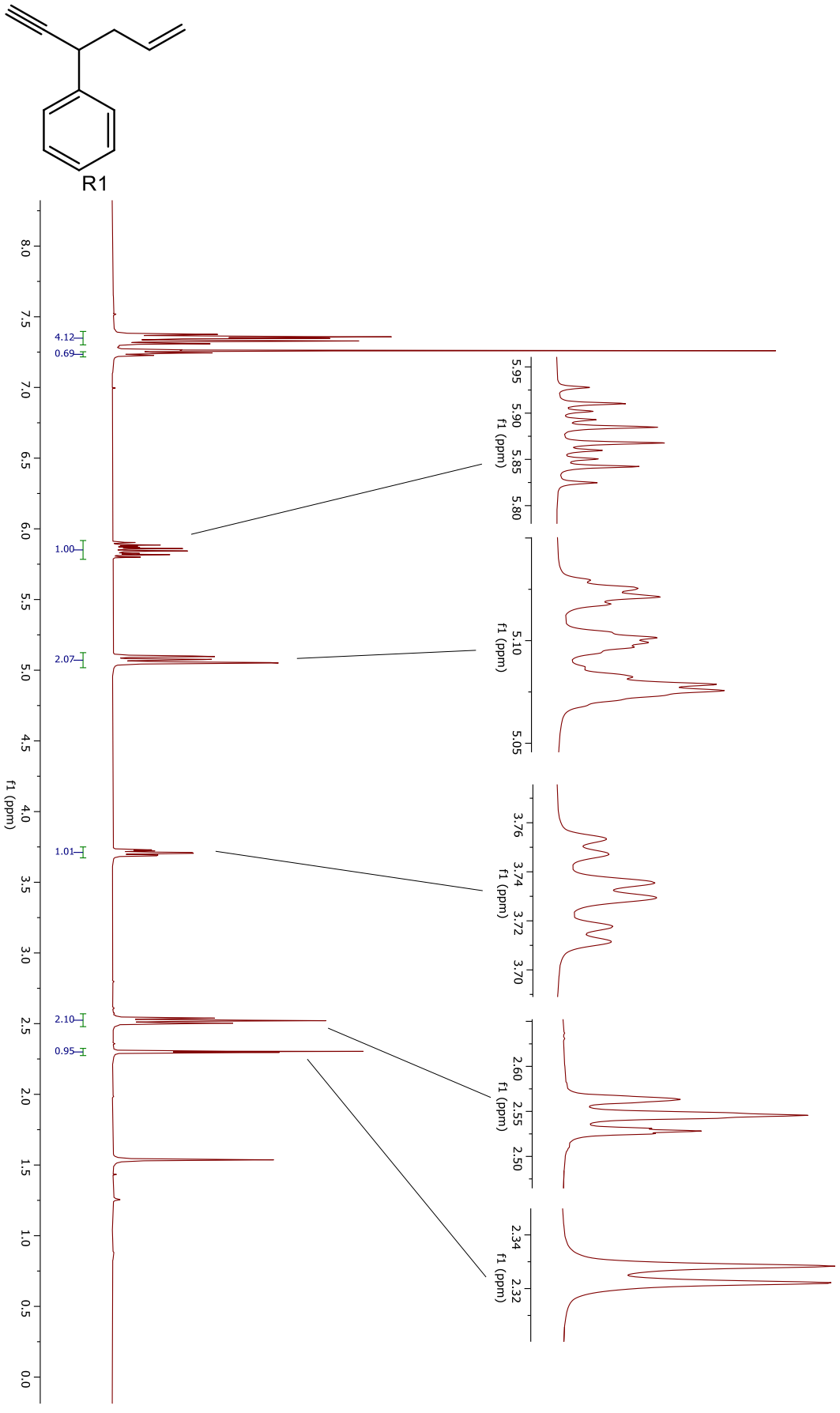

A 11. ^{1}H NMR (400 MHz, $CDCl_3$) spectrum of **R1** with embedded close-up view.

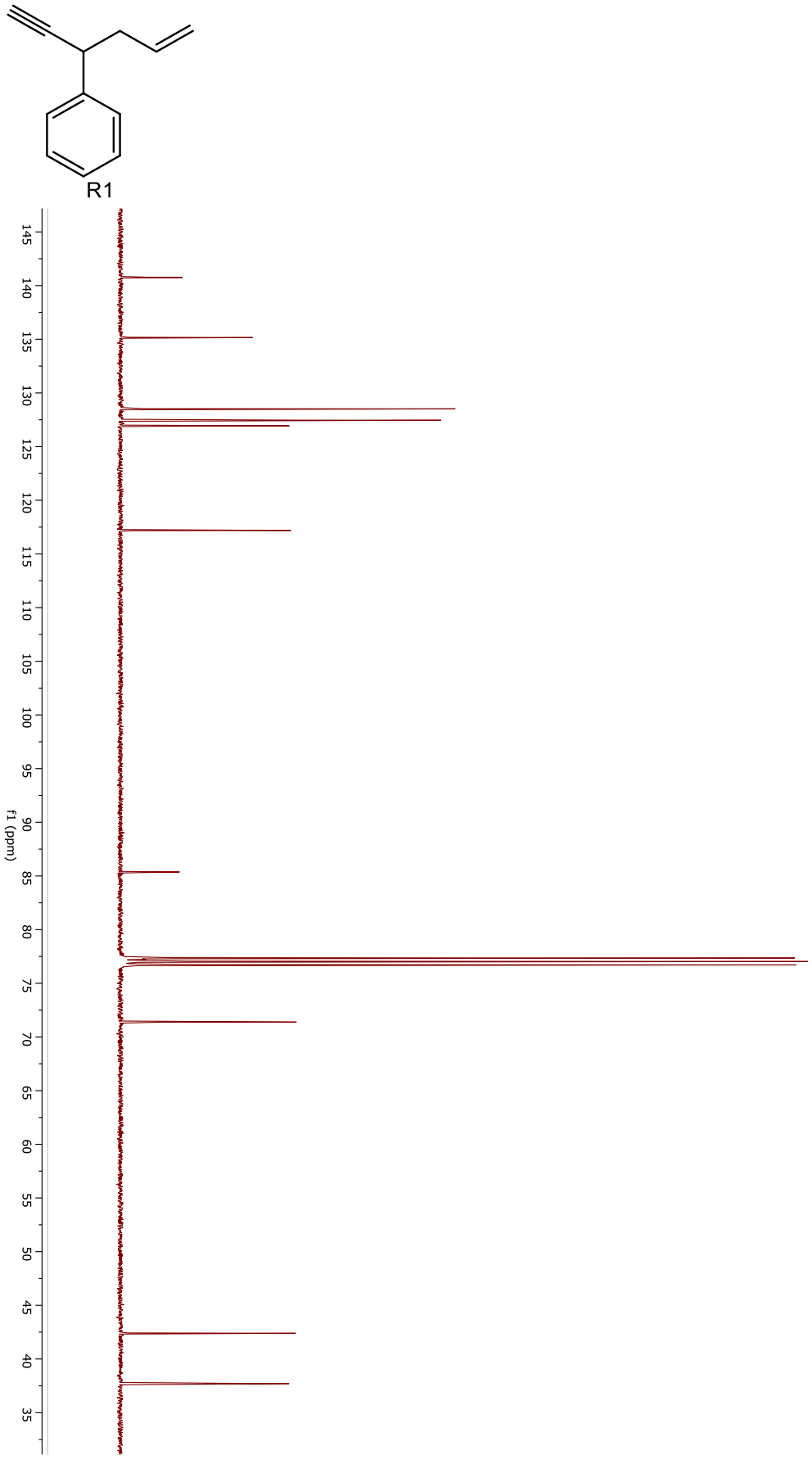

A 12. ^{13}C NMR (101 MHz, $CDCl_3$) spectrum of **R1**.

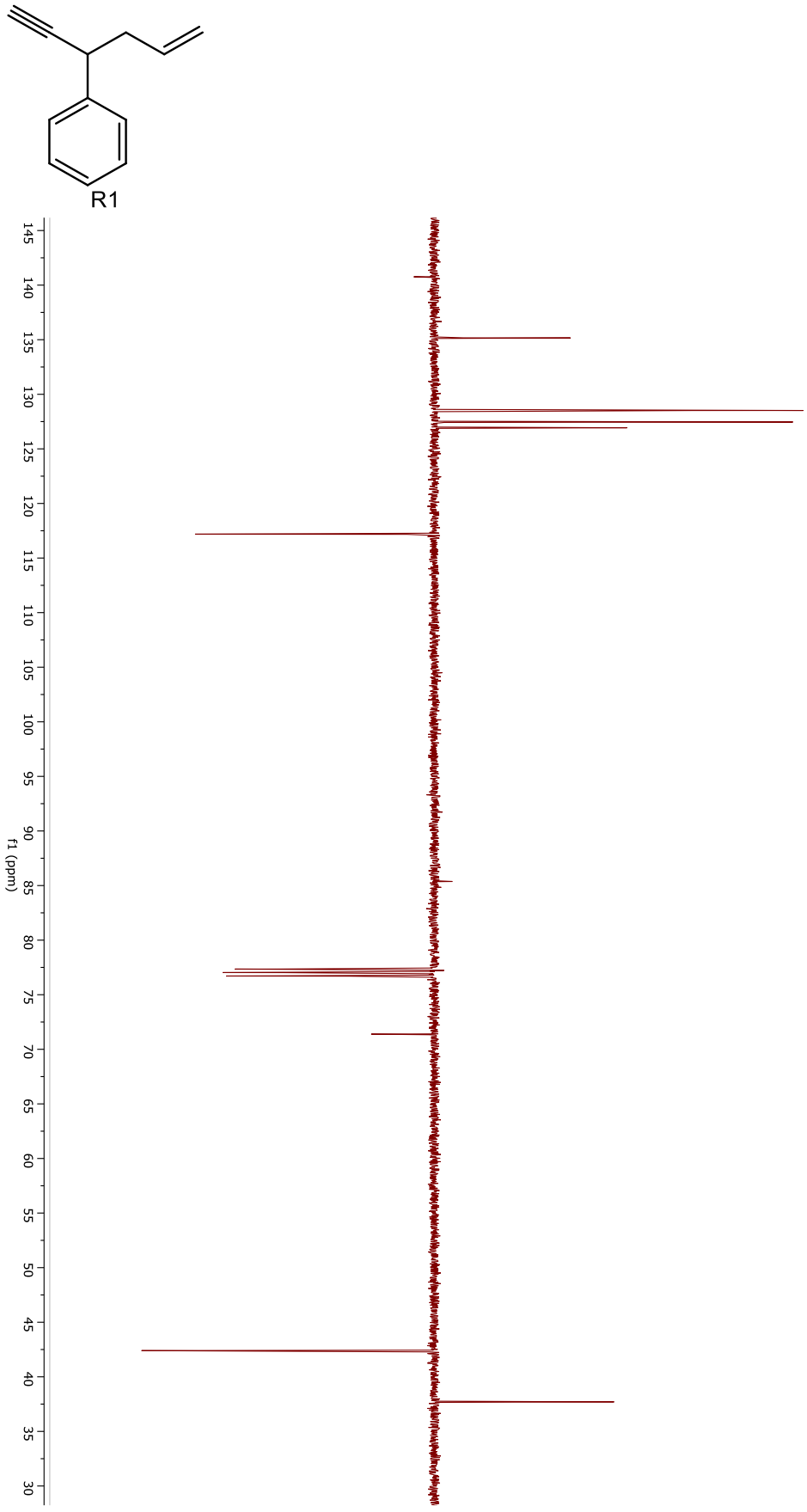

A 13. DEPTQ NMR (101 MHz, $CDCl_3$) spectrum of **R1**.

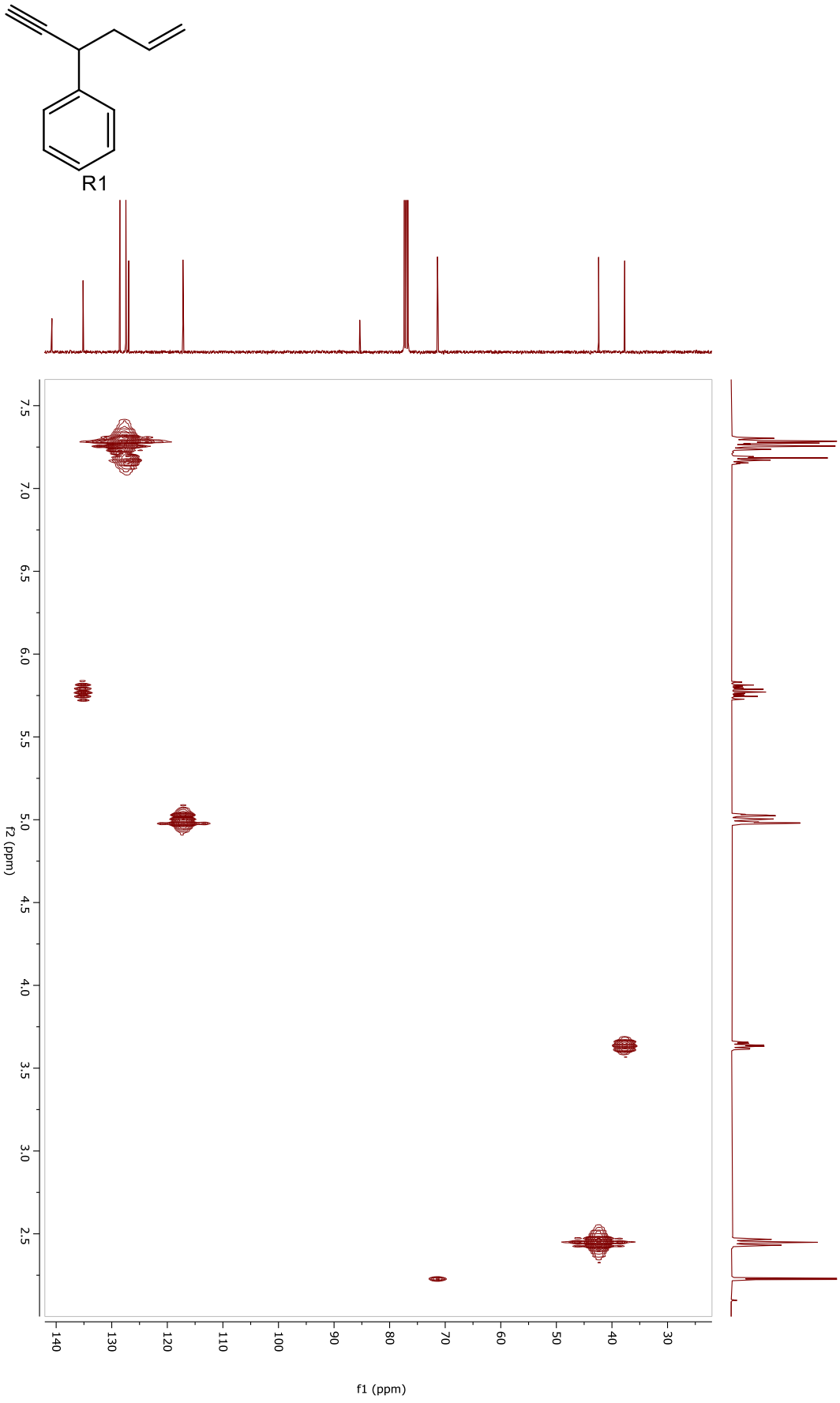

A 14. HSQC 2D NMR (400 MHz, $CDCl_3$) spectrum of **R1**.

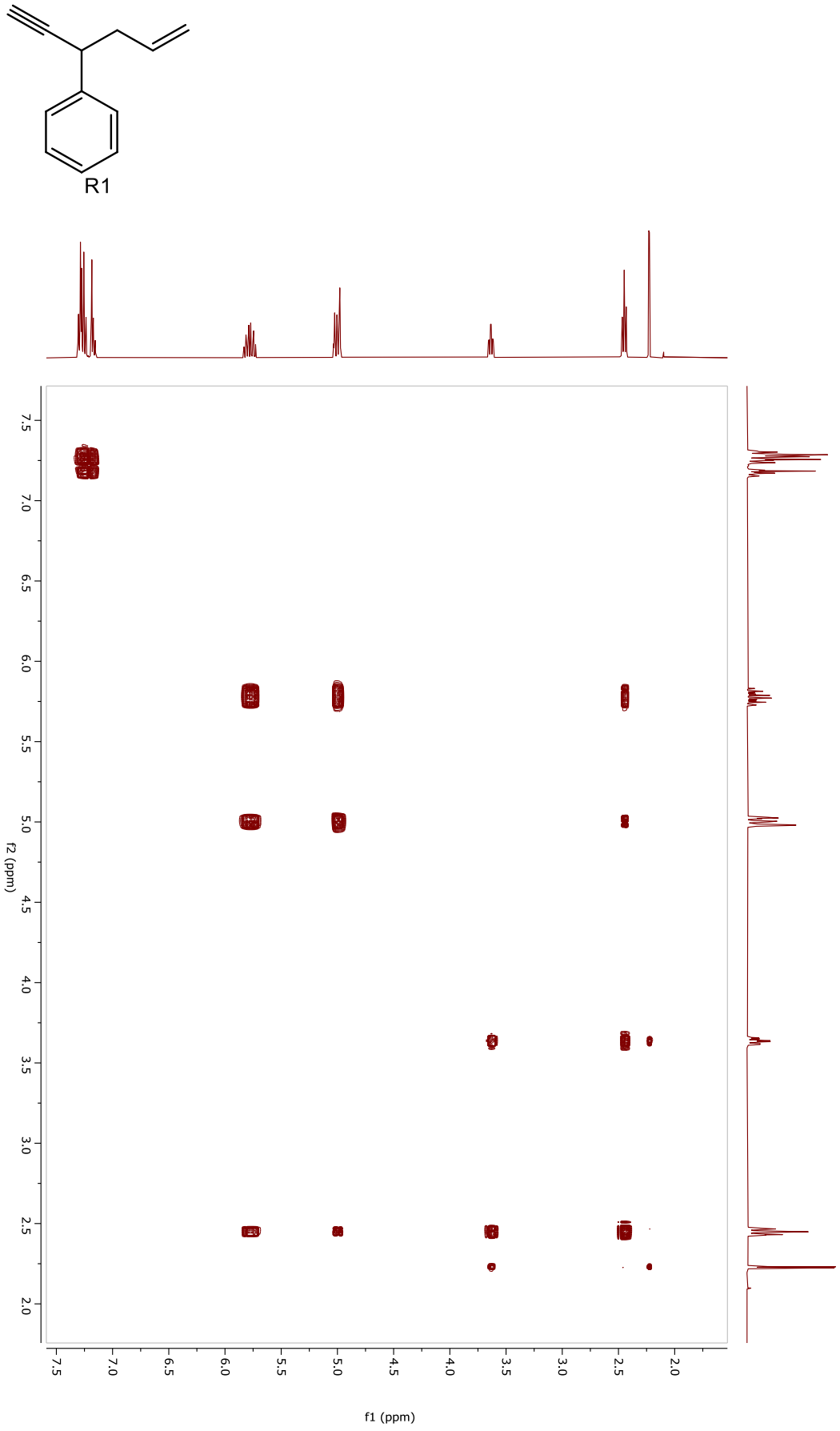

A 15. COSY 2D NMR (400 MHz, $CDCl_3$) spectrum of **R1**.

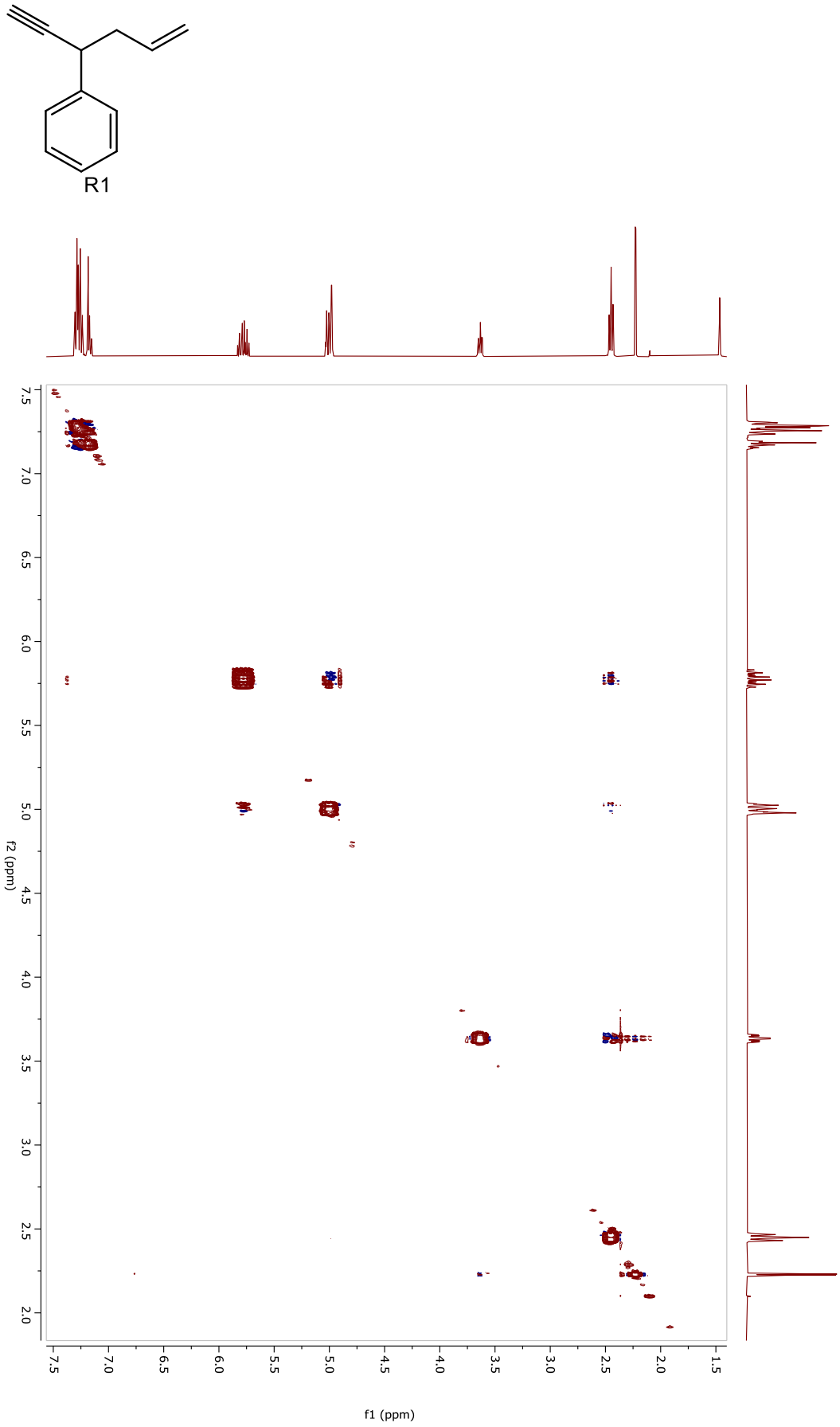

A 16. NOESY 2D NMR (400 MHz, $CDCl_3$) spectrum of **R1**.

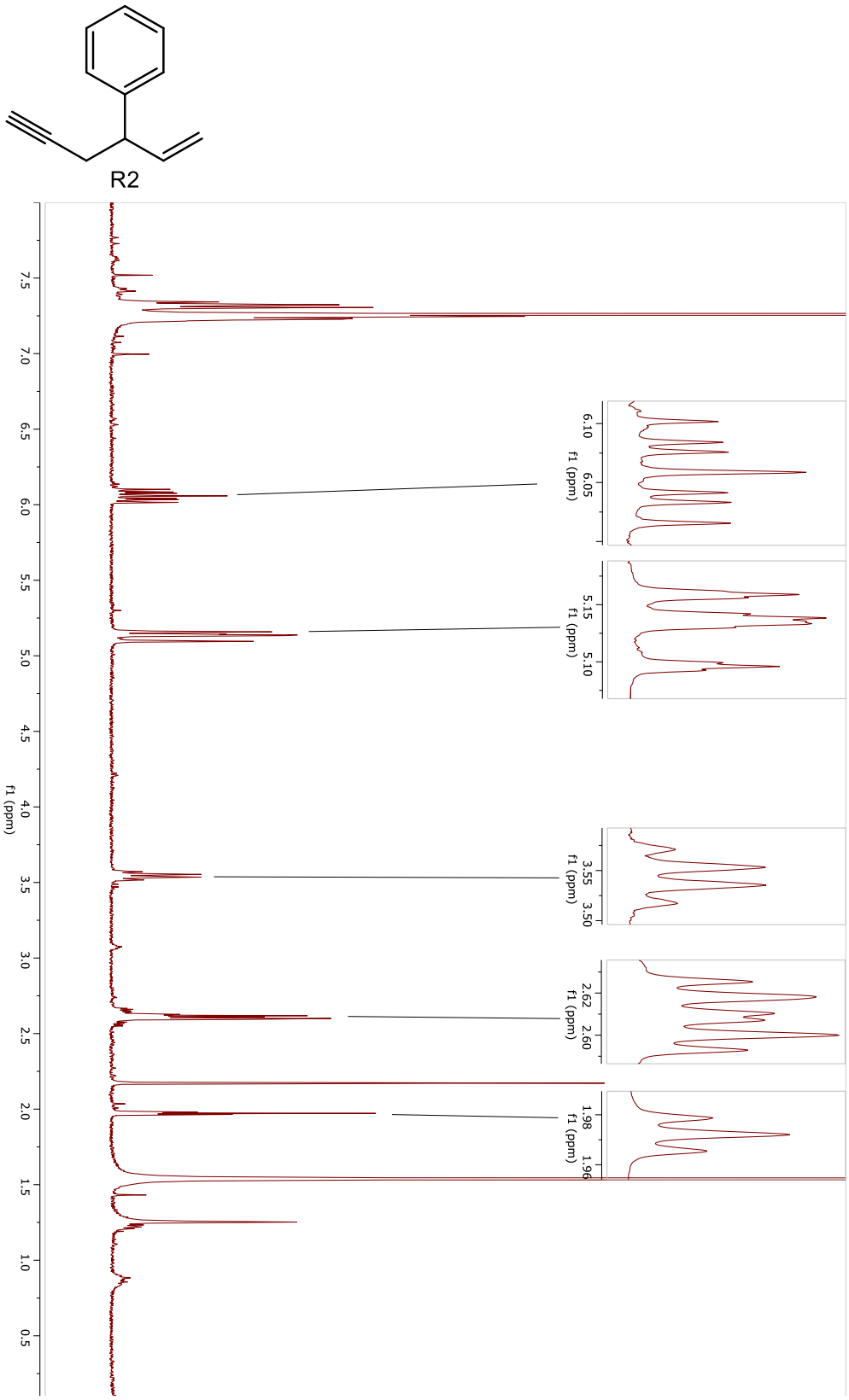

A 17. ^{1}H NMR (400 MHz, $CDCl_3$) spectrum of **R2** with embedded close-up view. The signal at 2.17 ppm identified as acetone, the signal at 1.54 as water form solvent. the signal at 1.25 ppm as grease and signal at 0.07 ppm as silicone grease. The sample size of **R2** was unusually small leading to deceptively large signals for mentioned contaminants.

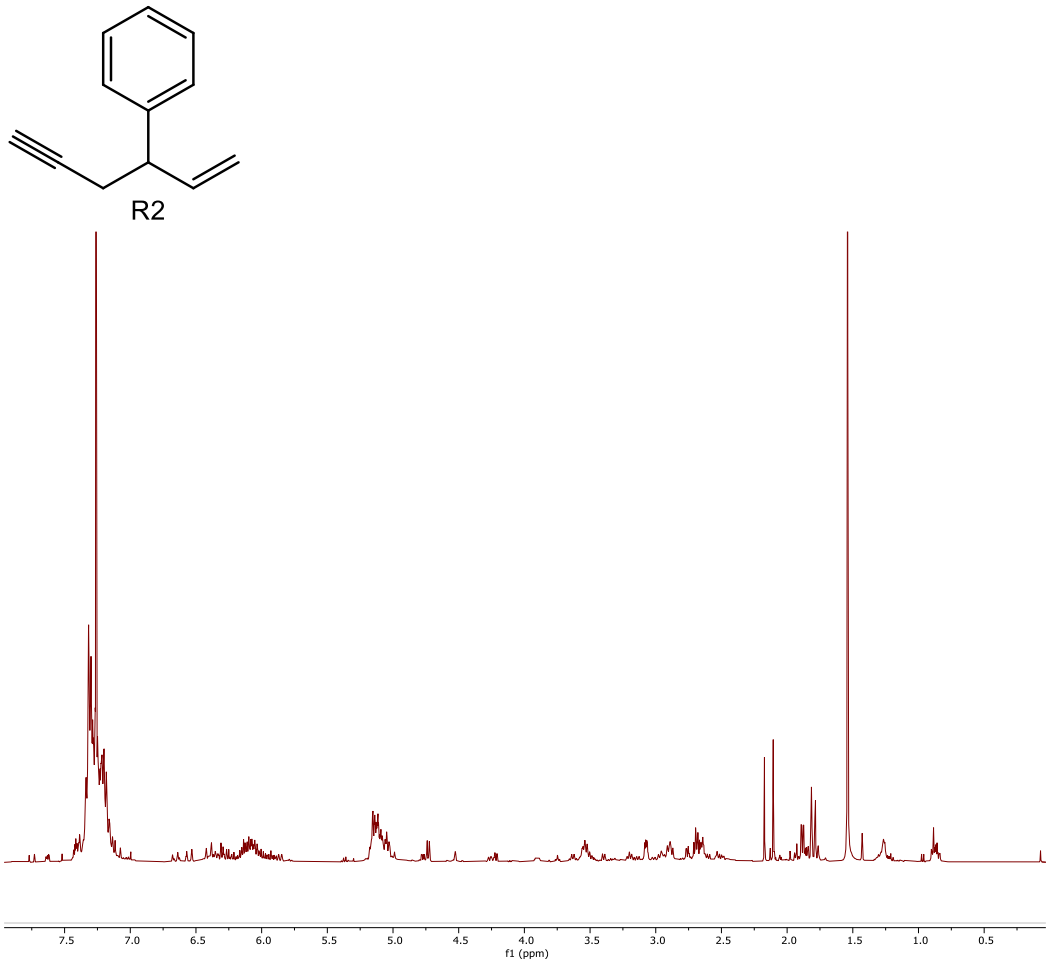

A 18. ^{1}H NMR (400 MHz, $CDCl_3$) spectrum of crude from synthesis of **R2** second attempt.

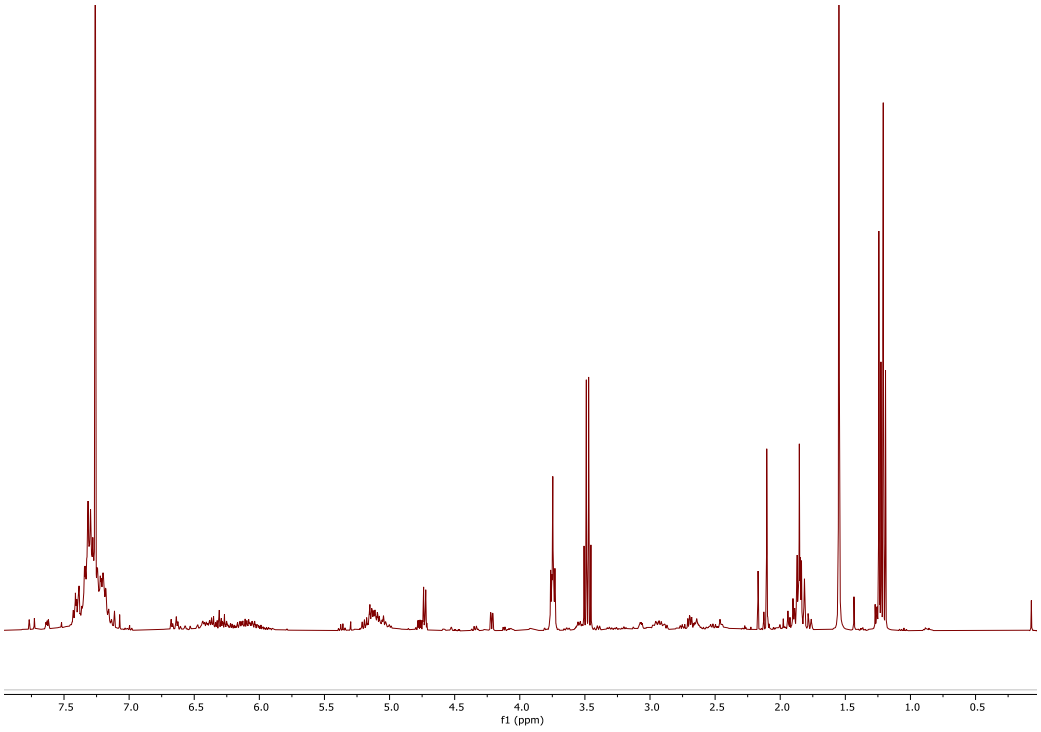

A 19. ^{1}H NMR (400 MHz, $CDCl_3$) spectrum of crude from synthesis of **R2** third attempt.

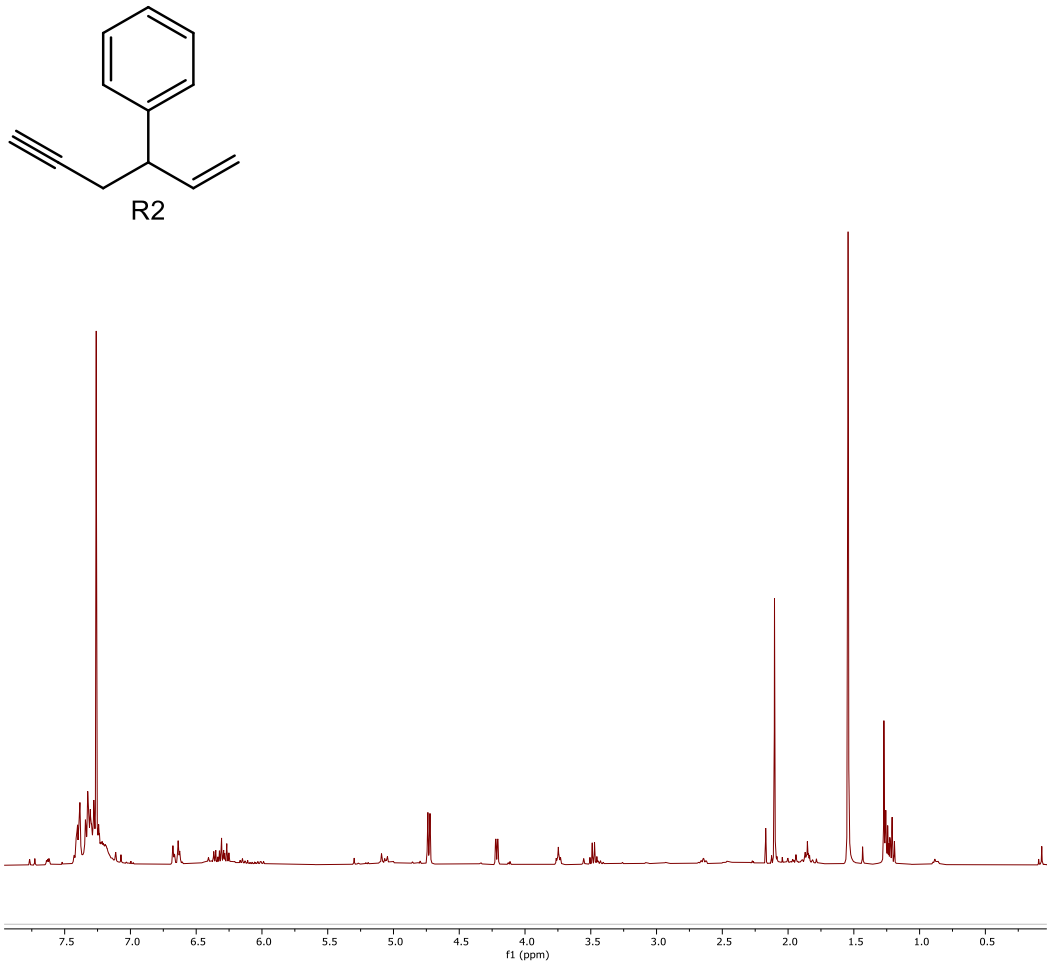

A 20. ^{1}H NMR (400 MHz, $CDCl_3$) spectrum of crude from synthesis of **R2** fourth attempt.

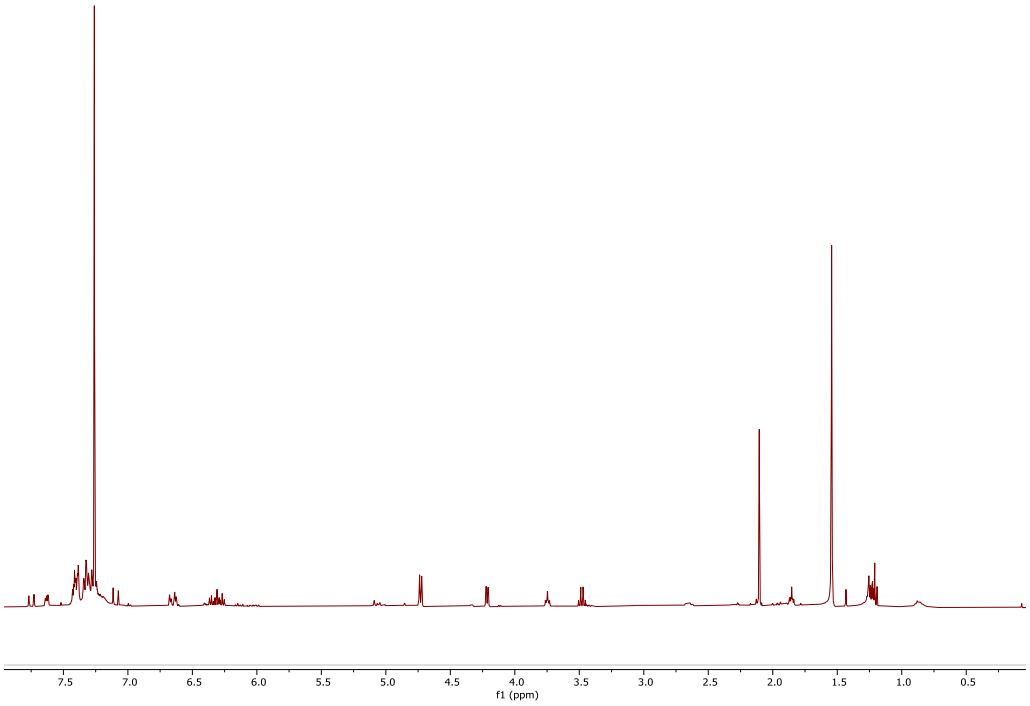

A 21. ^{1}H NMR (400 MHz, $CDCl_3$) spectrum of crude from synthesis of **R2** fifth attempt.

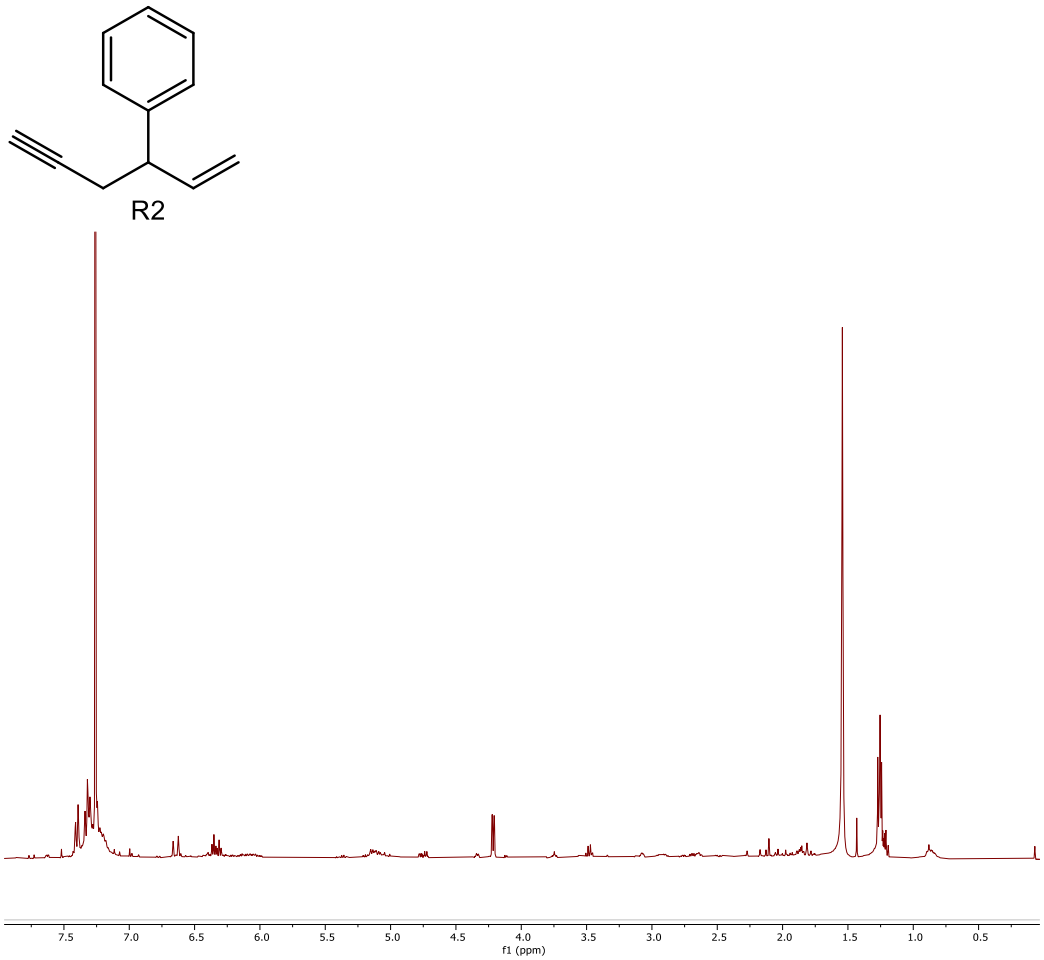

A 22. ^{1}H NMR (400 MHz, $CDCl_3$) spectrum of crude from synthesis of **R2** sixth attempt.

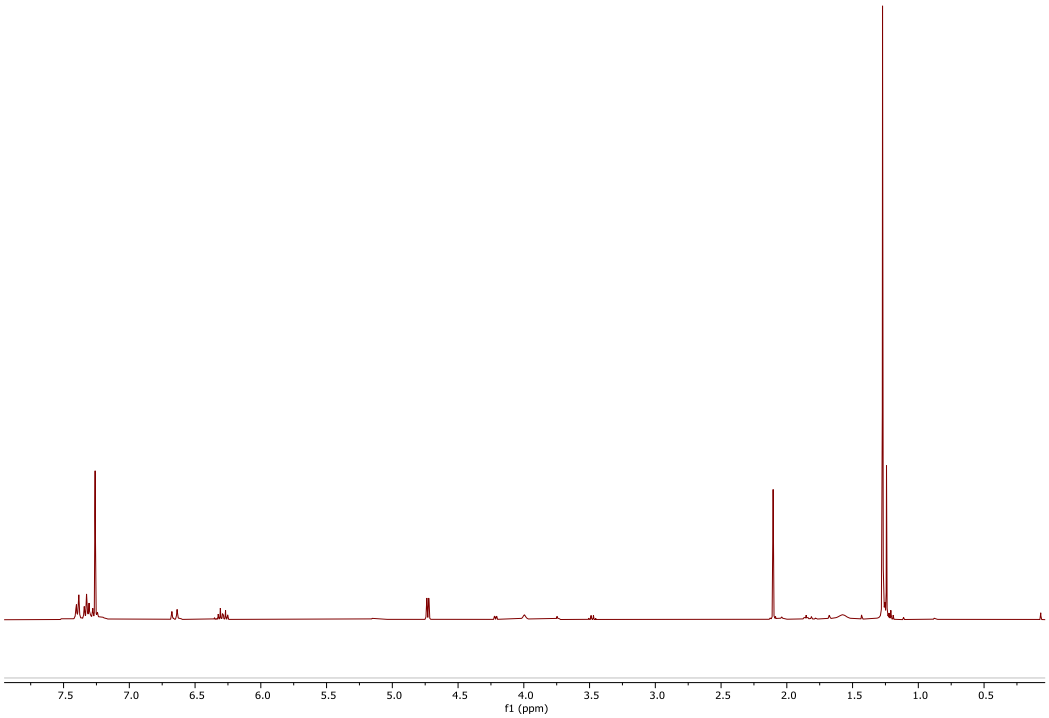

A 23. ^{1}H NMR (400 MHz, $CDCl_3$) spectrum of crude from synthesis of **R2** seventh attempt.

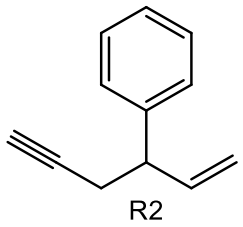

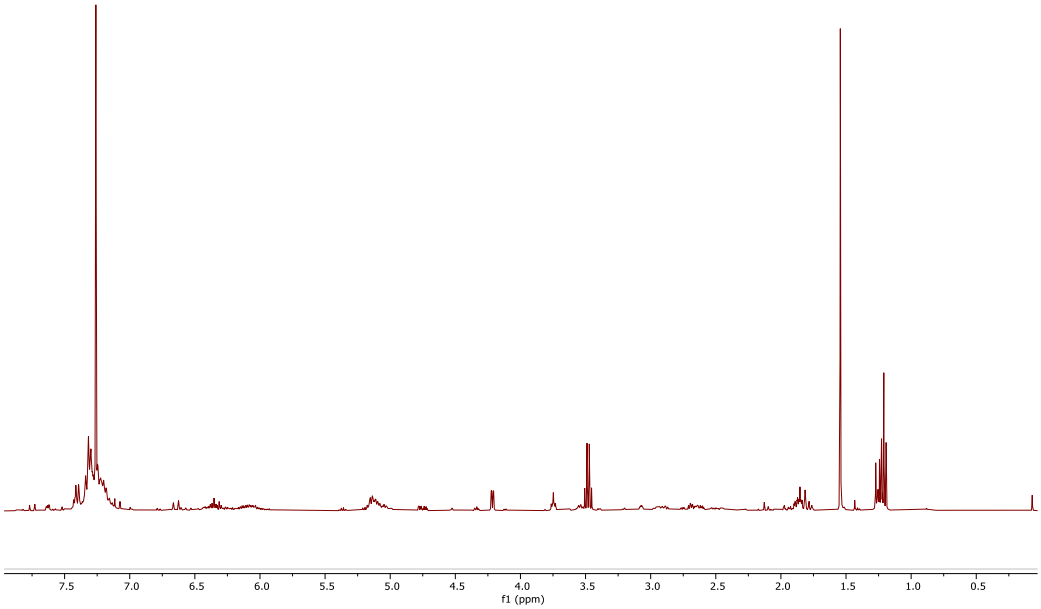

A 24. ^{1}H NMR (400 MHz, $CDCl_3$) spectrum of crude from synthesis of **R2** eighth attempt.

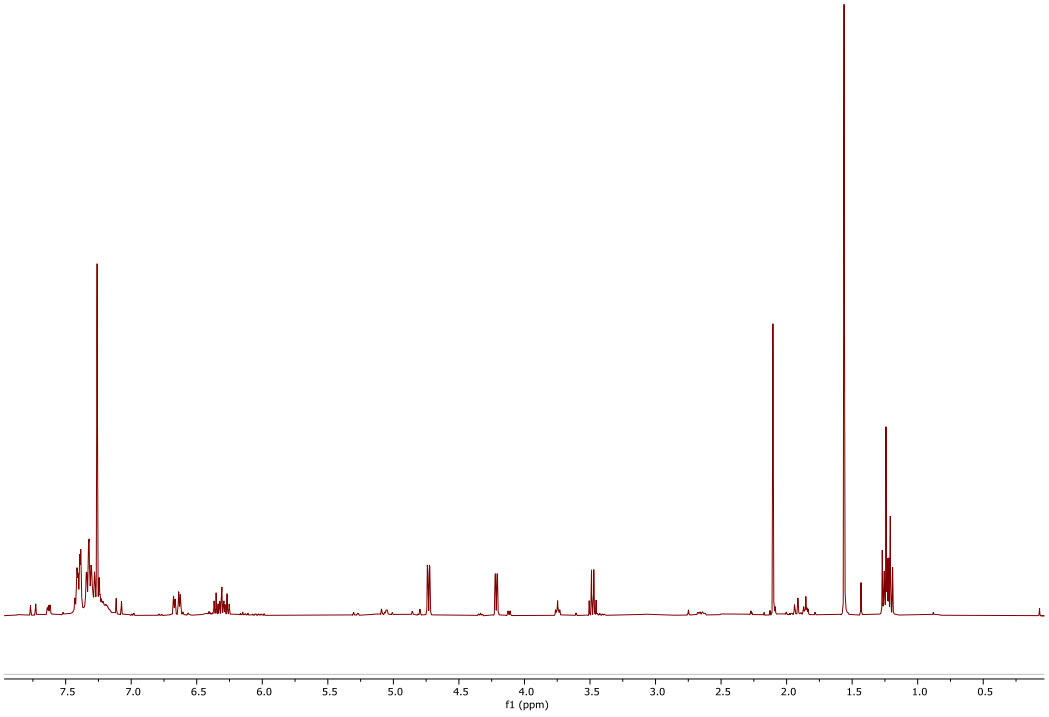

A 25. ^{1}H NMR (400 MHz, $CDCl_3$) spectrum of crude from synthesis of **R2** ninth attempt.

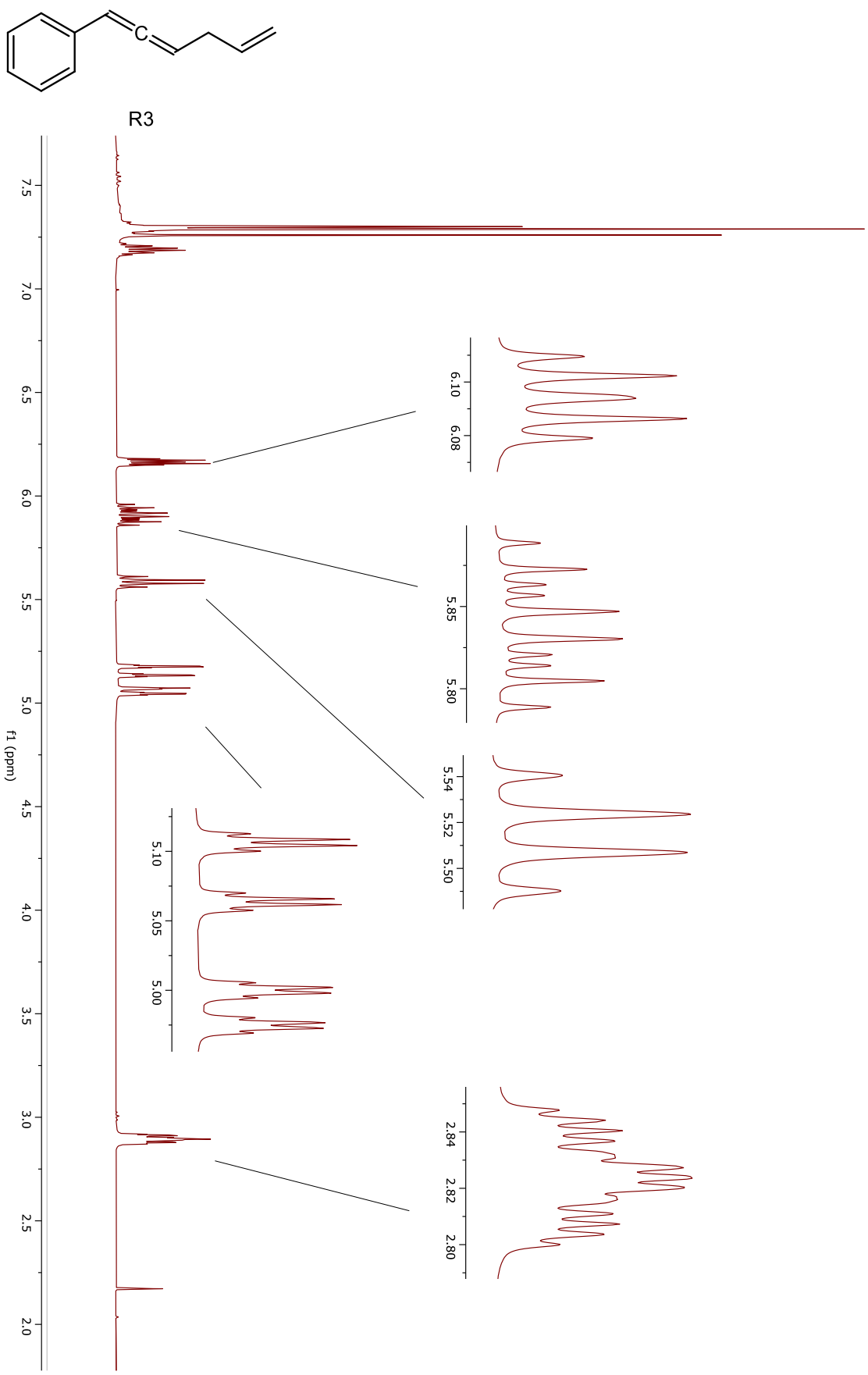

A 26. ^{1}H NMR (400 MHz, $CDCl_3$) spectrum of **R3** with embedded close-up view.

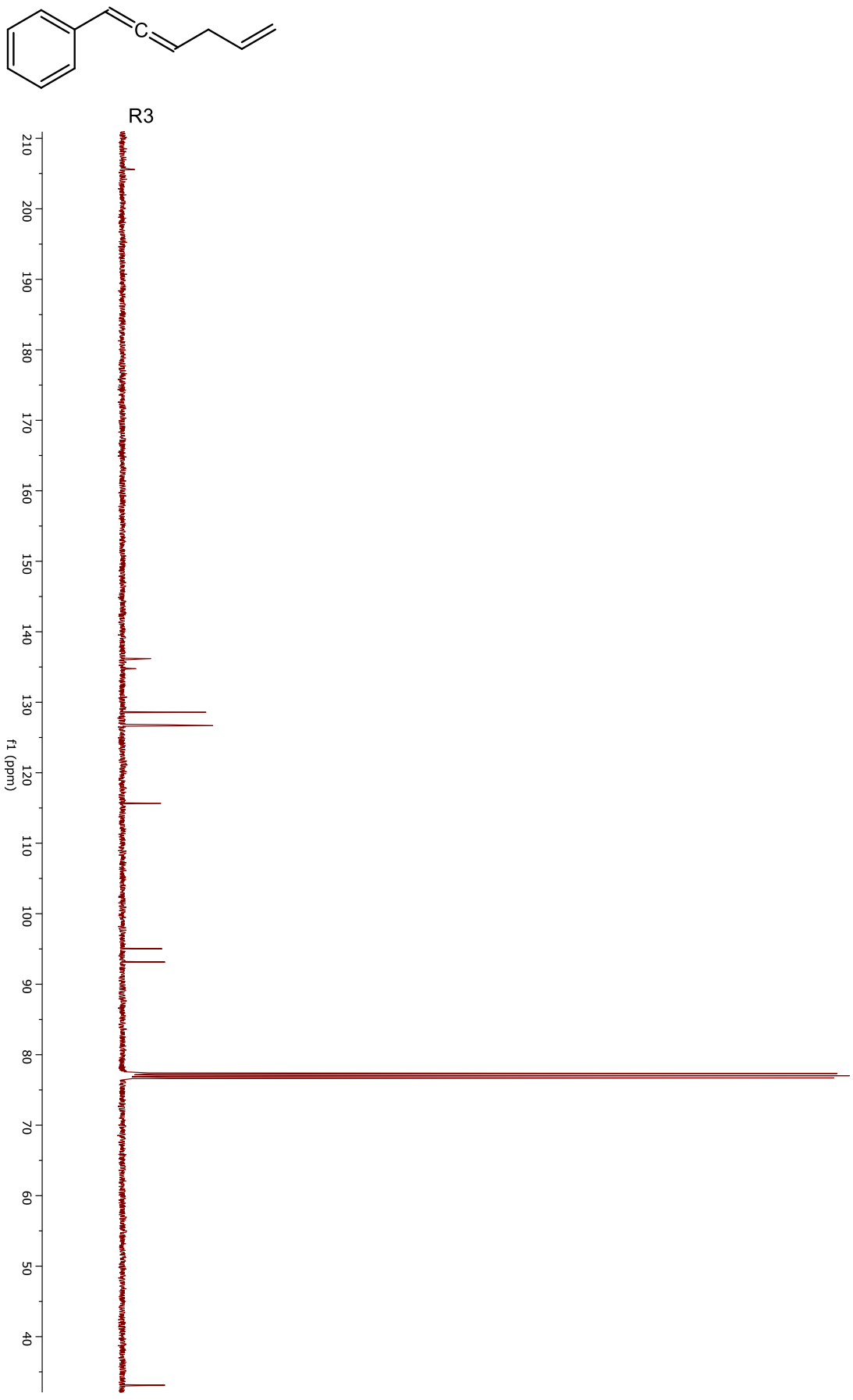

A 27. ^{13}C NMR (101 MHz, $CDCl_3$) spectrum of **R3**.

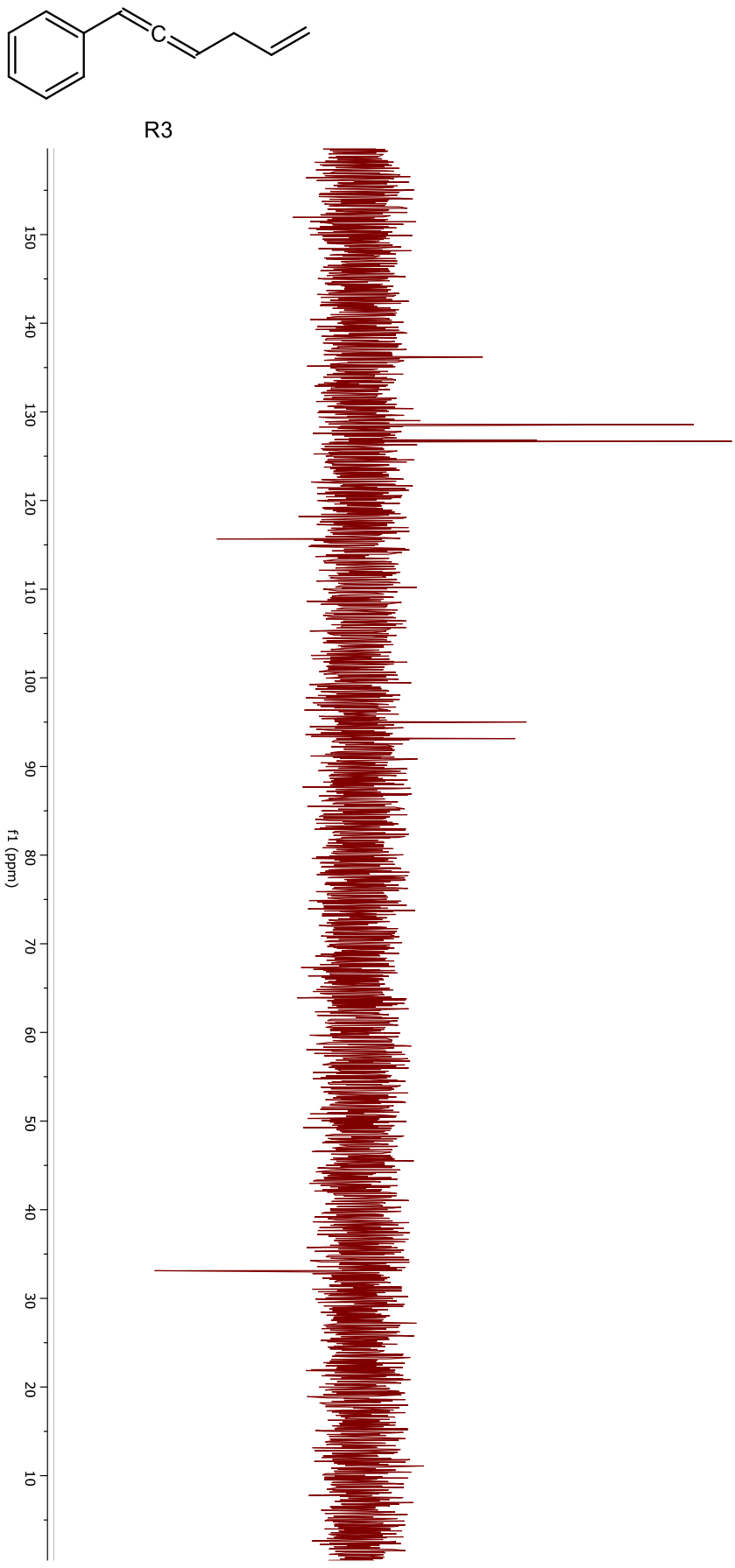

A 28. DEPT135 NMR (400 MHz, $CDCl_3$) spectrum of **R3**.

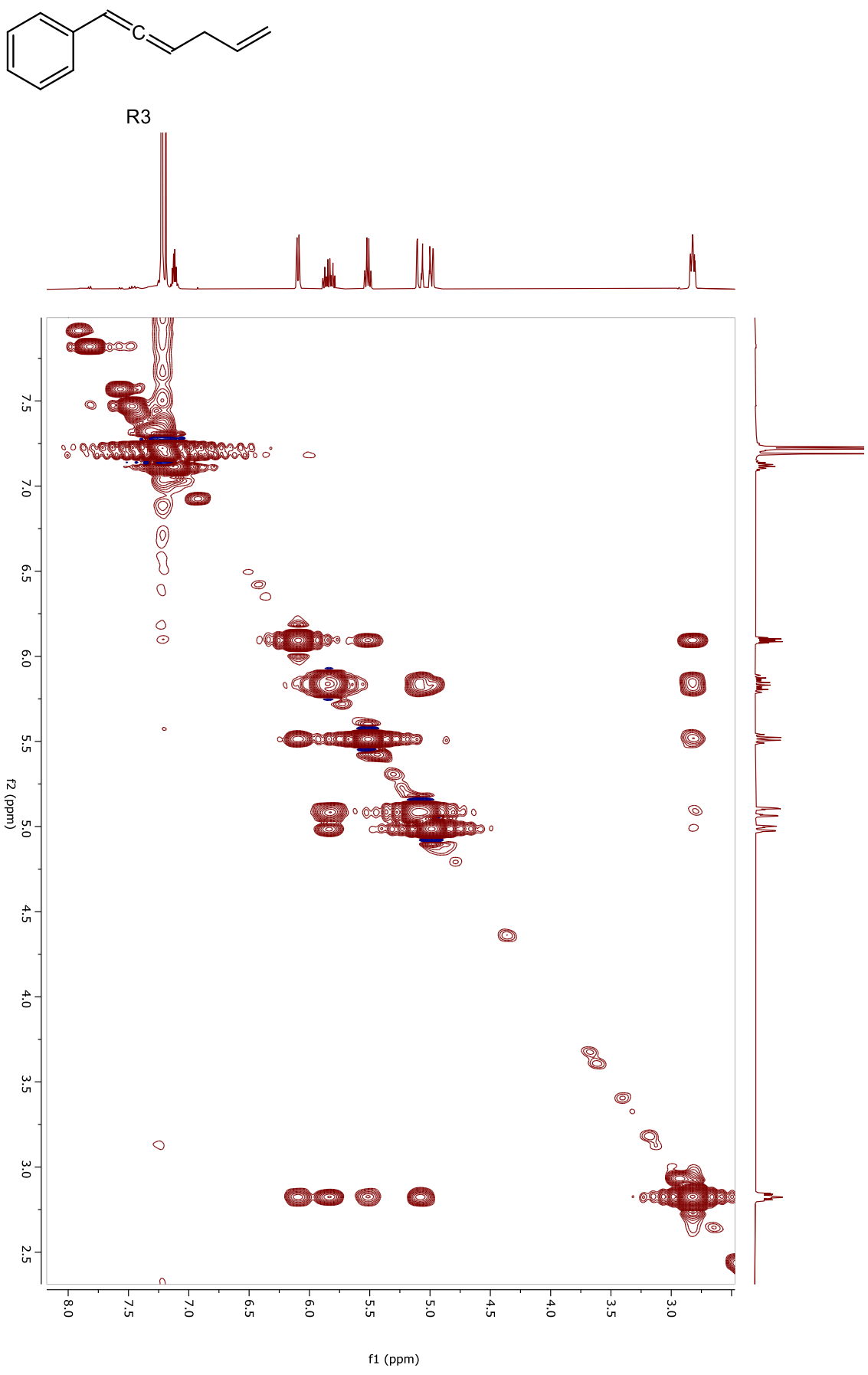

A 29. NOESY 2D NMR (400 MHz, $CDCl_3$) spectrum of **R3**.

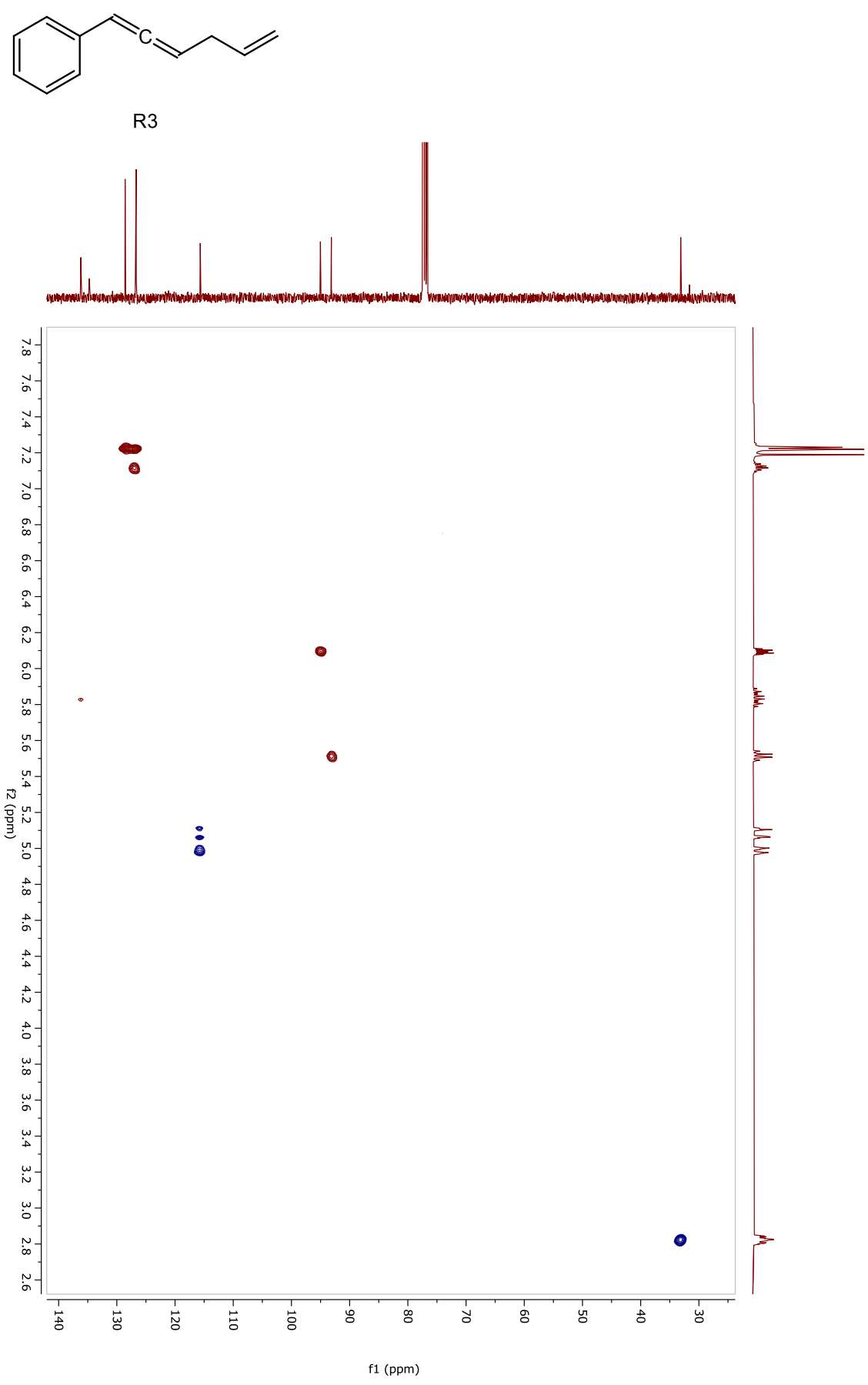

A 30. HSQC with DEPT NMR (400 MHz, $CDCl_3$) spectrum of **R3.**

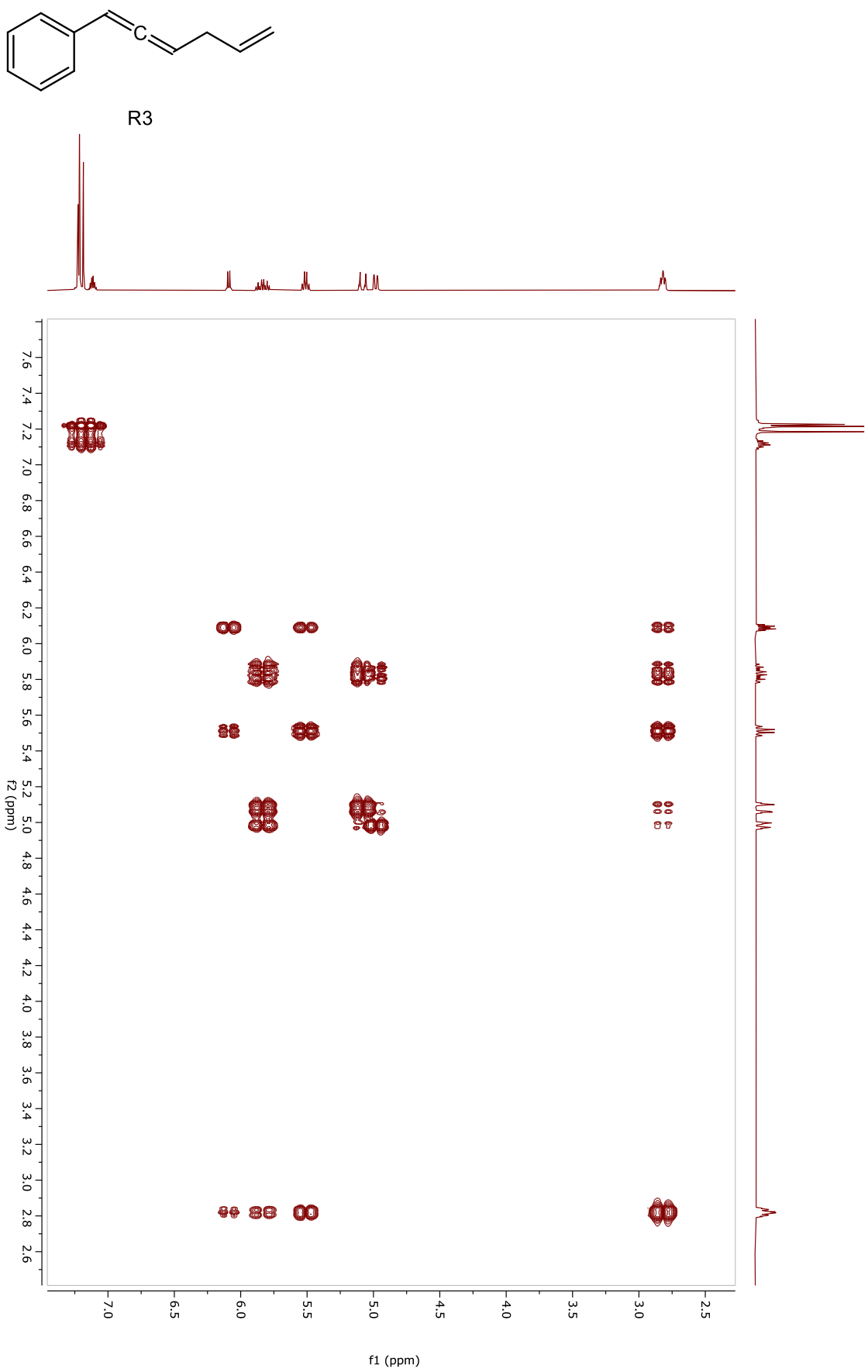

A 31. COSY 2D NMR (400 MHz, $CDCl_3$) spectrum of **R3**.

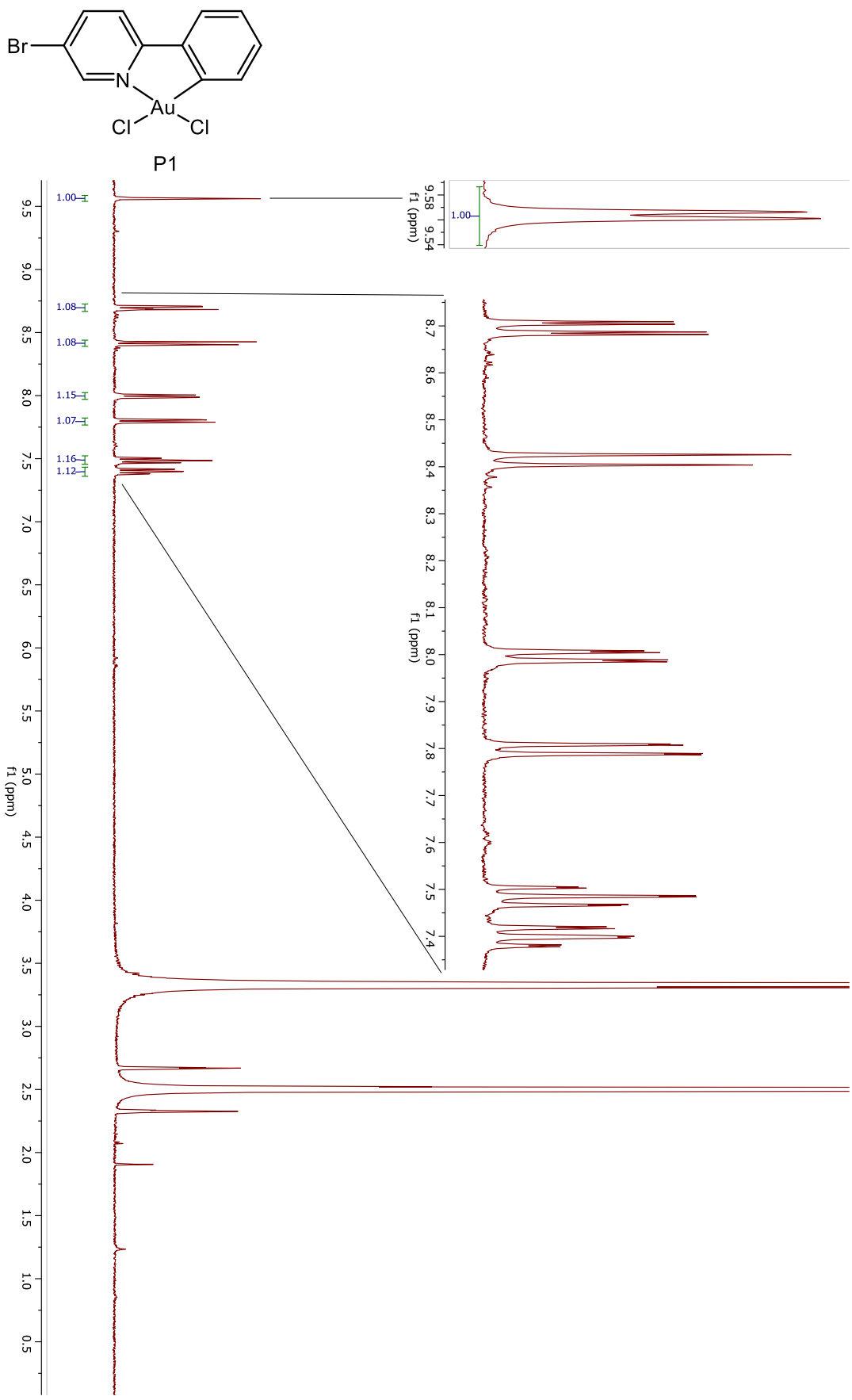

A 32. ^{1}H NMR (400 MHz, DMSO-d_6) spectrum of **P1**, with embedded close-up view.

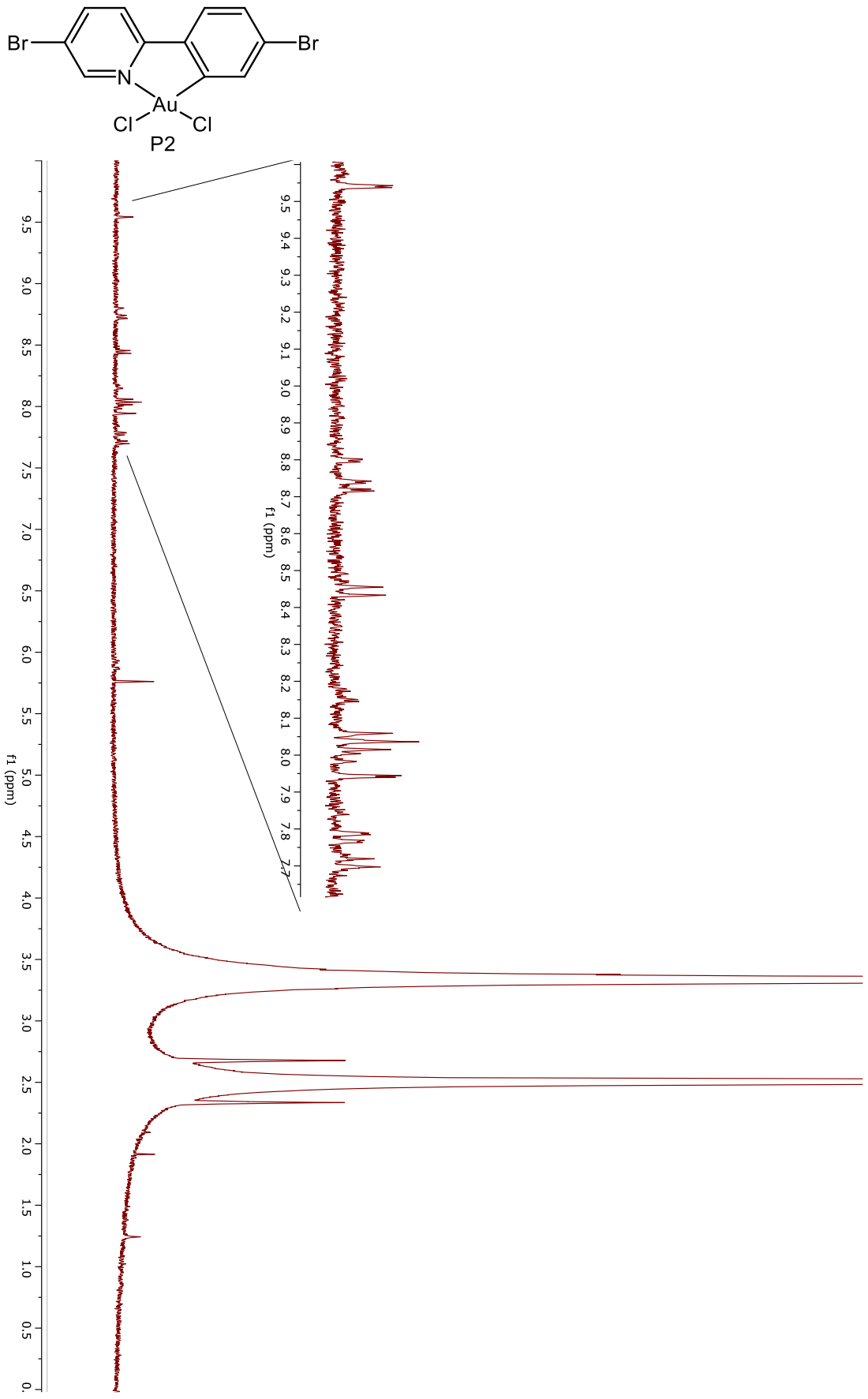

A 33. ^{1}H NMR (400 MHz, DMSO-d_6) spectrum of **P2** first attempt, with embedded close-up view.

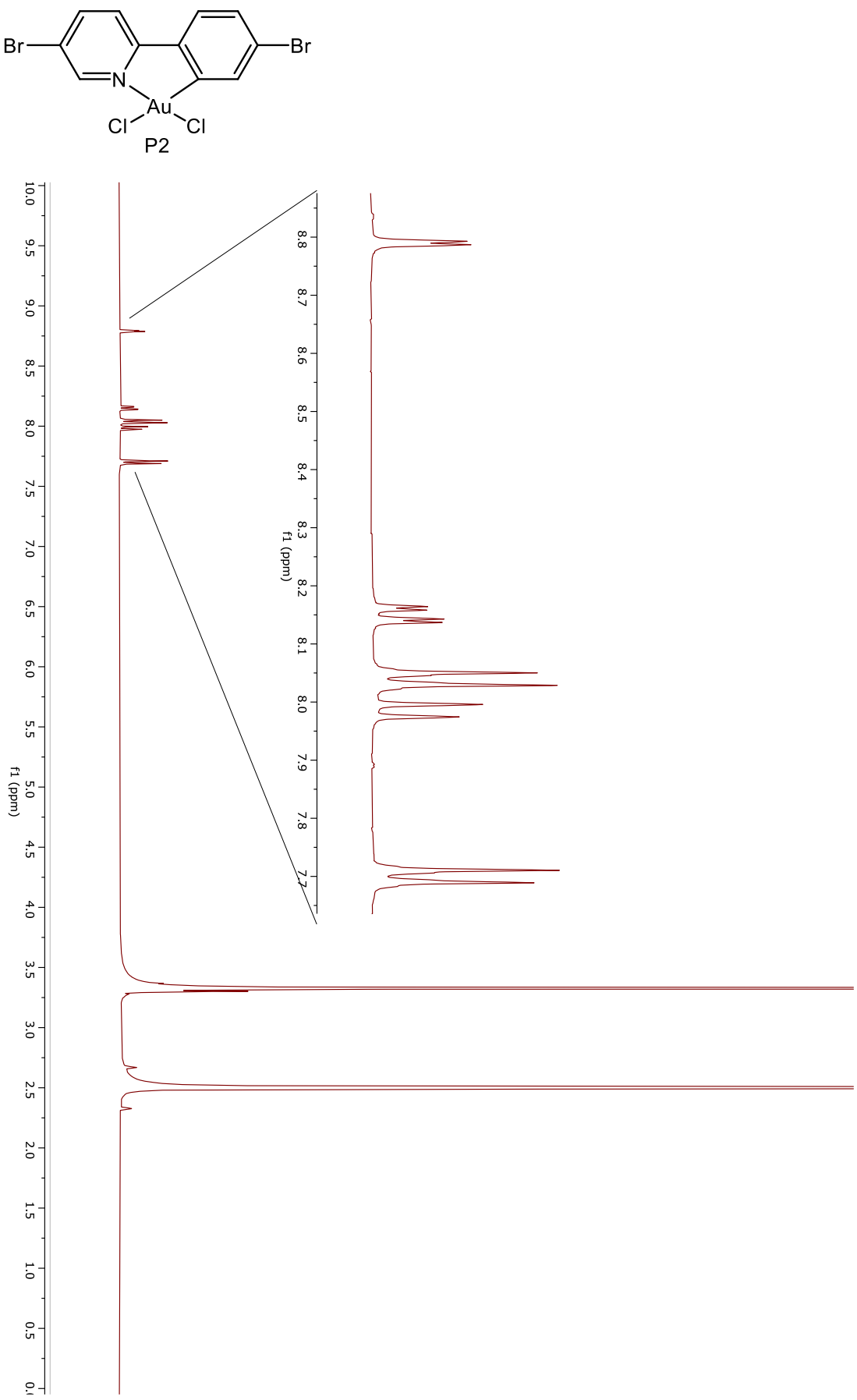

A 34. ^{1}H NMR (400 MHz, DMSO-d_6) spectrum of **P2** second attempt, with embedded close-up view.

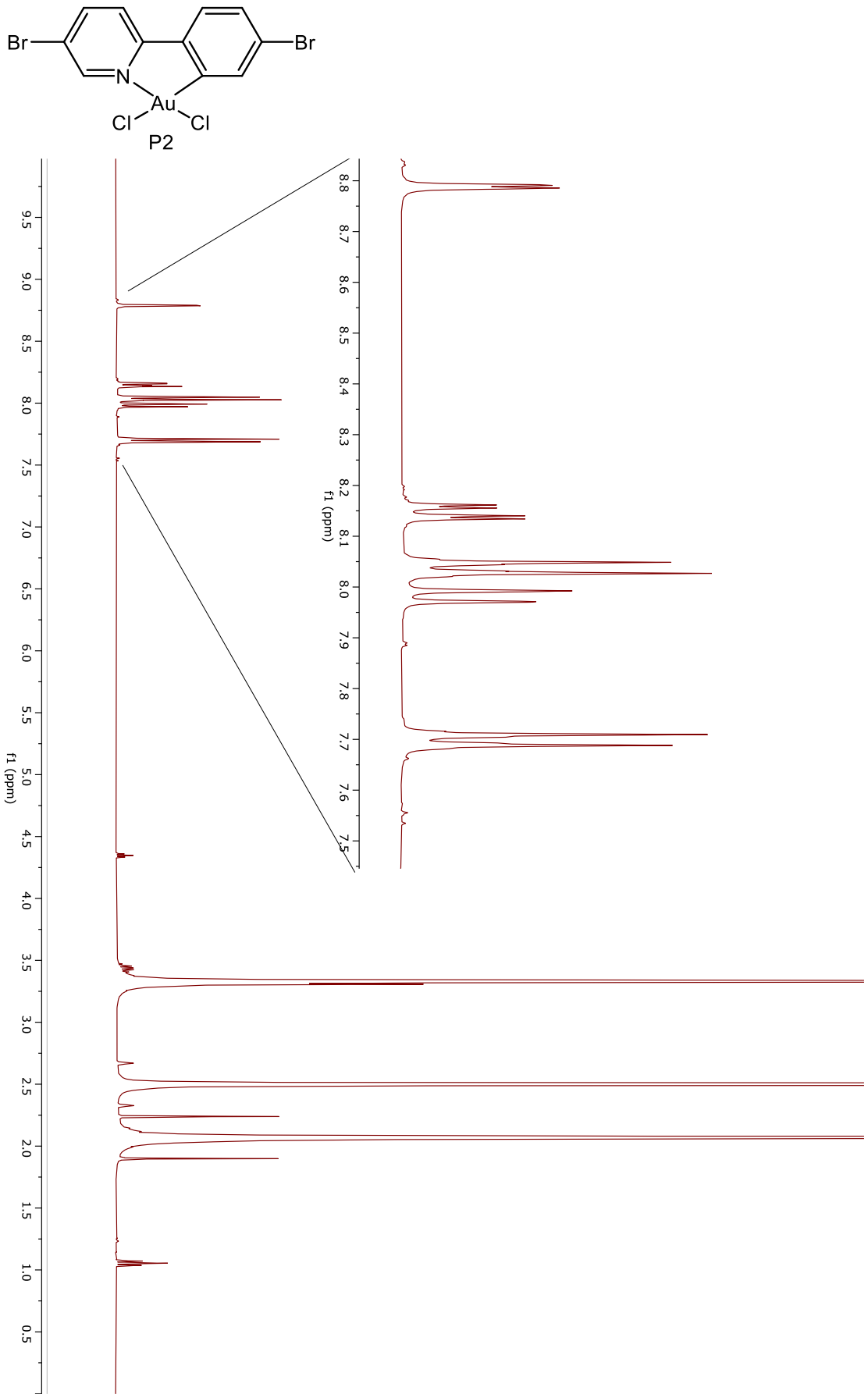

A 35. ^{1}H NMR (400 MHz, DMSO-d_6) spectrum of **P2** third attempt, with embedded close-up view.

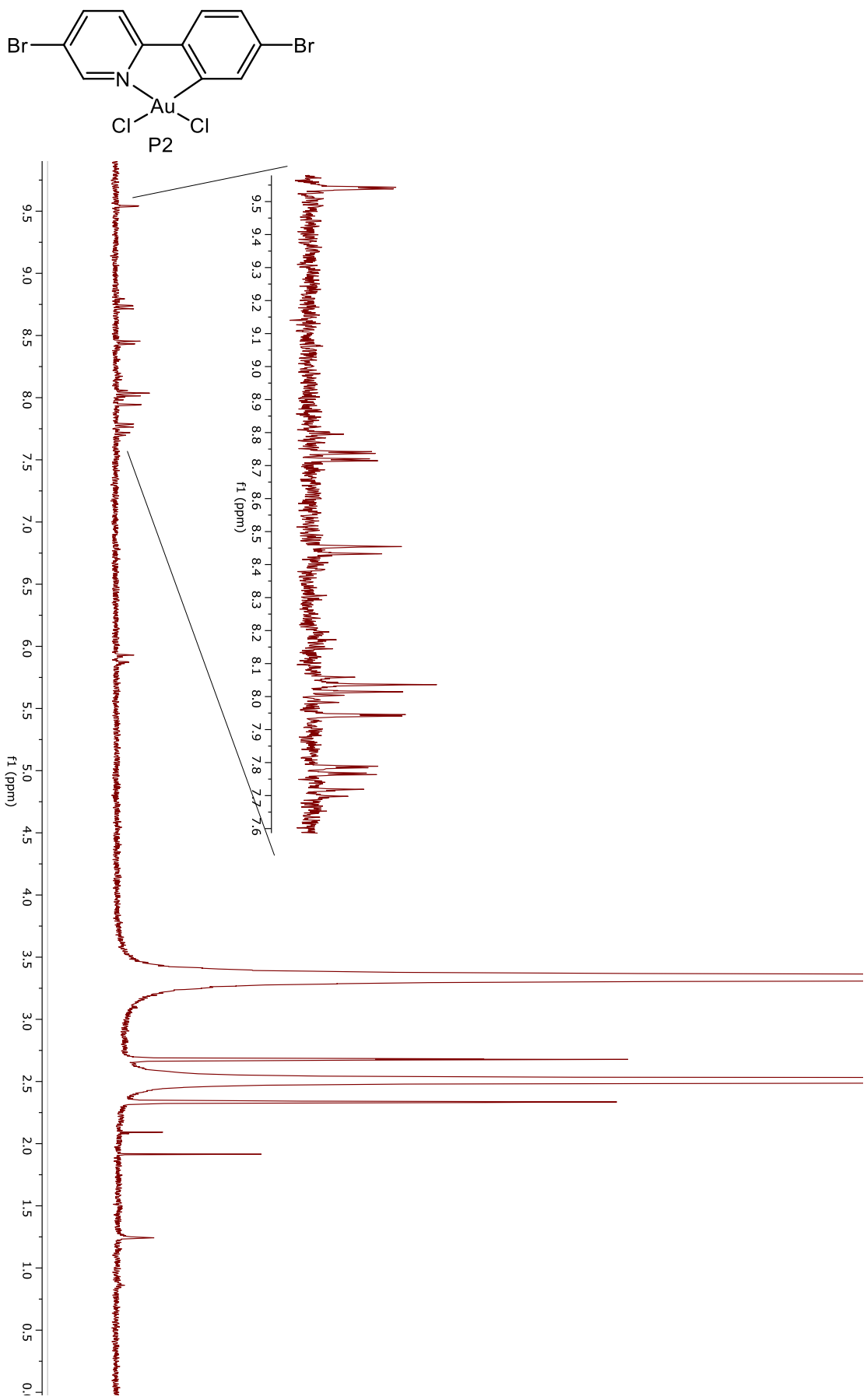

A 36. ^{1}H NMR (400 MHz, DMSO-d_6) spectrum of **P2** fourth attempt, with embedded close-up view.

MS

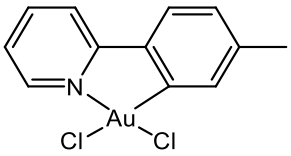

Au(tpy)

MS Spectrum Report

Analysis Info

Sample Name	SN-B2-02	Acquisition Date	3/5/2021 8:53:23 AM
Method	ESI_pos_50_1500_os.m	Analysis Name	D:\Data\maxis2021\17568.d

Acquisition Parameter

Source Type	ESI	Ion Polarity	Positive	Set Nebulizer	0.3 Bar
Focus	Not active	Set Capillary	3500 V	Set Dry Heater	200 °C
Scan Begin	50 m/z	Set End Plate Offset	-500 V	Set Dry Gas	4.0 l/min
Scan End	1500 m/z	Set Charging Voltage	2000 V	Set Divert Valve	Waste
		Set Corona	0 nA	Set APCI Heater	0 °C

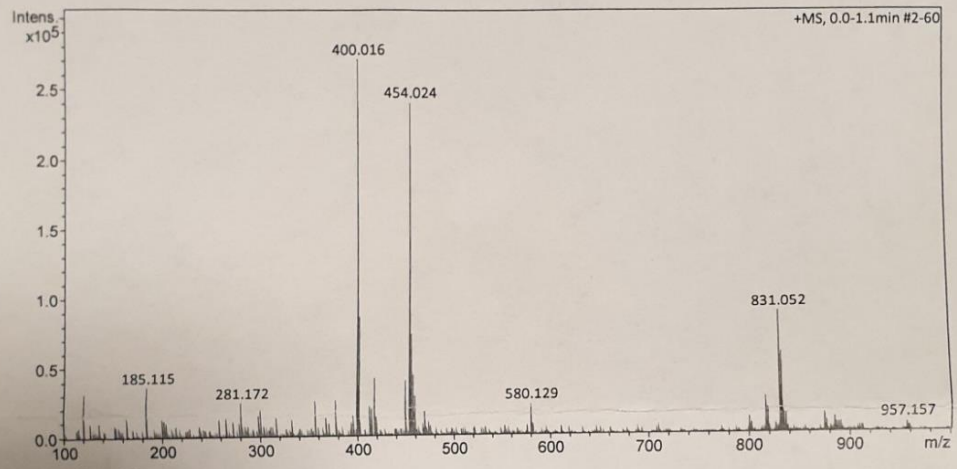

#	m/z	I %	
1	120.987	11.9	
2	185.115	13.5	
3	281.172	9.0	
4	356.976	9.4	
5	378.298	9.5	
6	400.016	100.0	M − Cl
7	401.020	13.4	
8	402.013	32.4	
9	418.027	15.7	
10	450.074	14.7	
11	454.024	88.9	
12	455.028	12.7	
13	456.022	27.4	
14	457.975	16.4	M + Na
15	459.972	10.7	
16	580.129	8.1	
17	817.037	9.6	
18	831.052	32.7	
19	832.056	9.0	
20	833.050	21.6	

17568.d
Bruker Compass DataAnalysis 4.3 printed: 3/5/2021 8:58:59 AM Page 1 of 1

A 37. ESI MS spectrum of **Au(tpy)Cl$_2$** with acetonitrile as solvent.

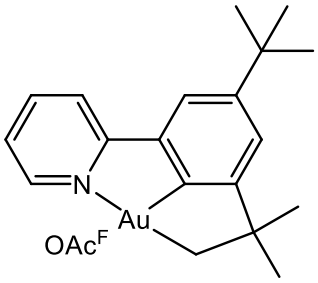

AuPinc

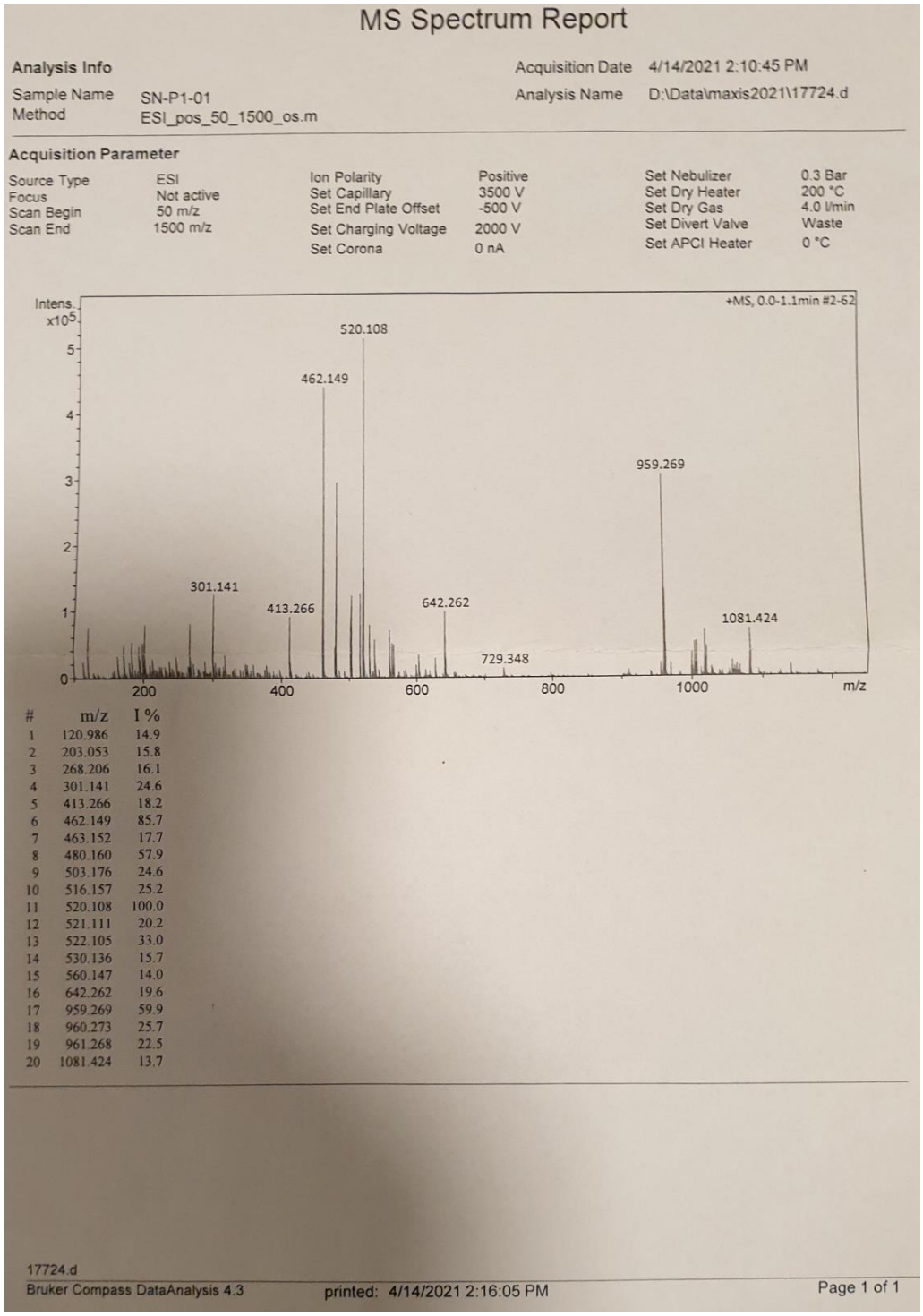

A 38. ESI MS spectrum of **AuPincOAc^{F}** with acetonitrile as solvent.

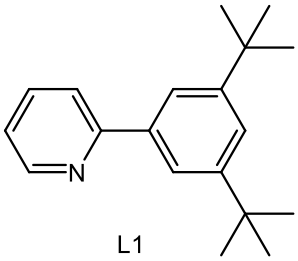

L1

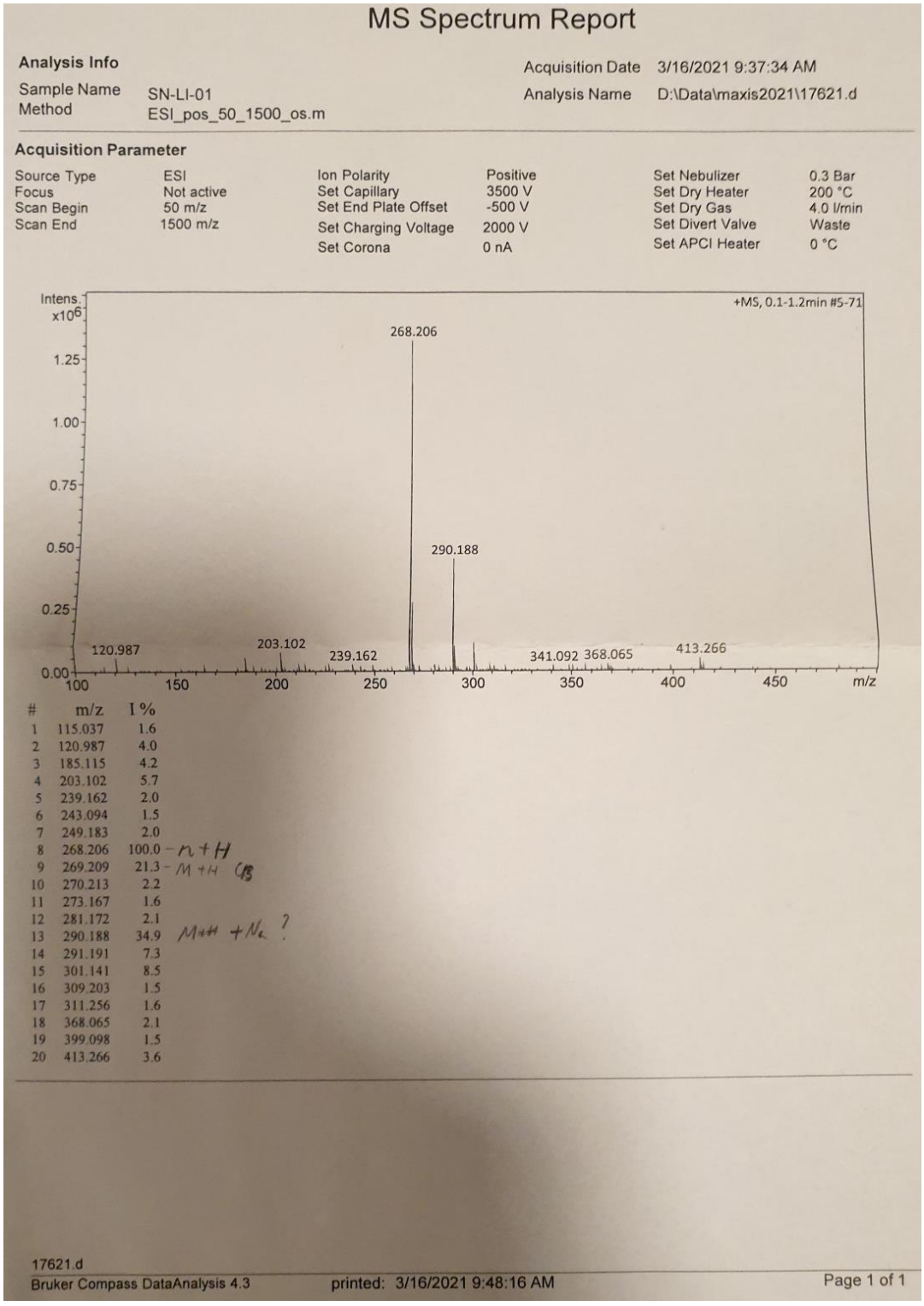

A 39. ESI MS spectrum of **L1** with acetonitrile as solvent.

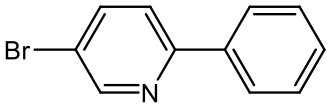

L2

Mass Spectrum List Report

Analysis Info

Analysis Name	D:\Data\maxis2022\19133.d	Acquisition Date	07-Nov-22 10:49:46 AM
Method	ESI_pos_50_1500_os.m	Operator	Mauritz
Sample Name	KSN-L2	Instrument	maXis II ETD 1823391.22318
Comment			

Acquisition Parameter

Source Type	ESI	Set Capillary	3500 V	Set Nebulizer	2.0 Bar
Focus	Not active	Set End Plate Offset	-500 V	Set Dry Heater	200 °C
Scan Begin	50 m/z	Set Charging Voltage	2000 V	Set Dry Gas	4.0 l/min
Scan End	1500 m/z	Set Corona	0 nA	Set Divert Valve	Waste
				Set APCI Heater	0 °C

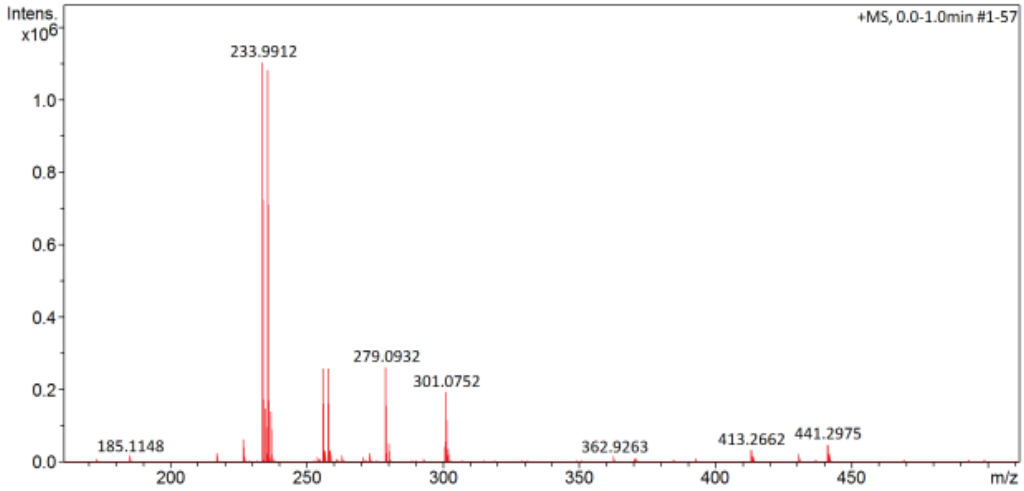

#	m/z	Res.	S/N	I	I %	FWHM
1	90.9766	23808	1764.0	17538	1.6	0.0038
2	158.9640	29078	1129.2	12227	1.1	0.0055
3	185.1148	29585	1231.5	14254	1.3	0.0063
4	217.1046	30578	1729.4	23976	2.2	0.0071
5	226.9515	32485	4289.9	62235	5.6	0.0070
6	227.1254	31285	1024.6	14911	1.4	0.0073
7	233.9912	30139	71958.7	1103560	100.0	0.0078
8	234.0823	35774	1317.8	20225	1.8	0.0065
9	234.9945	32204	9553.1	147054	13.3	0.0073
10	235.9891	30259	69840.3	1082216	98.1	0.0078
11	236.0807	36862	1222.5	18950	1.7	0.0064
12	236.9924	31664	9049.7	140511	12.7	0.0075
13	255.9731	32741	15553.5	260582	23.6	0.0078
14	256.9764	33330	1898.5	31950	2.9	0.0077
15	257.9711	33569	15389.1	260153	23.6	0.0077
16	258.9744	31630	1757.1	29853	2.7	0.0082
17	263.0984	33645	800.3	13989	1.3	0.0078
18	273.1672	33218	1319.1	24215	2.2	0.0082
19	279.0932	33164	13833.3	263697	23.9	0.0084
20	280.0967	32987	2671.7	51148	4.6	0.0085
21	301.0752	34147	9587.0	194375	17.6	0.0088
22	301.1411	34594	580.0	11758	1.1	0.0087
23	302.0786	34191	1866.9	37831	3.4	0.0088
24	362.9263	35570	593.8	12901	1.2	0.0102
25	413.2662	36010	1421.3	32860	3.0	0.0115
26	430.9138	37396	509.3	11957	1.1	0.0115
27	441.2975	36633	2043.7	48876	4.4	0.0120
28	442.3009	36531	598.0	14336	1.3	0.0121
29	560.0025	37868	454.9	12788	1.2	0.0148
30	587.1115	38509	695.8	19934	1.8	0.0152

A 40. ESI MS spectrum of **L2** with acetonitrile as solvent.

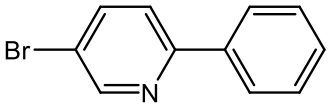

L2

Elemental Analysis Report

Analysis Info

Sample Name	KSN-L2	Acquisition Date	07-Nov-22 10:49:46 AM
Method	ESI_pos_50_1500_os.m	Analysis Name	D:\Data\maxis2022\19133.d

Acquisition Parameter

Source Type	ESI	Set Capillary	3500 V	Set Nebulizer	2.0 Bar
Focus	Not active	Set End Plate Offset	-500 V	Set Dry Heater	200 °C
Scan Begin	50 m/z	Set Charging Voltage	2000 V	Set Dry Gas	4.0 l/min
Scan End	1500 m/z	Set Corona	0 nA	Set Divert Valve	Waste
				Set APCI Heater	0 °C

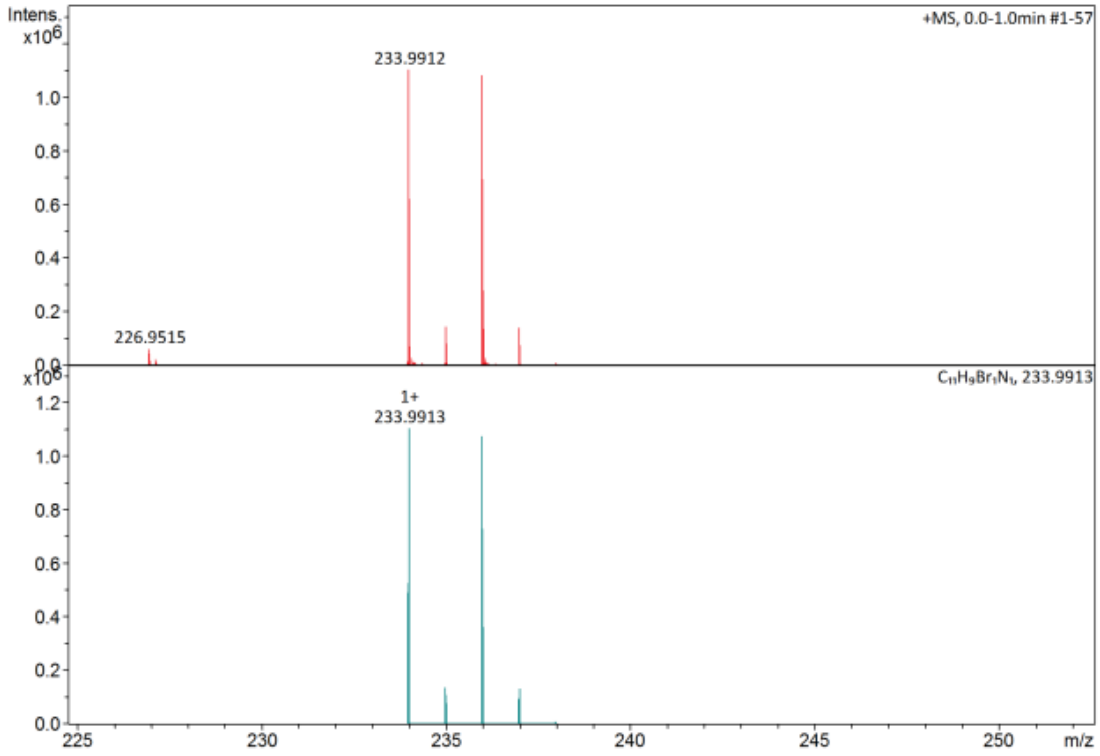

Meas. m/z	Ion Formula	m/z	err [ppm]
233.9912	C11H9BrN	233.9913	0.4
255.9731	C10H9BrO3	255.9730	-0.5
	C11H8BrNNa	255.9732	0.6

A 41. ESI elemental analysis at m/z 225 to 250 of **L2** with measured HRMS and suggested ion formula.

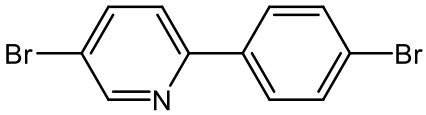

L3

Mass Spectrum List Report

Analysis Info

Analysis Name	D:\Data\maxis2022\19095.d	Acquisition Date	30-Sep-22 1:49:31 PM
Method	ESI_pos_50_1500_os.m	Operator	Erlend
Sample Name	SN_MA_L2_01	Instrument	maXis II ETD 1823391.22318
Comment			

Acquisition Parameter

Source Type	ESI	Set Capillary	3500 V	Set Nebulizer	0.3 Bar
Focus	Not active	Set End Plate Offset	-500 V	Set Dry Heater	200 °C
Scan Begin	50 m/z	Set Charging Voltage	2000 V	Set Dry Gas	4.0 l/min
Scan End	1500 m/z	Set Corona	0 nA	Set Divert Valve	Waste
				Set APCI Heater	0 °C

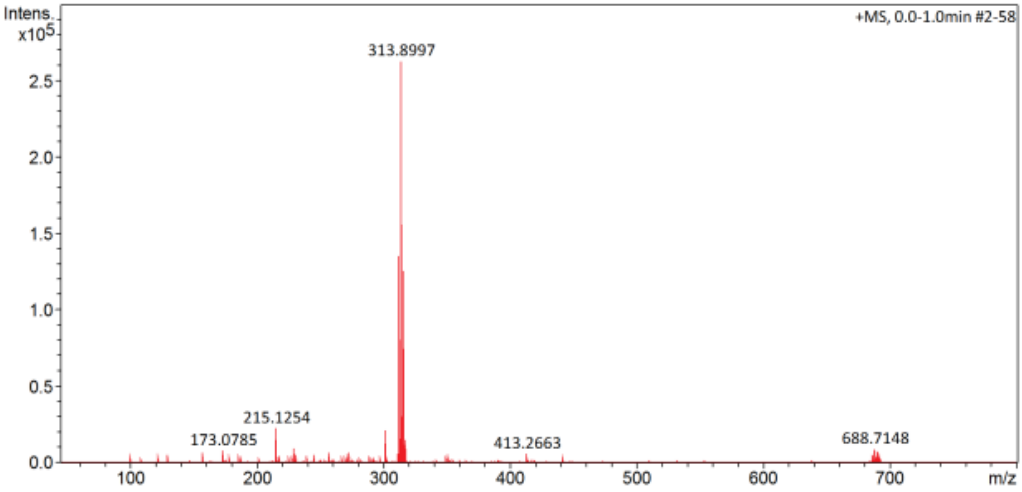

#	m/z	Res.	S/N	I	I %	FWHM
1	122.0576	25825	553.6	3954	1.5	0.0047
2	129.0522	26985	688.5	4930	1.9	0.0048
3	157.0836	29162	869.5	6415	2.4	0.0054
4	173.0785	30158	1055.3	7793	3.0	0.0057
5	215.1254	32561	3019.5	22343	8.5	0.0066
6	217.1047	31821	568.0	4207	1.6	0.0068
7	227.1254	32099	589.3	4396	1.7	0.0071
8	229.1410	32839	1215.7	9084	3.5	0.0070
9	231.1203	32887	677.2	5076	1.9	0.0070
10	239.0890	33397	646.1	4851	1.8	0.0072
11	245.1360	32894	653.3	4888	1.9	0.0075
12	257.1359	33708	900.6	6713	2.6	0.0076
13	271.1878	33229	512.7	3884	1.5	0.0082
14	273.1672	33735	825.6	6283	2.4	0.0081
15	301.1410	34282	2544.3	21475	8.2	0.0088
16	302.1443	34191	460.6	3906	1.5	0.0088
17	311.2557	34738	684.3	6057	2.3	0.0090
18	311.9018	35291	15236.8	135049	51.4	0.0088
19	312.9051	33765	1752.7	15591	5.9	0.0093
20	313.8997	35088	29403.9	262497	100.0	0.0089
21	314.9030	33851	3367.9	30125	11.5	0.0093
22	315.8977	34479	13993.0	125306	47.7	0.0092
23	316.9010	34577	1697.2	15218	5.8	0.0092
24	348.9901	35628	455.5	4339	1.7	0.0098
25	350.9871	35331	425.5	4073	1.6	0.0099
26	413.2663	37025	541.8	5710	2.2	0.0112
27	441.2975	36654	369.1	3960	1.5	0.0120
28	686.7166	40106	498.6	5135	2.0	0.0171
29	688.7148	40059	875.3	9004	3.4	0.0172
30	690.7129	38549	710.0	7293	2.8	0.0179

19095.d

Bruker Compass DataAnalysis 4.3 printed: 30-Sep-22 1:54:50 PM by: Erlend Page 1 of 1

A 42. ESI MS spectrum of **L3** with acetonitrile as solvent.

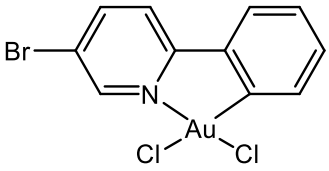

P1

Mass Spectrum List Report

Analysis Info

Analysis Name	D:\Data\maxis2022\19135.d	Acquisition Date	07-Nov-22 2:01:40 PM
Method	ESI_pos_50_1500_os.m	Operator	Mauritz
Sample Name	KSN-L2Au	Instrument	maXis II ETD 1823391.22318
Comment			

Acquisition Parameter

Source Type	ESI	Set Capillary	3500 V	Set Nebulizer	2.0 Bar
Focus	Not active	Set End Plate Offset	-500 V	Set Dry Heater	200 °C
Scan Begin	50 m/z	Set Charging Voltage	2000 V	Set Dry Gas	4.0 l/min
Scan End	1500 m/z	Set Corona	0 nA	Set Divert Valve	Waste
				Set APCI Heater	0 °C

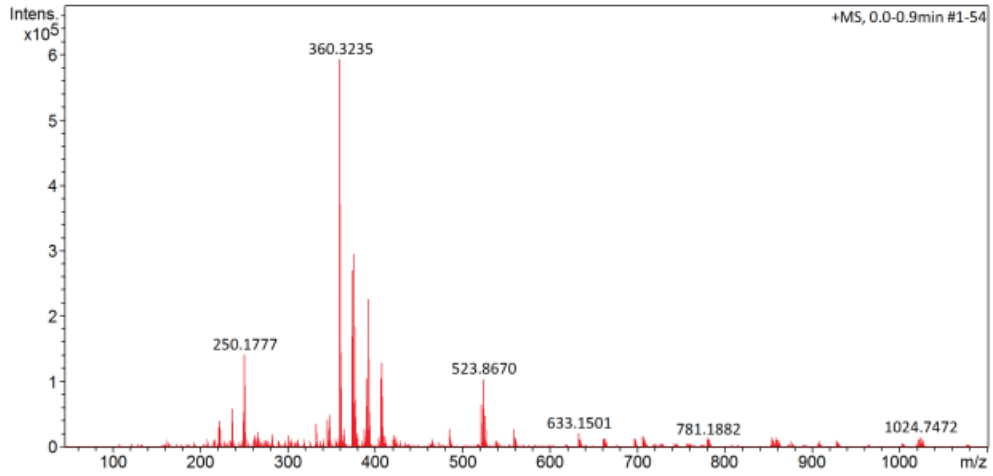

#	m/z	Res.	S/N	I	I %	FWHM
1	221.1750	30681	3189.4	31009	5.2	0.0072
2	222.1465	31722	4141.9	40447	6.8	0.0070
3	236.1622	32014	5283.0	58207	9.8	0.0074
4	250.1777	32925	11435.8	141584	23.9	0.0076
5	266.1726	32786	1398.8	22186	3.7	0.0081
6	332.2922	35373	1478.3	35758	6.0	0.0094
7	346.2715	35058	1595.6	41685	7.0	0.0099
8	348.2871	35049	1872.7	49433	8.3	0.0099
9	360.3235	35326	20493.6	592782	100.0	0.0102
10	361.3269	35462	5005.9	145053	24.5	0.0102
11	364.2820	35045	946.7	27773	4.7	0.0104
12	374.3027	35601	8564.7	270412	45.6	0.0105
13	375.3061	35289	2078.6	65908	11.1	0.0106
14	376.3183	35151	9241.9	295141	49.8	0.0107
15	377.3217	35522	2254.9	72454	12.2	0.0106
16	388.2820	35484	837.8	28145	4.7	0.0109
17	390.2976	35896	3130.8	105626	17.8	0.0109
18	391.3010	35144	756.8	25612	4.3	0.0111
19	392.3132	35649	6684.6	226473	38.2	0.0110
20	393.3167	35049	1610.4	54631	9.2	0.0112
21	394.3279	27469	736.6	25003	4.2	0.0144
22	406.2926	36148	3026.3	105187	17.7	0.0112
23	407.2959	36394	760.9	26470	4.5	0.0112
24	408.3081	35794	3719.7	129633	21.9	0.0114
25	409.3115	35306	882.0	30808	5.2	0.0116
26	485.1122	38299	717.1	27261	4.6	0.0127
27	521.8694	38550	1666.5	64841	10.9	0.0135
28	523.8670	38371	2677.3	104426	17.6	0.0137
29	525.8644	38675	1210.4	47228	8.0	0.0136
30	559.1311	38410	727.8	27069	4.6	0.0146

19135.d

Bruker Compass DataAnalysis 4.3 printed: 07-Nov-22 2:06:26 PM by: Mauritz Page 1 of 1

A 43. ESI MS spectrum of **P1** with acetonitrile as solvent.

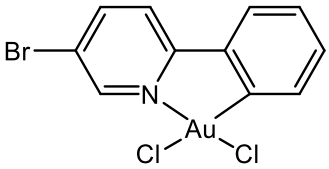

P1

Elemental Analysis Report

Analysis Info

Sample Name	KSN-L2Au	Acquisition Date	07-Nov-22 2:01:40 PM
Method	ESI_pos_50_1500_os.m	Analysis Name	D:\Data\maxis2022\19135.d

Acquisition Parameter

Source Type	ESI	Set Capillary	3500 V	Set Nebulizer	2.0 Bar
Focus	Not active	Set End Plate Offset	-500 V	Set Dry Heater	200 °C
Scan Begin	50 m/z	Set Charging Voltage	2000 V	Set Dry Gas	4.0 l/min
Scan End	1500 m/z	Set Corona	0 nA	Set Divert Valve	Waste
				Set APCI Heater	0 °C

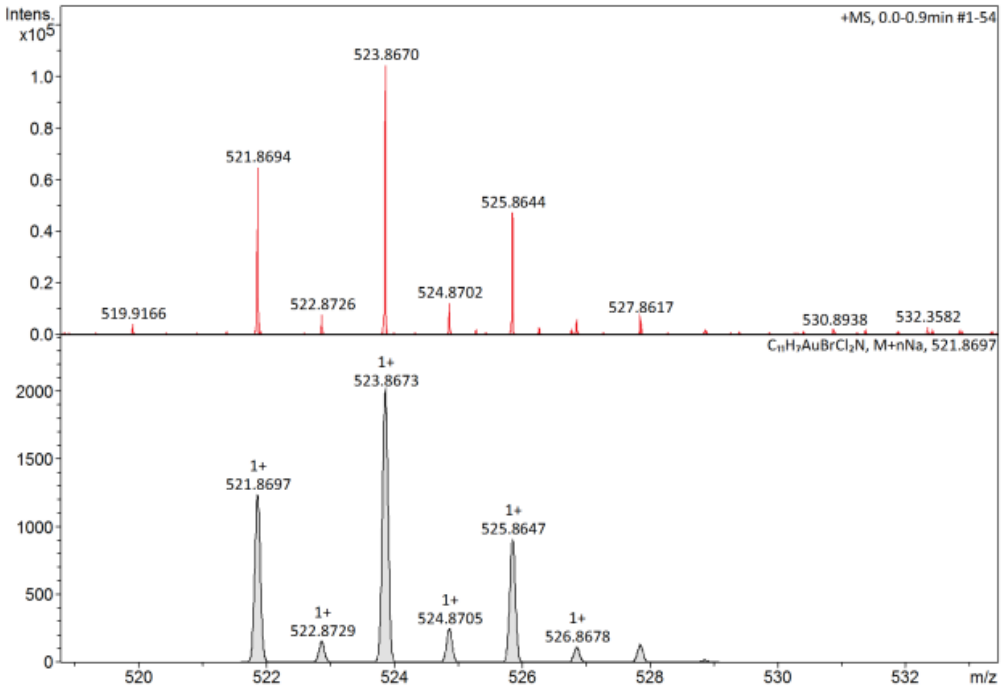

19135.d

Bruker Compass DataAnalysis 4.3 printed: 07-Nov-22 2:09:56 PM Page 1 of 1

A 44. ESI elemental analysis at m/z 519 to 533 of **P1** with measured HRMS and suggested ion formula.

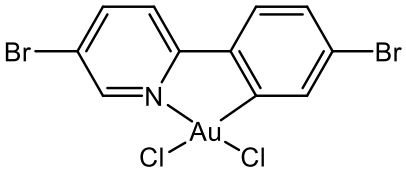

P2

Mass Spectrum List Report

Analysis Info

Analysis Name	D:\Data\maxis2022\19138.d	Acquisition Date	08-Nov-22 12:43:37 PM
Method	APPI_pos_50_1500_DIP.m	Operator	Mauritz
Sample Name	KSN L1Au	Instrument	maXis II ETD 1823391.22318
Comment			

Acquisition Parameter

Source Type	APPI	Set Capillary	700 V	Set Nebulizer	2.5 Bar
Focus	Not active	Set End Plate Offset	-500 V	Set Dry Heater	250 °C
Scan Begin	50 m/z	Set Charging Voltage	2000 V	Set Dry Gas	2.0 l/min
Scan End	1500 m/z	Set Corona	0 nA	Set Divert Valve	Source
				Set APCI Heater	50 °C

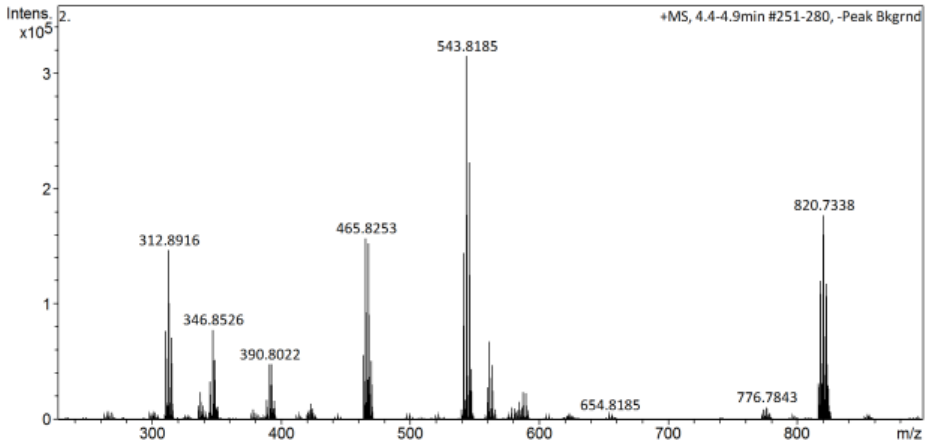

#	m/z	Res.	S/N	I	I %	FWHM
1	310.8936	35068	2528.5	77201	24.5	0.0089
2	312.8916	34832	4810.1	146657	46.6	0.0090
3	314.8896	34398	2342.2	71363	22.7	0.0092
4	344.8547	35298	1095.0	32749	10.4	0.0098
5	346.8526	35564	2624.9	78227	24.8	0.0098
6	348.8504	35405	1752.5	52055	16.5	0.0099
7	390.8022	36534	1727.8	48203	15.3	0.0107
8	392.8000	35990	1700.1	47527	15.1	0.0109
9	463.8274	37697	2131.5	55829	17.7	0.0123
10	465.8253	37407	5987.5	156991	49.9	0.0125
11	466.8294	34014	1323.6	34692	11.0	0.0137
12	467.8233	36507	5819.3	152381	48.4	0.0128
13	468.8275	35047	1401.7	36656	11.6	0.0134
14	469.8216	36002	1950.8	50963	16.2	0.0130
15	541.8207	38839	5941.9	144251	45.8	0.0140
16	543.8185	37977	12979.0	314848	100.0	0.0143
17	544.8218	37892	1559.4	37827	12.0	0.0144
18	545.8163	38355	9165.0	222310	70.6	0.0142
19	547.8140	38462	1808.4	43863	13.9	0.0142
20	559.8309	38039	1154.0	27801	8.8	0.0147
21	561.8290	38598	2819.9	67608	21.5	0.0146
22	563.8269	39103	1989.7	47391	15.1	0.0144
23	816.7379	40763	1697.9	31275	9.9	0.0200
24	818.7358	39995	6551.0	120350	38.2	0.0205
25	819.7383	39684	1695.8	31140	9.9	0.0207
26	820.7338	40119	9654.7	177179	56.3	0.0205
27	821.7366	38861	2347.7	43061	13.7	0.0211
28	822.7319	40711	6442.2	118099	37.5	0.0202
29	823.7348	40477	1541.6	28255	9.0	0.0204
30	824.7306	38899	1614.8	29582	9.4	0.0212

19138.d

Bruker Compass DataAnalysis 4.3 printed: 08-Nov-22 1:01:31 PM by: Mauritz Page 1 of 1

A 45. APPI MS spectrum of **P2** with acetonitrile as solvent and DIP introduction to the ion source.

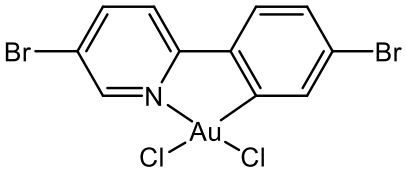

P2

Elemental Analysis Report

Analysis Info

Sample Name	KSN L1Au	Acquisition Date	08-Nov-22 12:43:37 PM
Method	APPI_pos_50_1500_DIP.m	Analysis Name	D:\Data\maxis2022\19138.d

Acquisition Parameter

Source Type	APPI	Set Capillary	700 V	Set Nebulizer	2.5 Bar
Focus	Not active	Set End Plate Offset	-500 V	Set Dry Heater	250 °C
Scan Begin	50 m/z	Set Charging Voltage	2000 V	Set Dry Gas	2.0 l/min
Scan End	1500 m/z	Set Corona	0 nA	Set Divert Valve	Source
				Set APCI Heater	50 °C

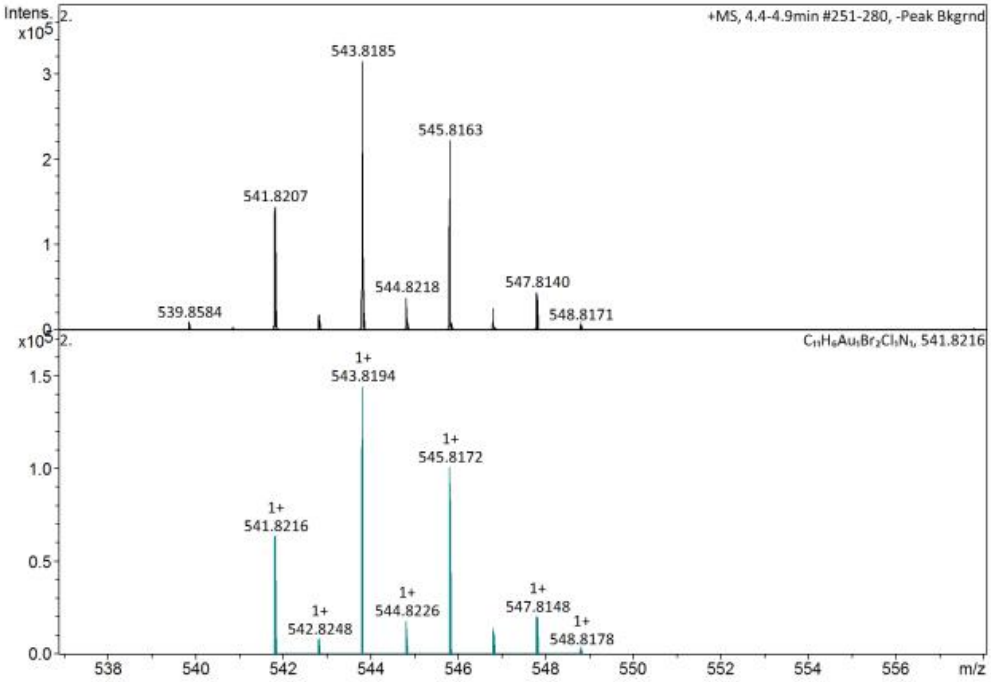

Meas. m/z	Ion Formula	m/z	err [ppm]
541.8207	C10H9Br2ClN2O12	541.8205	-0.3
	C11H6AuBr2ClN	541.8216	1.6

A 46. APPI elemental analysis at m/z 538 to 554 of **P2** with measured HRMS and suggested ion formula.